

Aus der Klinik und Poliklinik für Neurologie  
Direktor: Herr Prof. Dr. med. Heinz Reichmann

---

**Development of a human in-vitro pathophysiological model of FUS-ALS  
based on the induced pluripotent stem-cell technique and translation to  
patient phenotypes**

D i s s e r t a t i o n s s c h r i f t

zur Erlangung des akademischen Grades

Doctor rerum medicinalium (Dr. rer. medic.)

vorgelegt

der Medizinischen Fakultät Carl Gustav Carus

der Technischen Universität Dresden

von

Marcel Günter Naumann

Geboren am 23.11.1989 in Rochlitz/ Sachsen

Dresden, 2020

Gutachter

1. Gutachter: Prof. Dr. Dr. Andreas Hermann

2. Gutachter: Prof. Dr. Min Ae Lee-Kirsch

Tag der mündlichen Prüfung: 22.07.2021

gez.: -----

Vorsitzender der Promotionskommission

# Table of Contents

<b>Abbreviations</b> .....	<b>ii</b>
<b>1. Introduction</b> .....	<b>1</b>
1.1 Amyotrophic Lateral Sclerosis.....	1
1.2 Fused in Sarcoma.....	2
1.3 A Human Model System for ALS.....	5
<b>2. Aims of the thesis</b> .....	<b>7</b>
<b>3. Results</b> .....	<b>8</b>
3.1 Establishment of an In-Vitro Patient-Derived Cell Model of FUS-ALS to Investigate Pathological Pathways of Motor Neuron Degeneration.....	8
3.2 Application of the Established Model System for Pathophysiological Studies.....	10
3.2.1 Axonopathy and “Dying-Back” pathology is the prominent phenotype in FUS-ALS.....	10
3.2.2 Increased DNA damage is seen in FUS-ALS sMNs and induction of DNA damage mimics FUS-ALS distal axonopathy.....	11
3.2.3 Effect of <i>FUS</i> -NLS mutations on DNA repair mechanisms in patient-derived cells.....	12
3.3 Clinical Translation - Malignancy Rate and Further Clinical Aspects of FUS-ALS Patients .	32
<b>4. Discussion</b> .....	<b>45</b>
<b>5. Summary</b> .....	<b>52</b>
<b>6. Zusammenfassung</b> .....	<b>54</b>
<b>7. Acknowledgements</b> .....	<b>57</b>
<b>8. References</b> .....	<b>58</b>
<b>9. Appendix</b> .....	<b>70</b>
9.1 Anlage 1.....	70
9.2 Anlage 2.....	72
9.3 Erklärung zum Eigenanteil der gemeinschaftlichen Publikationen.....	73

## Abbreviations

A-T	<i>Ataxia telangiectasia</i>
AdOx	<i>Adenosine-2,3-dialdehyde</i>
ALS	<i>Amyotrophic lateral sclerosis</i>
AOA	<i>Ataxia oculomotor apraxia</i>
ATM	<i>Ataxia telangiectasia mutated</i>
C9ORF72	<i>Chromosome 9 open reading frame 72</i>
Cas9n	<i>Cas9 nickase</i>
ChAt	<i>Choline acetyltransferase</i>
CRISPR/Cas9	<i>Clustered regularly interspaced short palindromic repeat/CRISPR-associated 9 system</i>
DDR	<i>DNA damage response</i>
DDS	<i>DNA damage site</i>
DIV	<i>Day in vitro</i>
DNA-PK	<i>DNA-protein kinase</i>
DSB	<i>Double-strand break</i>
fALS	<i>familial ALS</i>
FTD	<i>Frontotemporal dementia</i>
FUS	<i>Fused in sarcoma</i>
gamma-H2AX	<i>Phosphorylated H2A.X</i>
GFAP	<i>Glial fibrillary acid protein</i>
GFP	<i>Green fluorescent protein</i>
HDAC1	<i>Histone Deacetylase 1</i>
hiPSC	<i>Human-induced pluripotent stem-cell</i>
ICC	<i>Immunocytochemistry</i>
MAP2	<i>Microtubule-associated protein 2</i>
MFC	<i>Microfluidic chamber</i>
MMP	<i>Mitochondrial membrane potential</i>
MN	<i>Motor neuron</i>
NHEJ	<i>Non-homologous end joining</i>
NLS	<i>Nuclear localization signal</i>
NPC	<i>Neural progenitor cell</i>
PAR	<i>Poly (ADP-ribose)</i>
PARG	<i>Poly (ADP-ribose) glycohydrolase</i>
PARP1	<i>Poly [ADP-ribose] polymerase 1</i>
PLD	<i>Prion-like domain</i>
ROS	<i>Reactive oxygen species</i>

SCA	<i>Spinocerebellar ataxia</i>
SCAN	<i>Spinocerebellar ataxia with axonal neuropathy</i>
SIRT1	<i>Sirtuin 1</i>
SMI32	<i>Neurofilament H</i>
SOD1	<i>Superoxide dismutase 1</i>
SOX2	<i>SRY (sex-determining region Y)-box 2</i>
SSB	<i>Single-strand breaks</i>
sMN	<i>Spinal motor neuron</i>
S/T-Q	<i>Serine/threonine - glutamine</i>
TDP-43	<i>TAR DNA-binding protein 43</i>
TLS	<i>Translocated in liposarcoma</i>
TRN	<i>Transportin 1</i>
WT	<i>Wild type</i>

# 1. Introduction

## 1.1 Amyotrophic Lateral Sclerosis

Amyotrophic lateral sclerosis (ALS) was first described by the French neurologist Jean-Martin Charcot in 1869 and is still considered as one of the most severe neurodegenerative diseases. Its characteristics are defined by a relatively selective and progressive loss of motor neurons (MN), which is mirrored by the clinical symptoms of the affected patients: The involvement of both, cortical and spinal motor neurons (sMNs) leads to characteristic symptoms such as spasticity, flaccid paralysis, muscle atrophy and fasciculations, which can occur simultaneously in different muscle groups. In general, the patients experience a progressive weakness of their voluntary muscle functions, which usually leads to death by respiratory failure about 2-5 years after disease onset (Rowland & Shneider, 2001; Zarei et al., 2015). It occurred with a constant incidence over the last decade of approximately 2.7-5/100000, which more or less equals the prevalence data due to the short survival time (Al-Chalabi & Hardiman, 2013; Hardiman et al., 2017; Kiernan et al., 2011; Mehta et al., 2018). About 70% of patients initially present with a spinal or limb onset of symptoms whereas only 25-30% have initial bulbar symptoms such as dysphagia or dysarthria resulting in shorter survival time compared to the former (Kiernan et al., 2011). On the other hand, ALS can be categorized with regards to its genetic background. In Western European ALS populations approximately 10% report a positive family history, while all other cases are considered sporadic. As a result, the term “familial ALS (fALS)” has been introduced. Mutations have been identified in more than 38 genes that are causative in a monogenetic way (Brenner & Weishaupt, 2019; Renton, Chiò, & Traynor, 2014). Homozygous and heterozygous mutations in *SOD1* were first identified to cause monogenetic ALS and account for 20% of genetic ALS cases, resulting in the establishment of several animal models, including preclinical pharmacological studies (Rosen et al., 1993). Ever since, a growing number of genes have been discovered coding for very different functional proteins. Hence, it was hypothesized that the pathophysiological pattern of ALS involves the dysfunction of a wide range of cellular pathways: Reactive oxygen species (ROS) accumulation, impaired autophagy, cellular transport defects, disbalance in RNA/DNA metabolism, mitochondrial dysfunction, impaired DNA damage response and insufficient degradation of cytoplasmatic proteins. The latter is of particular importance as it has been discovered that cytoplasmatic, ubiquitin-positive aggregates in MNs are found post mortem in all ALS patients. In more than 90% of all cases, they consist mainly of hyperphosphorylated TAR-DNA binding protein 43 (TDP-43) and have therefore become the pathohistological hallmark of sporadic and of most genetic ALS cases (Neumann et al., 2006). Thus, the discussion arose whether pathological protein aggregates *per se* might cause MN degeneration, similar to pathophysiological theories

on other neurodegenerative diseases such as Alzheimer's and Parkinson's disease (Hardy & Higgins, 1992; Spillantini et al., 1997).

Interestingly, mutations in *TARDBP* itself can cause ALS but only account for ~4% of genetic cases (Kabashi et al., 2008; Sreedharan et al., 2008). However, the most common mutation in genetic ALS is a hexanucleotide repeat expansion in *C9ORF72* (40-50%), followed by *SOD1* (20-25%), *FUS* (5%) and *TARDBP* (Ghasemi & Brown, 2018; Taylor, Brown, & Cleveland, 2016). *Fused in sarcoma (FUS)*, another gene with very similar structure and functions on the protein level as TDP-43, was found to be mutated in a few families with an abundance of ALS cases in their pedigrees in 2009 (Kwiatkowski et al., 2009; Vance, Rogelj, Hortobágyi, et al., 2009). This supports the idea of a central involvement of DNA/RNA-binding proteins in the pathology of familial and sporadic ALS, because both, FUS and TDP-43 share the nucleic acid binding capacity. However, despite the considerable efforts and success in unravelling the disease mechanisms, it is still not clear what mediates the MN degeneration, which is one reason why therapeutic options are still very limited. The established drug in the treatment of ALS, Riluzole, prolongs the survival by 2-3 months on average (Miller, Mitchell, Lyon, & Moore, 2003). There is no causal therapy because of the still existing lack of pathophysiological knowledge about disease development and of reliable disease models.

## 1.2 Fused in Sarcoma

Screening for novel therapeutic options to alleviate ALS has been challenging in the last decades. One of the complicating factors might have been the fact that most of the tested drugs resulted from research based on genetic ALS models with mutations in *SOD1* (Cudkowicz et al., 2010). It is speculative whether these models also reflect general sporadic ALS disease, considering that many other genetic variations in genes encoding for DNA/RNA-binding proteins associated with genetic ALS have been discovered in recent years. One of the affected genes is *FUS*, which is located on chromosome 16p11.2 (Kwiatkowski et al., 2009; Vance, Rogelj, Hortobágyi, et al., 2009). Because of the structural and functional similarity of FUS to TDP-43 it has been intensively studied in the last decade in the context of motoneuronal pathology, but it has been primarily described in malignant liposarcoma. Therein, fusion of *FUS* with the dominant negative transcription factor *CHOP* (C/EBP homologous protein) by chromosomal translocation was found to promote oncogenic transformation (Croizat, Aman, Mandahl, & Ron, 1993; Rabbitts, Forster, Larson, & Nathan, 1993). The *FUS* gene consists of 15 exons with a length of ~14.9 Kb. Its translated gene product contains 526 amino acids with several functional domains. The N-terminal domain comprises a Q/G/S/Y-rich region (1-165), which makes it a low complexity region also called a "prion-like-domain" (PLD) because of its

similarity to the yeast prion protein (King, Gitler, & Shorter, 2012). Furthermore, it contains an arginine-rich RNA-recognition-motif, two RGG-repeat regions, one zinc-finger motif and at the C-terminal site a non-conventional proline-tyrosine nuclear localisation sequence (PY-NLS) (Shang & Huang, 2016). Mutations in *FUS* have been detected in 1% of sporadic and up to 5% of familial cases making it the third most common genetic ALS form in Germany (Brenner & Weishaupt, 2019). Disease-relevant genetic alterations are mainly located in the C-terminal PY-NLS region of the protein resulting more frequently in a more severe disease course compared to sporadic ALS (Conte et al., 2012; Müller et al., 2018; Waibel et al., 2013), which was substantiated by the finding that *FUS* mutations are most prevalent in young onset ALS patients in Germany in general (Hübers et al., 2015). In contrast, others reported on strikingly old patients with evident *FUS* mutation (Akiyama et al., 2016; Shang & Huang, 2016) making individual disease prognosis an impossible task for the consulting physician.

As a molecular consequence of mutations in the NLS, the *FUS* protein shuttling is impaired, which impacts on the cellular localisation of the *FUS* protein and lowers its physiological nuclear abundance. Different types of NLS mutations lead to a very distinct extent of this pathological cytoplasmic shift in various cell models (Bosco et al., 2010; Dormann et al., 2010; Vance, Rogelj, Hortobágyi, et al., 2009). This has also been shown to be correlated with the clinical disease onset (Dormann et al., 2010; Waibel et al., 2013), suggesting an influence of the cytosolic *FUS* localisation on the clinical disease severity. It remains to be demonstrated how these different mutations in the same gene affect MN biology and survival. Nonetheless, the pathological cytoplasmic distribution and aggregation of *FUS* have become the disease hallmark of *FUS*-ALS clearly separating it from TDP43-ALS forms. It has been shown that the protein mislocalization is caused by impaired nucleocytoplasmic shuttling via at least two main pathways. First, it was found that the Transportin 1 (TRN)/Karyopherin-beta-2 mediated nuclear import of *FUS* across the nuclear pore complex is perturbed by *FUS*-NLS mutations (Dormann et al., 2010) and that its binding to TRN is modulated by arginine methylation of the RGG domain adjacent to the PY-NLS. As a consequence, cytoplasmic and methylated inclusions were found in post mortem specimens of *FUS*-ALS patients (Dormann et al., 2012). Recently, a human stem cell derived cell model of cortical neurons could reflect the same pattern in vitro (Japtok et al., 2015). Moreover, studies in mice with differently generated *FUS*-NLS mutations could reproduce the MN phenotype (Devoy et al., 2017; Scekcic-Zahirovic et al., 2017). Second, an active mechanism of exclusion from the nucleus of *FUS* was demonstrated. This involved N-terminal phosphorylation at 12 different putative serine/threonine residues followed by glutamine (S/T-Q), which was mediated by the DNA-protein kinase (DNA-PK) functioning downstream in the Non-homologous end joining (NHEJ) DNA double strand break repair pathway (Deng et al., 2014). This study offered an explanation for the phenomenon that WT-*FUS* aggregates were found in post mortem specimens of neurons in the frontal lobe in a



subset of patients with frontotemporal dementia (FTD) without germline mutations in *FUS* (Neumann et al., 2009).

Of note is that the presented genotype-phenotype correlation of impaired nucleocytoplasmic transport of *FUS* due to NLS mutations did not cover all aspects of *FUS*-ALS genetics. To a much lesser extent, mutations are also found within the N-terminal PLD or RGG domains without diminishing the nuclear presence of *FUS* (Dormann et al., 2012; Dormann et al., 2010). Recently, it has been shown that these N-terminal mutations might negatively influence the process of phase-separation (Murakami et al., 2015). This term describes the particular characteristics of some proteins to form tight molecular assemblies that change their physical properties. However, internally disordered, low complexity domains with an abundance of polar amino acids as they are found in the PLD of *FUS* are needed to fulfil this task. Tight intermolecular assembly between PLDs allows the creation of higher-order structures, which are membrane-less compartments within the cell with different physical properties reminiscent of an oil in water droplet (Murthy et al., 2019). It is currently assumed that such structures are highly advantageous for many biological processes like transcription, DNA damage repair or cellular stress response as they allow temporal and spatial control of involved proteins (Nott, Craggs, & Baldwin, 2016). However, this process might also give rise to the formation of pathological protein aggregates in neurons in case disassembly is impaired or the corresponding stress does not disappear (King et al., 2012). Therefore, the theory of PLD/phase separation has become an emerging research area in the field of neurodegenerative diseases in general.

*FUS* performs its function as a DNA/RNA binding protein and is centrally implicated in splicing regulation, stress granule formation and DNA repair (Bosco et al., 2010; Lattante, Rouleau, & Kabashi, 2013; Shang & Huang, 2016). More than 20 years ago it was demonstrated to promote homologous DNA-pairing and D-loop formation (Baechtold et al., 1999; Bertrand, Akhmedov, Delacote, Durrbach, & Lopez, 1999). However, clear evidence for an important role in the DNA damage repair process has only been found in recent years. Following oxidative DNA damage *FUS* was shown to be recruited to the DNA damage site (DDS) within seconds after the activation of Poly-[ADP-ribose]-polymerase 1 (PARP1), presumably by binding to Poly-[ADP-ribose] (PAR) chains via its RGG2 domain (Mastrocola, Kim, Trinh, Rodenkirch, & Tibbetts, 2013a; Rulten et al., 2014). The function of PARP1 is mainly explained by producing a molecular scaffold of negatively charged PAR as a posttranslational modification on itself and a variety of other proteins, thus providing the basis for efficient recruitment of factors of the DNA damage response (DDR) by chromatin modulation (Pascal, 2018). Given that PARP1 is regarded as a sensor of a variety of occurring DNA damage entities including DNA single and double-strand breaks implies a central role for *FUS* in the

early DDR (Beck, Robert, Reina-San-Martin, Schreiber, & Dantzer, 2014). Another important finding was its close relationship to the Histone Deacetylase 1 (HDAC1) in the DDR for both DNA single-strand and double-strand break repair. This was shown to be disturbed by *FUS*-NLS mutations (in that particular case, the R521C mutation), possibly by impairing chromatin dynamics or histone acetylation regulation (W. Y. Wang et al., 2013). Considering that *FUS* <sup>-/-</sup> mice and murine embryonic fibroblasts display abundant chromosomal instability and increased radiation sensitivity, underlines the importance of *FUS* in the context of DNA damage repair (Hicks et al., 2000; Kuroda et al., 2000).

### 1.3 A Human Model System for ALS

The investigation of heterozygous, *FUS* mutation-related ALS human cell models was set as the scientific perspective of this dissertation, which was realised by using the human-induced pluripotent stem-cell (hiPSC) technique as the novel gold standard of disease modelling. The hiPSC cell culture was established in 2006 for murine cells (Takahashi & Yamanaka, 2006) and 2007 for human cells (Takahashi et al., 2007) and has been reproduced and applied in a wide variety of different biochemical experiments and scientific work. Disease modelling has become one key adaptation of this technique because it offers the unique opportunity to potentially create any cell type of the human body derived from stem cell status without the necessity to perform hazardous biopsies, thus enabling for the first time ever the *in-vitro* cultivation and investigation of living human patient-derived MN. It also circumvents major ethical objections to the use of human embryonic stem cells.

The procedure of reprogramming was performed on patient cells that had been collected by skin biopsy prior to the presented work. Only ALS patients with evident heterozygous mutations in *FUS* detected by Sanger sequencing/next-generation sequencing were selected. Furthermore, healthy adult individuals were randomly selected to provide age- and gender-matched controls. Genetic testing was performed on them, and they were only included if this was negative for mutations in the four main ALS genes *C9ORF72*, *SOD1*, *FUS*, and *TDP43*. Moreover, no objections are given regarding the pathogenicity of the individual mutations as is the case with non-human or non-neurological models when artificially introducing the genetic modification.

To optimize the control conditions, an isogenic cell pair was generated using the CRISPR-Cas9n technique on an hiPSC line derived from a *FUS*-NLS patient with an R521C mutation. The original mutation was removed and either a new pathogenic P525L mutation or the physiological information for arginine was included at the locus 521. In both cell lines, a 9bp-linking DNA sequence was added after the C-terminal end, extended by a GFP tag to facilitate

the imaging of living cells. The correct genotype for both cell lines was confirmed by PCR, which revealed the heterozygous presence of either FUS-WT-GFP or FUS-P525L-GFP and endogenous FUS-WT, respectively.

However, it is important to note that the cells generated by the above steps were provided for the scientific work of this dissertation, but their creation was not part of this work.

## **2. Aims of the thesis**

The scientific perspectives of this dissertation were defined as follows: The initial aim was to establish a patient-derived human neuronal cell model of *FUS*-associated ALS in order to gain new pathophysiological insights into the still elusive disease mechanisms of spinal motor neuron demise. Importantly, in order to pursue in-depth biomolecular studies using this model system, it was primarily necessary to validate it by comparison with existing non-human models. Subsequently, hypothesis-driven assessments of pathophysiological changes were performed by comparing with WT control cells, which included therapeutic drug testing. Finally, the aim was to clinically translate the previously obtained results by extrapolating the biomolecular data to the *FUS*-ALS patient characteristics.

### 3. Results

#### 3.1 Establishment of an In-Vitro Patient-Derived Cell Model of FUS-ALS to Investigate Pathological Pathways of Motor Neuron Degeneration

The following sections refer to the first publication on which this dissertation is based:

**Naumann M**, Pal A, Goswami A, Lojewski X, Japtok J, Vehlow A, Naujock M, Günther R, Jin M, Stanslawski N, Reinhardt P, Sternecker J, Frickenhaus M, Pan-Montojo F, Storkebaum E, Poser I, Freischmidt A, Weishaupt JH, Holzmann K, Troost D, Ludolph AC, Boeckers TM, Liebau S, Petri S, Cordes N, Hyman A, Wegner F, Grill S, Weis J, Storch A, Hermann A. Impaired DNA damage response signaling by FUS-NLS mutations leads to neurodegeneration and aggregation formation. *Nature Communications* (2018), 9:335. DOI: 10.1038/s41467-017-02299-1

The first important step was the stable establishment of the sMN culture in our laboratory relying on the original protocol of *Reinhardt et al. 2013*. The basis for this procedure was the cell culture of neuronal progenitor cells, which were derived from patient-specific and control hiPSCs from healthy donors. A total of 5 cell lines from 3 FUS-ALS patients, 4 control cell lines, and the isogenic pair generated by CRISPR-Cas9n were included in the project (Table 1, Naumann & Pal et al. 2018).

The original *Reinhardt* protocol described the fast and efficient differentiation of NPC, which served as a resource for the production of sMNs (Reinhardt et al., 2013). This was facilitated by a differentiation step with pumorphamine, a sonic hedgehog agonist, and retinoic acid. Thereafter, neuronal maturation was required by adding neurotrophic factors. In between, it was possible to split the cells, which had the advantage that other cell culture application formats could be defined for different experimental approaches with NPCs in patterning. Moreover, to a certain extent it allowed a purification of matured neurons. The detailed protocol is shown in Figure 1a (Naumann & Pal et al. 2018). It was possible to keep the cells in this maturation medium for over 100 days.

Importantly, the neurons were positive for a range of specific markers of neuronal development. First, the neural progenitor cells showed immunocytochemical (ICC) staining for SOX2 and Nestin. In the same way, Hb9 (Homeobox gene 9) and Islet1 (Figure 1e; Naumann & Pal et al. 2018), which are early sMN markers, could be detected in differentiation after a few days. Prolonged cultivation with selected growth factors finally yielded mature sMNs as indicated by positive staining for Map2, Beta-III-Tubulin, and SMI32 (Figure 1b, Naumann & Pal et al 2018). Furthermore, all SMI32-positive neurons were co-stained for the enzyme choline acetyltransferase (ChAt), proving that the culture produced contained spinal MN, in contrast to cortical MN, which lack this protein. It is important to note that due to the absence

of a GFAP-ICC signal, no glial cells were detectable and that approximately 50% of all neurons were positive for specific MN markers.

Fourteen days after the start of differentiation, no clear difference was detectable between mutant and control cells regarding the ratio of sMNs over all neurons. The same was evident for the rate of spontaneous necrotic cell death observed in the staining for propidium iodide and Hoechst arguing against an early loss of MN. At that time, the cellular localisation of the FUS protein, which is known to be shifted into the cytoplasm in other FUS-ALS disease models, was normal in the *FUS* mutated neurons with the R521C or R521L amino acid change. However, extended culturing over a longer time span revealed the spontaneous appearance of FUS-immunoreactive dots in the cytoplasm and axons exclusively of mutated sMNs. This indicated a gradual development of pathological changes, which is perfectly consistent with the nature of a neurodegenerative disease.

A disadvantage of the established cell culture was its heterogeneous structure, which made it difficult to delineate anatomical changes during the expected disease progress. The cell bodies and large axons formed a complex network that made it impossible to adequately assess axon retraction or integrity. Therefore, a system was designed that ensured the directed growth of axons in a cell culture dish. This was realised by applying the microfluidic chamber (MFC) technique, which allowed the integration of small silicon chambers into the cell culture system, which required a special surface coating procedure in order to ensure MFC adherence with a given coating. The background was that the neurons in patterning were detached from their original culture plate and re-seeded into one side of the chamber system. However, the neuronal cell bodies were too large to grow within the microfluidic channels that connected one so-called main channel to the other. Only axons were capable of penetrating in this way, resulting in selective axonal sprouting at the exit site of the microchannels. In order to improve the rate of axonal sprouting, a growth factor gradient in favour of the exit site was designed serving as a guidance stimulus. By using a defined length of microchannels, contamination with dendrites was prevented, which allowed selective observation of different axonal compartments of the sMNs. Subsequent ICC within the MFC dish confirmed this by an exclusively positive signal for axonal proteins in the distal compartment (Figure 2 a,b; Naumann & Pal et al. 2018). Since its establishment in conjunction with primary neuronal mouse culture this was the first time the technique has been used for a human neuronal cell culture. Importantly, the application of the MFC technique facilitated the assessment of a purified axonal culture for more focussed experiments with sMN axons as the presumed mainly affected cellular compartment in ALS pathology.

## 3.2 Application of the Established Model System for Pathophysiological Studies

### 3.2.1 Axonopathy and “Dying-Back” pathology is the prominent phenotype in FUS-ALS

The following sections refer to:

**Naumann M**, Pal A, Goswami A, Lojewski X, Japtok J, Vehlow A, Naujock M, Günther R, Jin M, Stanslawski N, Reinhardt P, Sternecker J, Frickenhaus M, Pan-Montojo F, Storkebaum E, Poser I, Freischmidt A, Weishaupt JH, Holzmann K, Troost D, Ludolph AC, Boeckers TM, Liebau S, Petri S, Cordes N, Hyman A, Wegner F, Grill S, Weis J, Storch A, Hermann A. Impaired DNA damage response signaling by FUS-NLS mutations leads to neurodegeneration and aggregation formation. *Nature Communications* (2018), 9:335. DOI: 10.1038/s41467-017-02299-1

Pal A, Glaß H, **Naumann M**, Kreiter N, Japtok J, Sczech R, Hermann A. High content organelle trafficking enables disease state profiling as powerful tool for disease modelling. *Sci Data*. 2018 Nov 13;5:180241.

Remarkably, within the MFC dish time lapse assessment over several weeks revealed a continuous retraction of primarily well-grown axons from mutated neurons in comparison to controls, which were also characterized by axonal swellings and later axonal fragmentation. However, it was much later that significant neuronal cell loss was detected in conjunction with increased cleaved caspase 3 signal suggesting a primary event leading to axonal degeneration and secondary cell body demise (Figure 2c-I; Naumann & Pal et al. 2018).

It was therefore asked whether functional impairments of the axons occurred prior to structural changes. Indeed, axonal transport deficits have been discussed earlier as a theory for the pathogenesis of ALS (De Vos & Hafezparast, 2017). A convenient way to monitor such features was the live-cell microscopy of transported organelles like mitochondria or lysosomes. Fluorescent dyes (MitoTracker™/ LysoTracker™) are available for both, which enable quick and easy fluorescence staining with low toxicity.

Similar to the previously demonstrated temporal change in pathological features, a gradual loss of mitochondria and lysosomes and a virtual standstill in distal axons was observed in *FUS*-mutated sMNs (Figure 4a; Naumann & Pal et al. 2018). These results were already detectable on day *in-vitro* (DIV) 21, but organelle size and movement were normal on DIV 9. It is important that the findings occurred before any structural changes in the axons could be detected. Furthermore, on closer examination, the mitochondria showed a reduced length and an abolished mitochondrial membrane potential (MMP) selectively in the distal compartment of the microchannels. The MMP was analysed separately by the special mitochondrial

fluorescent probe JC-1, which emits light of different wavelength, depending on the MMP. This observation could be made for all different *FUS* mutations, including the P525L produced by CRISPR-Cas9n, whose counterpart, the isogenic control, was unremarkable. Importantly, the readout was semiautomated, which allowed the high-content assessment and quantification of a large number of organelle features beyond size and count. In this way, specific signatures of combined characteristics for different cell lines could be established, e.g. enabling high-throughput drug screening (Pal et al., 2018).

Together with the axonal retraction, these results also indicated a pathological involvement of the distal axons in *FUS* mutant sMNs. Neuropathological examinations of *FUS*-ALS patient material conducted by cooperation partners were in line with these findings and showed a denervated and severely degenerated skeletal musculature with a less pronounced loss of alpha-motor neuron cell soma, which suggested a primary axonopathy (Figure 3; Naumann & Pal et al. 2018).

### **3.2.2 Increased DNA damage is seen in *FUS*-ALS sMNs and induction of DNA damage mimics *FUS*-ALS distal axonopathy**

The following sections refer to parts of:

**Naumann M**, Pal A, Goswami A, Lojewski X, Japtok J, Vehlow A, Naujock M, Günther R, Jin M, Stanslowski N, Reinhardt P, Sternecker J, Frickenhaus M, Pan-Montojo F, Storkebaum E, Poser I, Freischmidt A, Weishaupt JH, Holzmann K, Troost D, Ludolph AC, Boeckers TM, Liebau S, Petri S, Cordes N, Hyman A, Wegner F, Grill S, Weis J, Storch A, Hermann A. Impaired DNA damage response signaling by *FUS*-NLS mutations leads to neurodegeneration and aggregation formation. *Nature Communications* (2018), 9:335. DOI: 10.1038/s41467-017-02299-1

Based on the initially stated important role of *FUS* in relation to the DDR, the hypothesis was made that *FUS* mutations might play a role in this setting, as previously demonstrated in murine neurons (W. Y. Wang et al., 2013) and that this might be related to the axonal phenotype. ICC staining of histone gamma-H2A.X phosphorylated by kinases such as Ataxia telangiectasia mutated protein kinase (ATM) or DNA-PK on Serine-139 as part of the DNA damage response pathway has been widely used for the quantitative assessment of DNA double-strand break (DSB) foci. As a control, 53BP1 was labelled in the same way, which is another protein in the DSB repair cascade and showed a similar localisation as gamma-H2A.X (Figure 5a, b, g; Naumann & Pal et al. 2018).



An increased signal and an increased amount of gamma-H2A.X dots could already be detected in NPC with different *FUS*-mutations compared to controls. The same was true for sMN DIV 14, which implied a generally elevated DDR as an early key element of *FUS*-mediated pathology. Etoposide was used as a positive control, which promoted the production of DSBs due to abortive transcription by irreversible binding and inhibition of the topoisomerase II. In fact, etoposide also significantly increased the gamma-H2A.X signal in the controls (Figure 5a-g; Naumann & Pal et al. 2018). Next, the hypothesis was put forward that the DNA damage itself is sufficient to cause axonal demise in MN. For this, etoposide was selectively added to the proximal compartment of the MFC (=soma side) containing healthy donor-derived sMNs. In fact, a pattern very similar to the results of *FUS* mutant sMNs was observed, including a lack of organelle movement and loss of MMP in distal axons, suggesting nucleo-axonal crosstalk (Figure 5h; Naumann & Pal et al. 2018). This implied DNA damage as an upstream event in the lethal cascade of *FUS*-ALS, which is why this pathway was studied in more detail.

### 3.2.3 Effect of *FUS*-NLS mutations on DNA repair mechanisms in patient-derived cells.

The following sections refer to parts of:

**Naumann M**, Pal A, Goswami A, Lojewski X, Japtok J, Vehlow A, Naujock M, Günther R, Jin M, Stanslawski N, Reinhardt P, Sternecker J, Frickenhaus M, Pan-Montojo F, Storkebaum E, Poser I, Freischmidt A, Weishaupt JH, Holzmann K, Troost D, Ludolph AC, Boeckers TM, Liebau S, Petri S, Cordes N, Hyman A, Wegner F, Grill S, Weis J, Storch A, Hermann A. Impaired DNA damage response signaling by *FUS*-NLS mutations leads to neurodegeneration and aggregation formation. *Nature Communications* (2018), 9:335. DOI: 10.1038/s41467-017-02299-1

Martinez-Macias MI, Moore DA, Green RL, Gomez-Herreros F, **Naumann M**, Hermann A, Van Damme P, Hafezparast M, Caldecott KW. *FUS* (fused in sarcoma) is a component of the cellular response to topoisomerase I-induced DNA breakage and transcriptional stress. *Life Sci Alliance*. 2019 Feb 26;2(2).

Since the repair of DNA damage is a fast and strictly regulated process, a different approach was needed to monitor rapid changes in neurons. It has been shown previously that *FUS* is rapidly recruited within seconds to the site of DNA damage induced by UV laser irradiation (Mastrocola, Kim, Trinh, Rodenkirch, & Tibbetts, 2013b; Rulten et al., 2014). Using a very similar laser ablation microscope as described in the publications mentioned above, these results could be confirmed for human *FUS*-GFP hiPSC-derived sMNs (Figure 6a; Naumann & Pal et al. 2018). UV laser irradiation through a laser ablation microscope with a spinning disc

module allowed the precise induction of spatially and temporally controlled DNA damage, although it was not possible to clearly distinguish between different qualities of DNA damage. The human FUS-WT-GFP was recruited to the DNA damage site (DDS) within seconds, which was not the case with the FUS-P525L-GFP variant in the mutated cell line. Most of the FUS-P525L-GFP signal was detected outside the nucleus, suggesting a redistribution problem to be causative for the aborted DDS recruitment (Figure 6a; Naumann & Pal et al. 2018). Therefore, experimental conditions were necessary to intervene in the relevant DDR pathways FUS is involved in in order to gradually reflect the pathological changes. It has been shown that FUS is recruited secondarily to the activity of PARP1 (Rulten et al., 2014). The addition of an inhibitor of PARP to the control cell lines confirmed these findings in human sMNs. Not only a complete loss of FUS-WT-GFP recruitment was observed but also a shift of the FUS-WT-GFP into the cytoplasm. On the other hand, blocking the activity of the main PAR-cleaving enzyme poly (ADP-ribose) glycohydrolase (PARG) with a selective inhibitor resulted in a partial redistribution of FUS-P525L-GFP into the nucleus in the mutated cells. This was accompanied by an improvement in the recruitment to the DDS in the mutated cells. Inhibition of DNA-PK activity with a selective inhibitor similarly caused a redistribution into the nucleus of FUS-P525L-GFP and restored its recruitment at DNA damage sites (Figure 6c, e; Naumann & Pal et al. 2018). In accordance with these results, the treatment of control cells with etoposide led to a shift of nuclear FUS-WT-GFP into the cytoplasm, probably due to the DNA-PK activity induced by the DNA damage occurring. However, the observation was different from that for the use of the PARP inhibitor (Figure 7; Naumann & Pal et al. 2018). Etoposide needed several hours to change the balance of FUS in favour of the cytoplasm, and only then FUS-WT-GFP could no longer be recruited to the irradiated DDS. In contrast, PARP inhibition primarily inhibited the DDS recruitment and later led to a cytoplasmic shift of FUS-WT-GFP. Importantly, double treatment experiments with DNA-PK inhibition and either PARP inhibitor or etoposide revealed the preservation of nuclear FUS-WT-GFP in both mutant and control cell lines when incubated primarily with the DNA-PK inhibiting factor.

Furthermore, the mechanism presented in the last section also had an influence on the axonal integrity of the treated neurons. It was hypothesized that the functional conservation of the mutant FUS-P525L-GFP in the nucleus could also have an influence on the axonal phenotype previously observed in this work and, on the contrary, if the same could be reproduced when abrogating FUS-WT-GFP in the nucleus. In fact, both etoposide and PARP inhibition treatment in the proximal compartment of MFCs led to a stillstand of lysosomes and mitochondria and loss of the MMP in distal axons of WT sMNs (Figure 6g; Naumann & Pal et al. 2018). On the other hand, in the *FUS* mutated sMNs, this phenotype could be prevented by the addition of the PARG1 or DNA-PK inhibitors to the proximal site of the MFCs, resulting in a condition indistinguishable from the WT control.

In summary, the presented results provide evidence for a novel pathomechanism in mutated *FUS* neurons: a primary nuclear dysfunction of FUS due to reduced nuclear import as a result of ALS-associated NLS mutations leads to a secondary distal axonopathy and a progressive axonal retraction. Furthermore, the aggregate formation of cytoplasmic FUS could be modulated by intervening in the important DDR pathways in both FUS-WT and FUS-P525L, suggesting that this is a downstream event.

In addition to this work, the role of FUS in transcription-associated DNA damage was investigated, which was done in collaboration with the laboratory of Prof. Dr. Keith Caldecott (Martinez-Macias et al., 2019). In particular, transcription-associated stress is a major source of DNA damage in neurons, considering their high transcriptional activity (McKinnon, 2017), and FUS was previously implicated in the repair of transcription-associated DNA damage (Hill et al., 2016). The arrest of mRNA transcription either by direct inhibition of RNA Pol II or by inhibition of the topoisomerase I, which produced transcription-associated SSB, led to a shift of FUS from the transcription site to the nucleolus, irrespective of its usual dependence on PAR production. This process was not abrogated by the presence of FUS-P525L-GFP. However, fibroblasts from patients with various *FUS-NLS* mutations, including the P525L amino acid alteration, showed a reduced survival when exposed to topoisomerase I inhibition compared to control cells.

ARTICLE

DOI: 10.1038/s41467-017-02299-1

OPEN

# Impaired DNA damage response signaling by FUS-NLS mutations leads to neurodegeneration and FUS aggregate formation

Marcel Naumann<sup>1</sup>, Arun Pal<sup>1</sup>, Anand Goswami<sup>2</sup>, Xenia Lojewski<sup>1</sup>, Julia Japtok<sup>1</sup>, Anne Vehlow<sup>3,4,5</sup>, Maximilian Naujock<sup>6,21</sup>, René Günther<sup>1</sup>, Mengmeng Jin<sup>1</sup>, Nancy Stanslowsky<sup>6</sup>, Peter Reinhardt<sup>7,22</sup>, Jared Sternecker<sup>7</sup>, Marie Frickenhaus<sup>8,9</sup>, Francisco Pan-Montojo<sup>10</sup>, Erik Storkebaum<sup>8,9,23</sup>, Ina Poser<sup>11</sup>, Axel Freischmidt<sup>12</sup>, Jochen H. Weishaupt<sup>12</sup>, Karlheinz Holzmann<sup>13</sup>, Dirk Troost<sup>14</sup>, Albert C. Ludolph<sup>12</sup>, Tobias M. Boeckers<sup>15</sup>, Stefan Liebau<sup>16</sup>, Susanne Petri<sup>6</sup>, Nils Cordes<sup>3,4,5,17</sup>, Anthony A. Hyman<sup>11</sup>, Florian Wegner<sup>6</sup>, Stephan W. Grill<sup>11,18</sup>, Joachim Weis<sup>2</sup>, Alexander Storch<sup>1,7,19,20</sup> & Andreas Hermann<sup>1,7,19</sup>

Amyotrophic lateral sclerosis (ALS) is the most frequent motor neuron disease. Cytoplasmic fused in sarcoma (FUS) aggregates are pathological hallmarks of FUS-ALS. Proper shuttling between the nucleus and cytoplasm is essential for physiological cell function. However, the initial event in the pathophysiology of FUS-ALS remains enigmatic. Using human induced pluripotent stem cell (hiPSCs)-derived motor neurons (MNs), we show that impairment of poly(ADP-ribose) polymerase (PARP)-dependent DNA damage response (DDR) signaling due to mutations in the FUS nuclear localization sequence (NLS) induces additional cytoplasmic FUS mislocalization which in turn results in neurodegeneration and FUS aggregate formation. Our work suggests that a key pathophysiologic event in ALS is upstream of aggregate formation. Targeting DDR signaling could lead to novel therapeutic routes for ameliorating ALS.

<sup>1</sup> Department of Neurology, Technische Universität Dresden, 01307 Dresden, Germany. <sup>2</sup> Institute of Neuropathology, RWTH Aachen University Hospital, Pauwelsstrasse-30, 52074 Aachen, Germany. <sup>3</sup> OncoRay—National Center for Radiation Research in Oncology, Faculty of Medicine and University Hospital Carl Gustav Carus, Technische Universität Dresden, Helmholtz-Zentrum Dresden-Rossendorf, Dresden 01307, Germany. <sup>4</sup> German Cancer Consortium (DKTK), partner site Dresden, and German Cancer Research Center (DKFZ), 69192 Heidelberg, Germany. <sup>5</sup> Helmholtz-Zentrum Dresden-Rossendorf, Institute of Radiooncology—OncoRay, 01328 Dresden, Germany. <sup>6</sup> Department of Neurology, Hannover Medical School, 30625 Hannover, Germany. <sup>7</sup> Center for Regenerative Therapies Dresden (CRTD), Technische Universität Dresden, 01307 Dresden, Germany. <sup>8</sup> Molecular Neurogenetics Laboratory, Max Planck Institute for Molecular Biomedicine, 48149 Münster, Germany. <sup>9</sup> Faculty of Medicine, University of Münster, 48149 Münster, Germany. <sup>10</sup> Department of Neurology, Klinikum der Universität München, and Munich Cluster for Systems Neurology, SyNergy, 81377 Munich, Germany. <sup>11</sup> Max Planck Institute of Molecular Cell Biology and Genetics, 01307 Dresden, Germany. <sup>12</sup> Department of Neurology, University Ulm, 89081 Ulm, Germany. <sup>13</sup> Genomics-Core Facility, University Hospital Ulm, Centre for Biomedical Research, 89081 Ulm, Germany. <sup>14</sup> Division of Neuropathology, Department of Pathology, Academic Medical Centre, 1105 AZ Amsterdam, The Netherlands. <sup>15</sup> Institute of Anatomy and Cell Biology, University of Ulm, 89081 Ulm, Germany. <sup>16</sup> Institute of Neuroanatomy & Developmental Biology, Eberhard Karls University of Tübingen, 72074 Tübingen, Germany. <sup>17</sup> Department of Radiotherapy and Radiation Oncology, Faculty of Medicine and University Hospital Carl Gustav Carus, Technische Universität Dresden, 01307 Dresden, Germany. <sup>18</sup> BIOTEC, Technische Universität Dresden, 01307 Dresden, Germany. <sup>19</sup> German Center for Neurodegenerative Diseases (DZNE), Research Site Rostock, 18147 Rostock, Germany. <sup>20</sup> Department of Neurology, University of Rostock, 18147 Rostock, Germany. <sup>21</sup> Present address: CNS Research Department, Boehringer Ingelheim Pharma GmbH & Co. KG, Binger Strasse 173, 55216 Ingelheim am Rhein, Germany. <sup>22</sup> Present address: AbbVie Deutschland GmbH & Co. KG, 67061 Ludwigshafen, Germany. <sup>23</sup> Present address: Department of Molecular Neurobiology, Donders Institute for Brain, Cognition and Behaviour, Radboud University, Nijmegen, The Netherlands. Marcel Naumann and Arun Pal contributed equally to this work. Correspondence and requests for materials should be addressed to A.H. (email: [Andreas.Hermann@uniklinikum-dresden.de](mailto:Andreas.Hermann@uniklinikum-dresden.de))

**A**myotrophic lateral sclerosis (ALS) is a devastating neurodegenerative disease leading to death within 2–5 years of symptom onset. Fused in Sarcoma (FUS) is one of the most frequently mutated genes in familial ALS (fALS), being responsible for approx. 5% of fALS and up to 1% of sporadic ALS (sALS)<sup>1,2</sup> cases. Autosomal-dominant mutations within the nuclear localization signal (NLS) region of FUS are by far the most prevalent mutations and clearly pathogenic<sup>3</sup>, with the R521C and R521H point mutations being the most common<sup>2</sup>. While physiological FUS function depends on proper shuttling between the nucleus and cytoplasm, cytoplasmic FUS aggregates are a pathological hallmark of FUS-ALS.

FUS mislocalization due to nucleo-cytoplasmic shuttling<sup>4</sup> depends on two main pathways. First, Transportin (TRN)-mediated nuclear import of FUS is known to be disrupted by FUS-NLS mutations<sup>4–6</sup>. Arginine methylation of the PY-NLS domain modulates TRN binding to FUS and its nuclear import. Inhibition of arginine methylation is known to restore TRN-mediated nuclear import in FUS-NLS mutant HeLa cell culture models<sup>5</sup>. Similarly, FUS<sup>+</sup> aggregates in ALS postmortem specimens contain methylated FUS<sup>5</sup>, which was also recently reported for iPSC-derived cortical neurons<sup>7</sup>. Second, Deng and colleagues reported DNA-damage-induced FUS phosphorylation by the DNA-dependent protein kinase (DNA-PK), leading to nuclear export of FUS<sup>8</sup>.

Previous reports on human motor neuronal cell culture models of FUS-ALS showed the acquirement of typical neuropathology, such as cytoplasmic mislocalization of mutant FUS as well as appearance of FUS<sup>+</sup> cytoplasmic inclusions<sup>7,9–11</sup>. However, mechanistic insights into how these events cause neurodegeneration and about upstream events are still lacking.

FUS is physiologically involved in RNA metabolism (transcription, splicing, and export to cytoplasm) and DNA repair<sup>3</sup>. Recent data suggest a significant role in DNA damage response (DDR) downstream of poly(ADP-ribose) polymerase (PARP) not involving ATM or DNA-dependent protein kinase (DNA-PK)<sup>12–14</sup>. DNA damage is the primary activator of PAR polymerase 1 (PARP1) that catalyzes the reaction of poly(ADP-ribosylation) (for review see ref. <sup>15</sup>). Previous studies showed that FUS is rapidly recruited to DNA damage sites (DDS) in a PAR-dependent manner<sup>13,14,16</sup>. Indeed, PARP1 arrives within seconds of DNA damage followed immediately by FUS<sup>17</sup>. PAR is degraded by poly(ADP-ribose) glycohydrolase (PARG)<sup>18</sup> and PARG inhibition leads to prolonged recruitment of FUS to DDS<sup>17</sup>. In addition, an interaction of FUS and Histone deacetylase 1 (HDAC1) was reported to be diminished by FUS-NLS mutations resulting in impairment of proper DDR<sup>14,19</sup>. FUS directly interacts with PAR<sup>13</sup> and PARylation was shown to induce additional PARP1 recruitment to DDS<sup>20</sup>.

Wang and colleagues reported two FUS-NLS cases that exhibited increased DNA damage in the postmortem motor cortex<sup>14</sup>. In addition, increased levels of oxidative DNA damage were reported in the spinal cord of both sporadic and familial ALS patients<sup>21</sup>. While mice carrying FUS-NLS mutations also showed signs of increased DNA damage<sup>19</sup>, FUS<sup>-/-</sup> mice have obvious signs of genetic instability<sup>22</sup>.

Recent studies suggest that PARP is involved in forming liquid compartments of FUS at DDS, and that aberrant phase transition of the liquid compartments to solid-like aggregates could be involved in the onset of the disease<sup>17,23–25</sup>. However, the relationship between DNA damage and the formation of cytoplasmic aggregates and to neurodegeneration is unknown. Here, we (i) develop a human MN model of FUS-ALS with endogenously tagged protein, (ii) investigate DNA damage in MNs and (iii) link DDR signaling to aggregate formation and neurodegeneration. Moreover, we report a neuronopathy with distal axon

degeneration as the major phenotype of FUS-ALS prior to FUS aggregation. Furthermore, we show that inappropriate DDR signaling due to FUS-NLS mutations is a key upstream event in FUS-ALS enhancing/inducing a vicious cycle by increasing cytoplasmic FUS shuttling. This study suggests that targeting DNA damage could be a new therapeutic strategy for ALS.

## Results

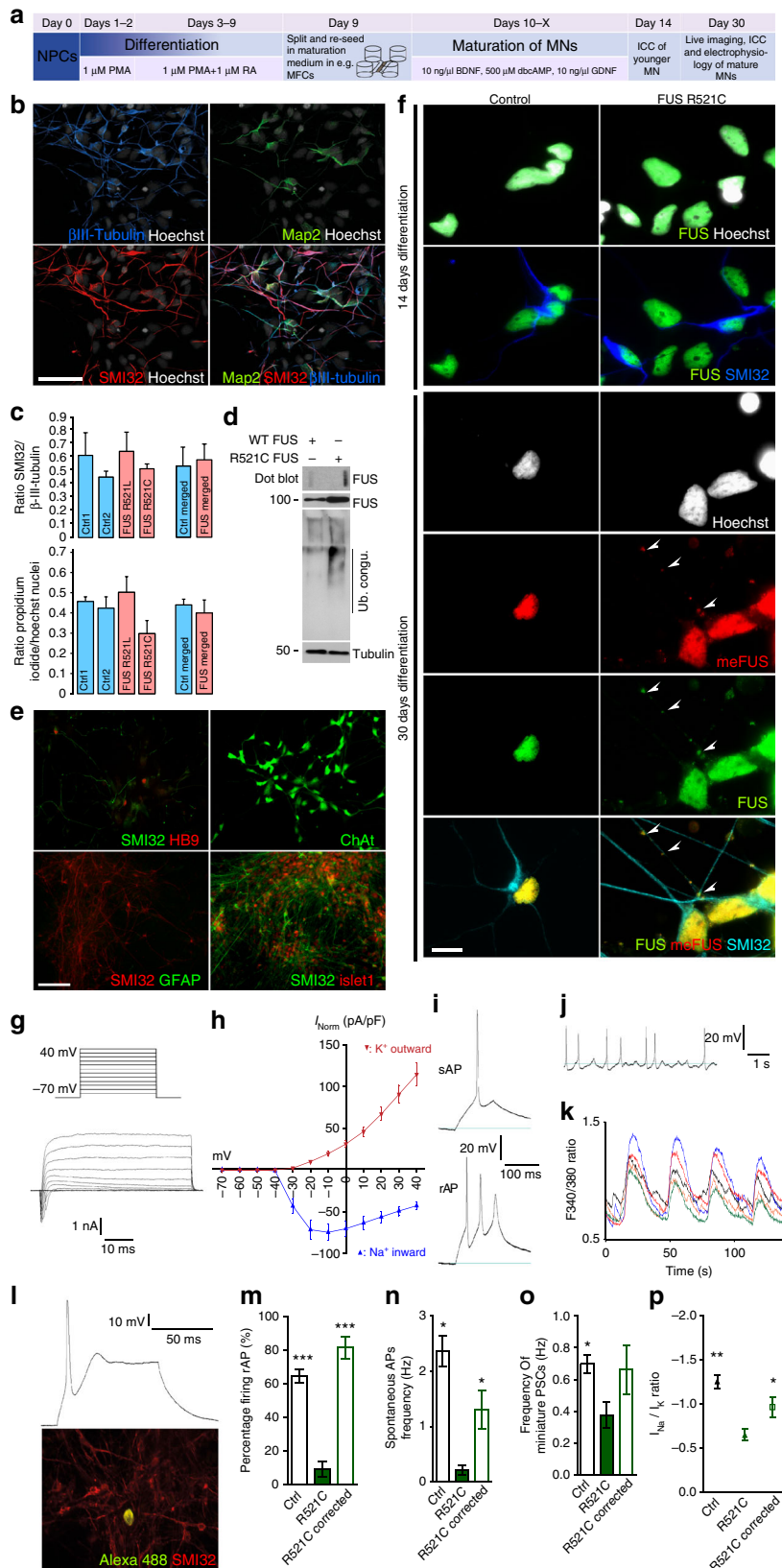
**Patient-specific FUSmt motor neurons reproduce key pathology.** To develop a human MN model of FUS-ALS, we generated human induced pluripotent stem cells (hiPSCs), by classical retroviral “Yamanaka-factor” reprogramming, from three different FUS-ALS patients carrying diverse NLS mutations (R521C, R521L, R495QfsX527; Fig. 1, Table 1). Additionally, we generated isogenic iPSC lines by CRISPR/Cas9n from one clone of the R521C hiPSC lines by generating both a wildtype and a new (P525L) mutation carrying an additional c-terminal GFP tag (Supplementary Fig. 1). We included only fully characterized hiPSC with a normal karyotype and confirmed mutations in our study (see Methods). We generated fully functional MNs and then tested for acquisition of hallmark pathology (Fig. 1a–e)<sup>26</sup>. Spinal MN differentiation yielded ≈50% MNs with no difference between healthy controls and FUS-ALS patient lines (Fig. 1c). MNs expressed typical markers for spinal MNs, including HB9, Islet, SMI32 and ChAt (Fig. 1b, e)<sup>27</sup>. We neither observed increased cell death nor pathological FUS aggregation in the early stages of MN differentiation (Fig. 1c, f). Electrophysiology revealed the presence of voltage-gated sodium and potassium channels (Fig. 1g, h, l), firing of evoked and spontaneous action potentials (Fig. 1i, j) and periodical spontaneous increases of intracellular calcium (Fig. 1k), providing evidence of neuronal function<sup>28</sup>. Interestingly, we show a hypoexcitability in FUSmt MNs that was abolished by genotype correction (Fig. 1m–p). After extended maturation (>30 days of differentiation), FUS-ALS—but not control-derived—spinal MNs increasingly showed cytoplasmic FUS translocation and spontaneous appearance of cytoplasmic FUS inclusions (Fig. 1f). Those inclusions were also positive for methylated FUS as typically seen in FUS-ALS (Fig. 1f)<sup>5,7</sup>. Immunoblot analysis of spinal MNs further confirmed Triton-x insoluble FUS aggregates (dot blot) and increased polyubiquitylation in R521C FUS MNs (Fig. 1d, Supplementary Fig. 11). Taken together, we have developed an iPSC-based human spinal MN disease model of FUS-ALS showing normal differentiation into fully functional spinal MNs with subsequent acquisition of hallmark pathology—including neuronal dysfunction and protein aggregation—during cellular aging. This model is ideal for pathophysiological studies.

**Mutant FUS predominantly affects distal axons.** To further characterize the FUSmt MNs, we focused on structural changes in the MNs during in vitro maturation and aging. MNs were observed using microfluidic chambers (MFCs) (Fig. 2a, b). There was no obvious structural phenotype after 21 days of maturation (Fig. 2c–i), but this changed during longer in vitro aging (Fig. 2c–i). First, we identified significant increased axonal swelling followed by complete loss of motor axons at the distal exit site in FUSmt only (Fig. 2c, d). Following complete degeneration of distal axons, there was still no corresponding neuron loss at the proximal MFC site until 60 DIV (Fig. 2e–g); however, there were significantly increased caspase3-positive MNs (Fig. 2j–l, Supplementary Fig. S10). This was caused by the underlying FUS mutation as isogenic lines generated using the CRISPR/Cas9n technique showed significantly higher numbers of caspase3-positive MNs in FUSmt during cellular aging (Fig. 2l,

Supplementary Fig. S10). Cultivation for additional 50 days yielded an increased MN loss in FUS mutants (Fig. 2g–i).

Consistently, human postmortem tissue from FUS-ALS patients exhibited severe atrophy of skeletal muscles and

replacement of skeletal muscle parenchyma by connective and fat tissue (Fig. 3c) indicative of almost complete loss of skeletal muscle innervation. There was also considerable but not complete loss of lumbar spinal cord  $\alpha$ -MNs with the presence of FUS



aggregates in surviving  $\alpha$ -MNs (Fig. 3a, b-, e, f), and corresponding partial degeneration of ventral root axons (Fig. 3d). These data suggest that the neurodegenerative processes predominantly, however not exclusively, affected the distal axons, consistent with the results obtained with our in vitro model (Fig. 2). Thus, the data presented here with our iPSC-derived MN model are in agreement with a prominent distal axonopathy combined with a less severe neuropathy in FUS ALS patients.

We next looked for early events in this neurodegenerative cascade. We performed live cell imaging of lysosomes and mitochondria between days 9–30 of maturation (Fig. 4), prior to the appearance of a structural phenotype (Fig. 2). We detected an overall reduction in organelle number (data not shown). In compartmentalized MN cultures using microfluidic chambers (MFCs), we observed the appearance of an axonal phenotype in

FUS-ALS with a virtual arrest of mitochondria and lysosomes distally as opposed to normal motility proximally (Fig. 4a–i, Supplementary Movies 1–3, for detailed statistics of all box plots refer to Supplementary Tables 1–17). These axon trafficking defects were not detected in very early time points (9 DIV) but became obvious from 21 DIV onwards (Fig. 4a–c, Supplementary Movies 1 and 2). Analysis of Mitotracker JC-1—revealing the mitochondrial membrane potential—showed a loss of membrane potential only in the distal axon (Fig. 4d, g, Supplementary Movie 3) along with reduced mitochondria length (Fig. 4h), consistent with a recent report on non-neuronal cell models<sup>29</sup>. Lysosomes, however, remained normal in size (Fig. 4i). We confirmed that all control and FUS lines were phenotypically similar, thereby excluding clonal variability (Supplementary Figs. 2–9). The phenotypes were caused by the underlying FUS

**Table 1 Patient/proband characteristics**

	Sex	Age at biopsy (years)	Mutation	Age at disease onset	Clinical phenotype	Disease duration (months)	
Controls	hiPSC	Female					
		Male					
		Female					
		Female					
	Autopsies	Female					
		Male					
		Male					
		Male					
		Male					
		Male					
FUS-ALS	hiPSC	Female	R521C	57	Spinal	7	
		Isogenic control	WT-GFP				
		Isogenic mutant	P525L-GFP				
		Female	R521L	61	Spinal	60	
	Autopsies	Male	29	R495QfsX527	n.d.	Spinal	n.d.
		Male	40	R521C	n.d.	Spinal	n.d.
		Female	70	R521C	n.d.	Spinal	n.d.
		Female	35	Y526C <sup>49</sup>	n.d.	Spinal/bulbar	n.d.

n.d.: no data

**Fig. 1** Basal characterization of iPSC-derived FUS spinal MNs from ALS patients and controls. **a** Differentiation scheme of FUS and control MNs. **b** ICC of maturation markers (Map2,  $\beta$ III-Tubulin, SMI32) highlighting MNs, bar: 50  $\mu$ m. **c** Top: quantification of **(b)**, bottom: quantification of cell death in mutant FUS versus WT controls, counts of pyknotic nuclei (ratio Propidium Iodide/Hoechst),  $N = 3$ , error bars = STDEV. **d** Western blots and dot blot analysis of WT (left lane) and FUS mutant (right lane; R521C), iPSC-derived MNs. Cell lysates were either subjected to dot blot analysis for FUS aggregates (top), or immunoblot analysis and probed with antibodies against FUS, ubiquitin, and tubulin. Note the augmented ubiquitination and aggregation of FUS in FUS MNs over WT. **e** Same as **b** but for more markers to further confirm MN identity: SMI32 (Neurofilament H), Hb9 (Homeobox gene 9), Cholinacetyltransferase (ChAt), Islet1 (ISL LIM homeobox 1). No glial cells were present in this cell culture indicated by the lack of GFAP- (glial fibrillary acid protein) positive cells, bar: 100  $\mu$ m. **f** Aged FUS MNs displayed cytoplasmic, methylated FUS aggregates (white arrowheads), bar: 10  $\mu$ m. **g–p** FUS mutant iPSC-derived MNs were functional and spontaneously active. **g** Illustration of stepwise depolarization in increments of 10 mV from a holding potential of  $-70$  to 40 mV. **h** The potassium outward currents and sodium inward currents were normalized for the cell capacitance (mutant FUS cell line R521L,  $n = 21$ ). **i** Recorded in the current-clamp mode during week 7 of differentiation, a majority of mutant FUS iPSC-derived MNs fired a single action potential (sAP;  $90.7 \pm 9.3\%$ ; 19 out of 21 cells) upon stepwise depolarization or repetitive action potentials (rAP;  $32.7 \pm 4.3\%$ ; 7 out of 21 cells). **j** Mutant FUS iPSC-derived MNs ( $48.5 \pm 1.5\%$ ) were also spontaneously firing APs in varying frequencies ( $0.77 \pm 0.19$  Hz). **k** Calcium-imaging analysis revealed the periodical spontaneous rise of intracellular calcium. **l** Patch clamp recordings of MN's. After recording, cells were filled with alexa 488, then labeled with neurofilament marker SMI32 validating MN identity. **m–p** Whole-cell patch-clamp data of MN recordings from healthy control (left bars,  $N = 213$ ), mutant FUS (R521C.2, green middle bars,  $N = 24$ ) and corresponding genetically corrected isogenic control line (R521C.2 corrected, right bars,  $N = 16$ ) confirm the hypoexcitability phenotype of mutant FUS and suggest a functional recovery of the isogenic controls to healthy control level in terms of repetitive (**m**) and spontaneous APs (**n**), the frequency of post synaptic currents (PSCs) (**o**) as well as the  $\text{Na}^+/\text{K}^+$ -ratio (**p**). Data are plotted as mean, statistical comparison of healthy and isogenic control with mutant FUS using an unpaired  $t$ -test, \*, \*\*, \*\*\* $P$  values of 0.05, 0.01, and 0.001, respectively, error bars = STDEV (**c**) or SEM (**h, m–p**)



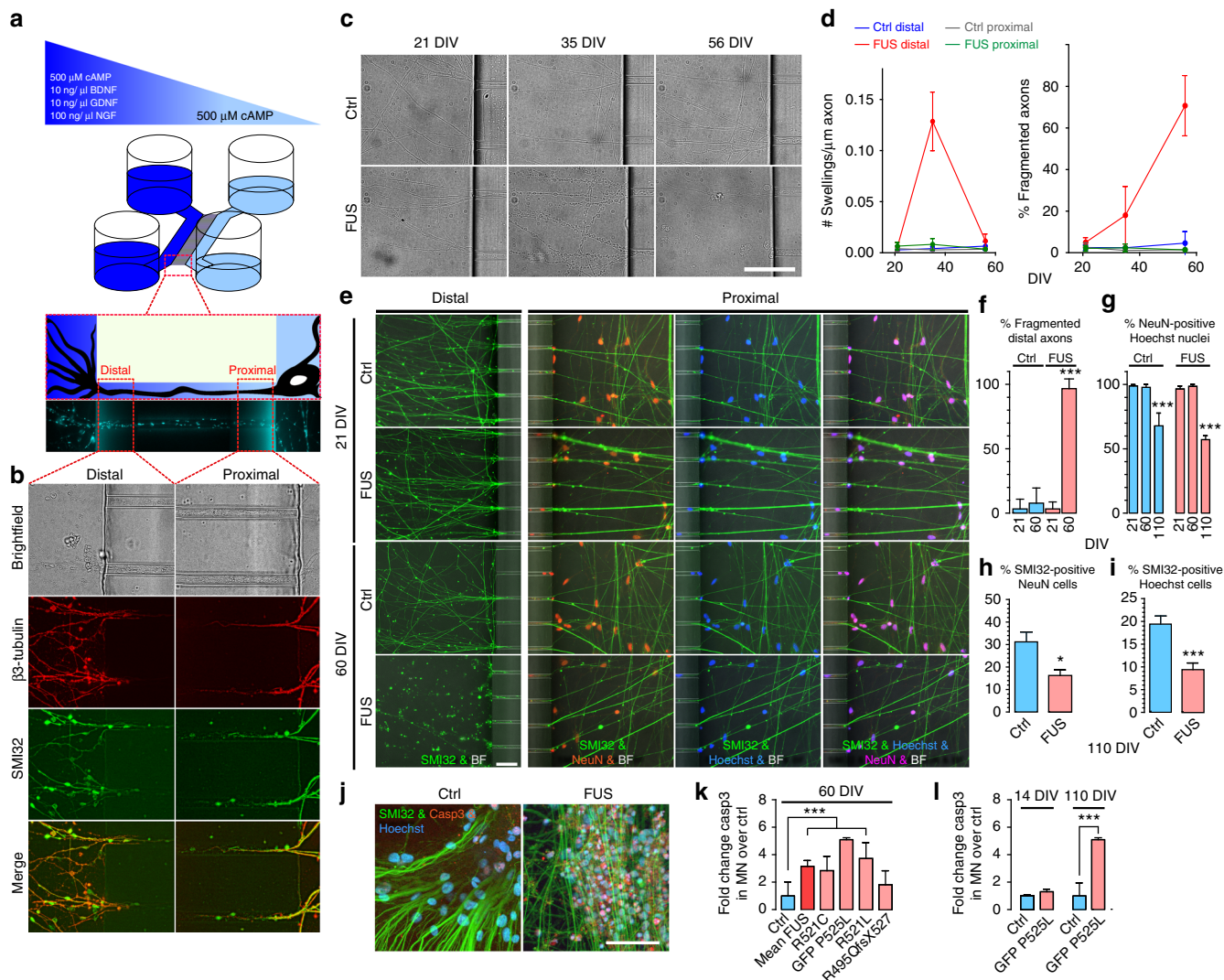


**Fig. 2** Sequential development of neurodegeneration in FUS-ALS MNs. **a** Cells were differentiated and afterwards seeded to one side (light blue). Directed growth of axons through 900  $\mu\text{m}$  long microchannels to the other side (dark blue) was realized by the application of a volume and maturation factor gradient functioning as a guidance cue. For a standardized statistical readout the “Distal” and “Proximal” Windows were defined. **b** Phase contrast and ICC of MN (representative example: Ctrl1, Table 1) cultivated in the MFCs. All grown-through axons were positive for  $\beta$ III Tubulin and SMI32, labeling them as originated from MNs, bar: 20  $\mu\text{m}$ . **c** Brightfield (BF) images acquired over aging of MN at the distal MFC exit revealed prominent axonal swelling and fragmentation beyond 21 DIV in FUS-GFP P525L as opposed to FUS-GFP WT control cells, bar: 50  $\mu\text{m}$ . **d** Quantification of **c**, left: count swellings, right: % fragmented distal axons,  $N = 10$ , error bars = STDEV. **e** IF images acquired over aging of MN at the distal exit versus proximal entry site with distal stainings for SMI32 (MN marker Neurofilament H) and proximal stainings for NeuN (neuronal nuclear marker) and Hoechst, Ctrl: FUS-GFP WT, FUS: FUS-GFP P525L. Note the complete loss of SMI32-positive distal axons (i.e. fragmentation) in FUS at 60 DIV as opposed to healthy control cells whereas the soma and network integrity remained intact at the proximal site, indicating a dying-back in FUSmts, bar: 50  $\mu\text{m}$ . **f-i** Quantification of **e** and in addition at 110 DIV, **f** distal axon integrity (% fragmented SMI32-positive axons), **g** % NeuN-positive Hoechst nuclei, **h** % SMI32-positive NeuN cells and **i** % SMI32-positive Hoechst cells,  $N = 10$ . **j** Increased apoptosis in FUS-GFP P525L MNs at 60 DIV as indicated by Caspase 3 IF staining (see Supplementary Fig. 10 for detailed gallery). **k** Quantification of **j** and all other mutant FUS MNs (see Table 1) at 60 DIV,  $N$  (ctrl) = 31,  $N$  (mean FUS) = 41,  $N$  (R521C) = 8,  $N$  (GFP-P525L) = 2,  $N$  (R521L) = 10,  $N$  (R495QfsX527) = 10, error bars = STDEV. **l** Isogenic ctrl/P525L MNs show increase of Caspase 3 MNs in the mutant line during cellular aging (14 versus 110 DIV),  $N = 8$ . All data are plotted as mean, statistics (**f-i**, **k**, **l**): one-way ANOVA with post-hoc Bonferroni test (\*, \*\*, \*\*\*P values of 0.05, 0.01, and 0.001, error bars = STDEV)

mutation as isogenic controls generated using the CRISPR/Cas9n technique presented a normal phenotype (Supplementary Fig. 1, Fig. 4e, Supplementary Movie 3).

**DNA damage causes neurodegeneration in FUS-ALS iPSC MNs.** Recent evidence suggests that DNA damage occurs in animal models of FUS<sup>19</sup> and in patients with FUS-ALS<sup>14</sup>. Therefore, we tested for the occurrence of DNA double strand

breaks (DSBs) in our hiPSC-derived FUS-ALS MN model. Immunofluorescence analysis suggested significantly increased DSBs ( $\gamma$ H2AX immunoreactivity) in FUS-ALS-derived neuronal cells (Fig. 5a–d), in fact increased DSBs were evident in both mature spinal MNs and in the neural progenitor cells (Fig. 5a–d), suggesting that these observations correspond to an early event in the FUS-ALS pathophysiology. This is strengthened by the fact that increased DSBs were already visible in MNs on DIV14 (Fig. 5b) prior to cytoplasmic FUS mislocalization (Fig. 1f). There



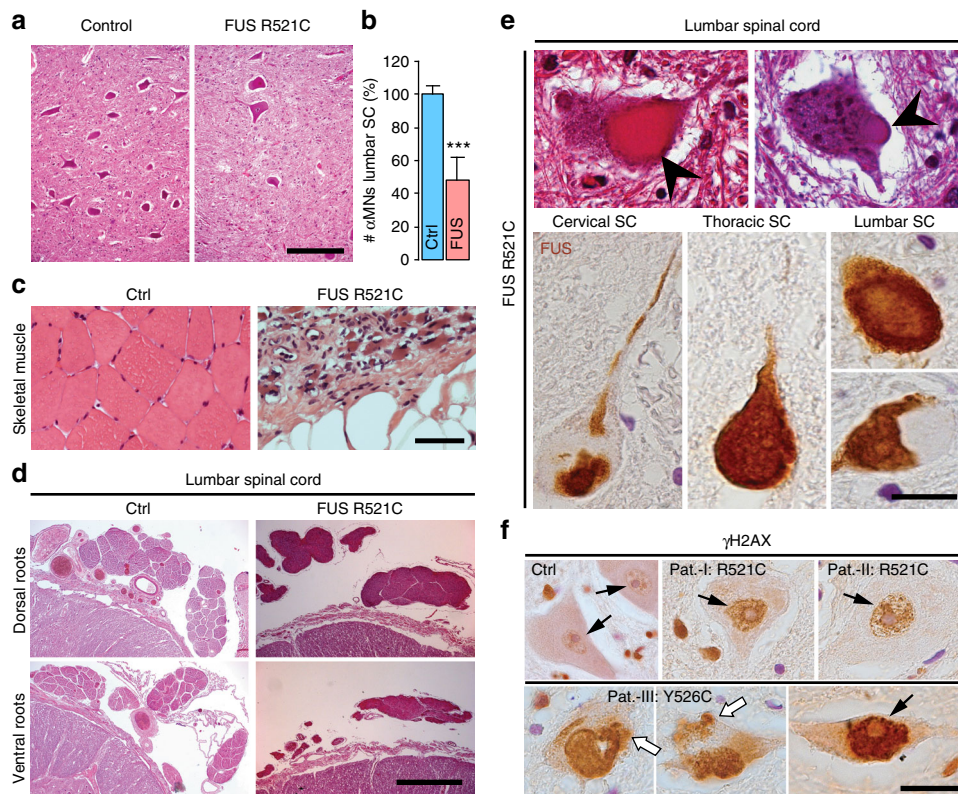


**Fig. 3** Human FUS lumbar spinal cord and skeletal muscle histology. **a** Human FUS lumbar spinal cord histology: reduced  $\alpha$ -MNs in the ventral horn, bar: 200  $\mu$ m. **b** Quantification of **a** from controls ( $n = 5$ ) compared to the FUSmTs ( $n = 4$ ) cases. Quantification done on H&E staining; 5 consecutive paraffin sections per case. Data are plotted as mean, error bars = STDEV, unpaired *t*-test (\*, \*\*, \*\*\**P* values of 0.05, 0.01, and 0.001, respectively). **c** Severe atrophy of skeletal muscles and replacement of skeletal muscle parenchyma by connective and fat tissue in FUSmTs, bar: 200  $\mu$ m. **d** Ventral versus dorsal roots atrophy, bar: 900  $\mu$ m. **e** FUS aggregates in lumbar spinal cord  $\alpha$ -MNs (arrow in upper panel), HE staining, bar: 40  $\mu$ m; lower panel, FUS-inclusions in  $\alpha$ -MNs (different spinal cord levels: cervical, thoracic, lumbar), bar: 30  $\mu$ m. **f** Representative IHC of human ALS-FUS cases with DSB marker  $\gamma$ H2AX antibody (black arrows), of lumbar spinal cord  $\alpha$ -MNs. Note the peculiar cytoplasmic staining of  $\gamma$ H2AX in one particular case (white arrows). Paraffin section, bar: 50  $\mu$ m

were significantly more DSBs in the P525L line compared to the isogenic control line (Fig. 5e). Similar to untreated conditions, DSBs were significantly increased in P525L neurons compared to isogenic controls 24 h after treating with etoposide for 1 h (Fig. 5e). Interestingly, P525L neurons were still able to repair DNA damage as shown by recovery experiments after etoposide treatment (Fig. 5e, f).

$\alpha$ -MNs of lumbar spinal cord from FUS-ALS patients (Table 1) consistently showed DNA DSBs as suggested by a robust immunoreactivity of  $\gamma$ H2AX in the nucleus (Figs. 3f and 5n, black arrows). Surprisingly, however, a few  $\alpha$ -MNs from one patient (Y526C) showed increased  $\gamma$ H2AX labeling both in the nucleus (Fig. 3f; black arrows) as well as in the cytoplasm (Fig. 3f; white arrows). Immunofluorescence analysis confirmed the aberrant co-localization of  $\gamma$ H2AX accumulations with FUS aggregates in the cytoplasm of surviving  $\alpha$ -MNs (Fig. 5o, yellow arrow) in the lumbar spinal cord of this particular patient. Taken together, our results support the notion that DNA damage is probably an early event in FUS-ALS.

We next asked whether DNA damage is the cause or consequence of FUS-ALS pathophysiology<sup>30</sup>. First, we induced DNA damage in spinal MNs derived from healthy controls. Proximal (soma site) etoposide treatment increased DNA DSBs in controls dramatically (Fig. 5b, d). In addition, this caused a loss of mitochondrial and lysosomal motility in distal axons (Fig. 5h–j, Supplementary Movies 4 and 5), a drop in mitochondrial membrane potential (Fig. 5h, k, Supplementary Movie 4) and

mitochondrial fragmentation (Fig. 5l). These effects were absent in the proximal axon parts (Supplementary Figs. 3–5, Supplementary Movies 4 and 5), thus mimicking the FUS-ALS phenotype (Fig. 4). Importantly these effects were also absent when etoposide or arsenite was added to distal axons only (Supplementary Figs. 3–5, Supplementary Movies 4 and 5). Finally, etoposide treatment of hiPSC-derived MNs leads to FUS mislocalization with the appearance of cytosolic FUS inclusions (Figs. 5b and 6e), confirming that the DNA damage is upstream of neurodegeneration and aggregate formation.

#### Impaired FUS shuttling is the upstream event in FUS-ALS.

To further substantiate the link between DDR, FUS aggregation and neurodegeneration, we investigated various aspects of DNA repair signaling in hiPSC-derived MNs (Figs. 6 and 7). At first, we asked whether NLS mutations in the *FUS* gene are sufficient to impair recruitment to DDS in patient-derived human MNs, as recently reported in heterologous (over-)expression models<sup>12–14,19</sup>. For this, we generated isogenic iPSCs with a carboxyterminal GFP tag on the endogenous FUS protein (wildtype (wt) and mutant (mt) P525L) (Supplementary Fig. 1, Table 1). Laser microirradiation caused fast and transient recruitment of FUS-GFP to DNA damage sites in wt MNs (Fig. 6a, b, Supplementary Movie 6), however, this process of FUS recruitment was diminished in FUS-NLS mutant lines (Fig. 6a, b, Supplementary Movie 6) consistent with the recently reported studies using heterologous expression in

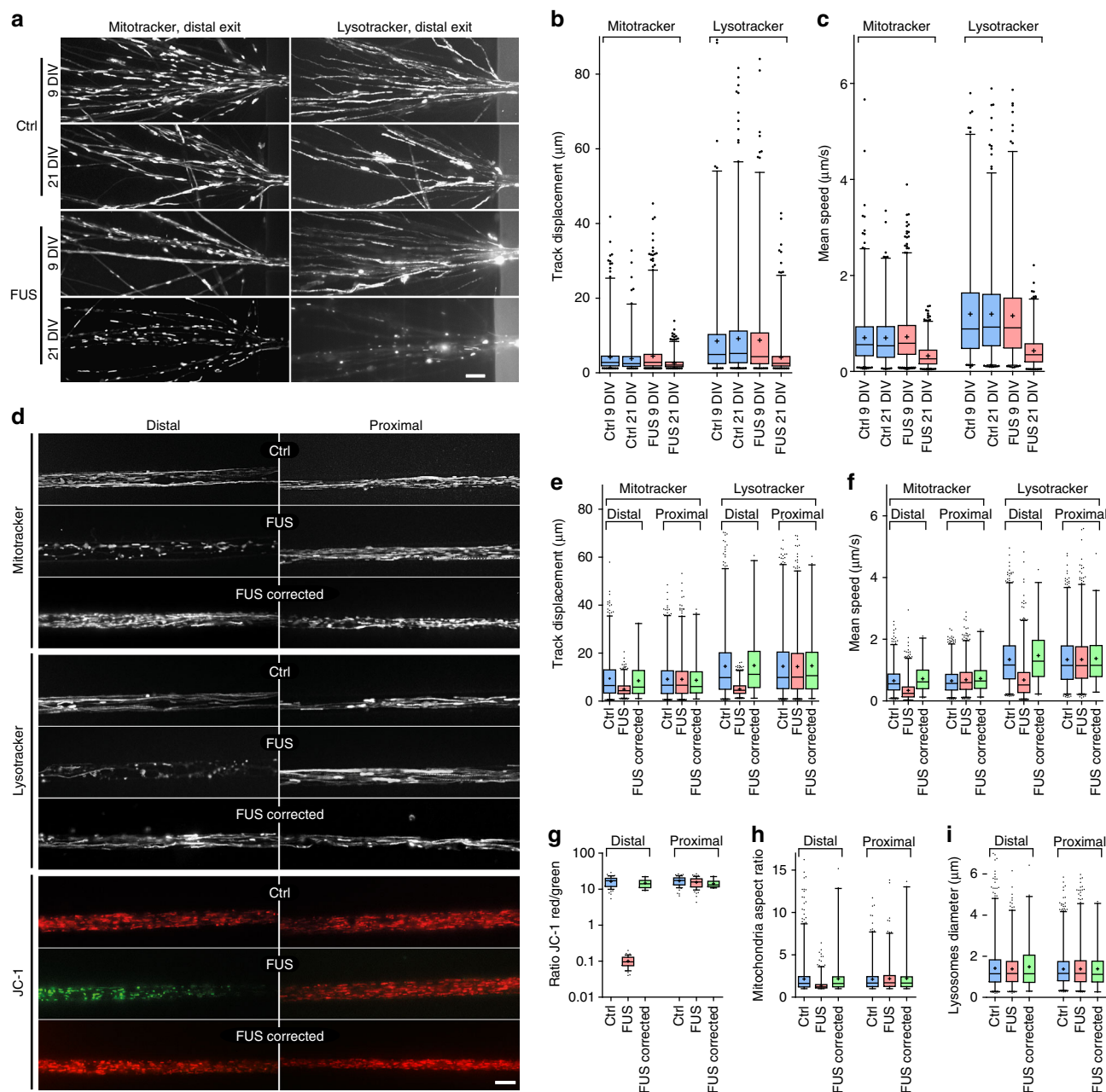


**Fig. 4** MNs develop trafficking defects of mitochondria and lysosomes over time along with loss of mitochondria function in distal axons. **a** FUS MN movies of shorter 150  $\mu\text{m}$ -MFC's at earlier maturation stage (9 DIV) versus standard endpoint time (21 DIV). Shown is the motility of mitochondria (left, Supplementary Movie 1) and lysosomes (right, Supplementary Movie 2) at the distal exit as maximum intensity projection. **b, c** Organelle tracking analysis as box plots, Ctrl: FUS-GFP WT, FUS: FUS-GFP P525L as described in Table 1. **d** FUS MN movies: distal organelle arrest and loss of mitochondrial membrane potential at 21 DIV in 900  $\mu\text{m}$ -MFC's (representative examples: Ctrl1 versus FUS R521C), bar: 10  $\mu\text{m}$  (Supplementary Movie 3). Note the rescue in isogenic FUS R521C corrected control cells. Shown is maximum intensity projection except for JC-1 movies, in which first frame of movie is shown. **e-i** Organelle tracking (**e, f**), mitochondrial membrane potential (**g**) and shape (**h, i**) analyses as box plots, batch analysis of Ctrl1-3 (Ctrl) and FUS R521C, R521L, R495QfsX527 (FUS) as described in Table 1

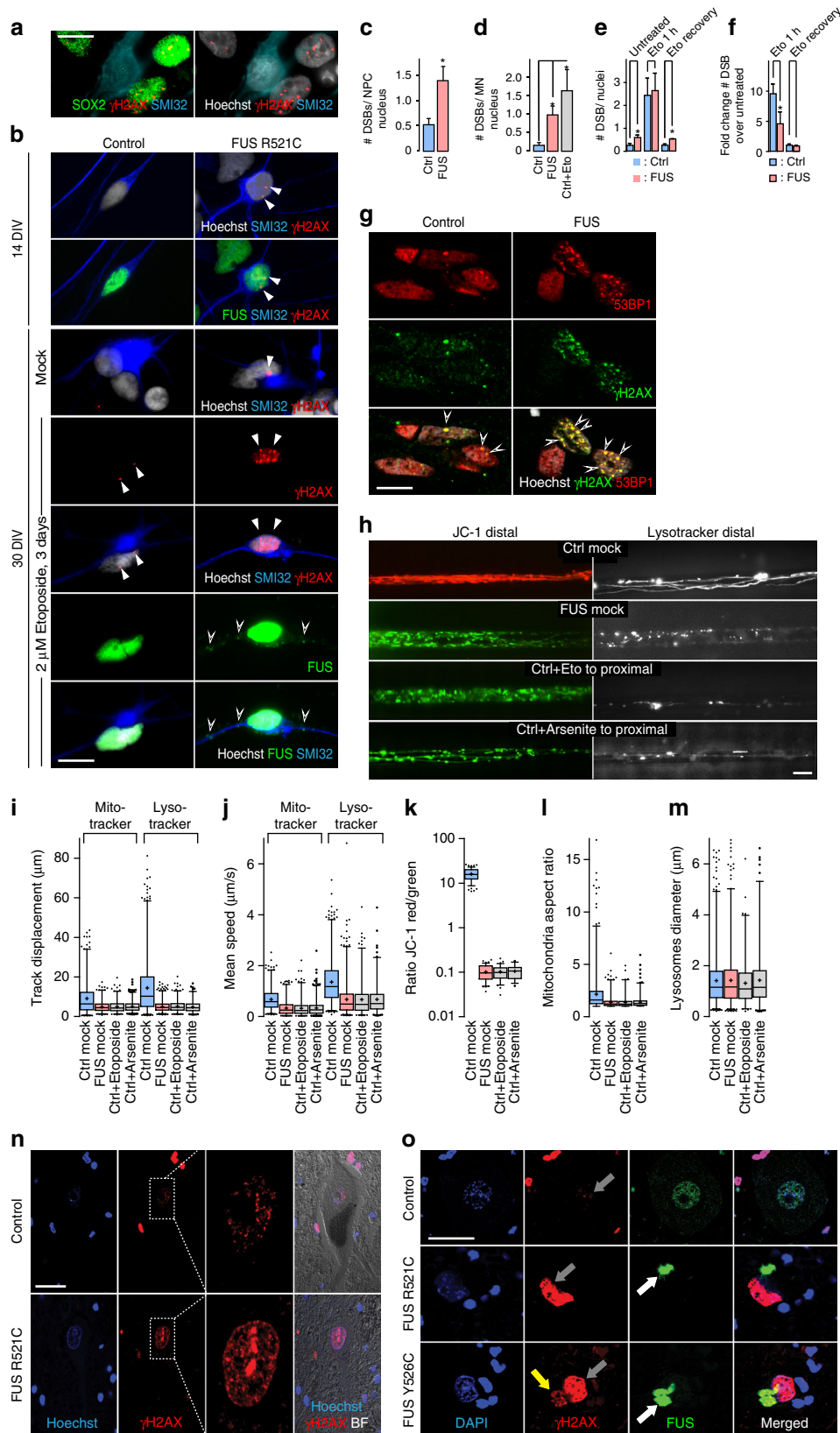
HeLa cells<sup>12,13,17</sup>, U2OS cells and murine primary neurons<sup>14</sup>. In fact, this inhibition was already observed in neural progenitor cells (NPCs) (Supplementary Movie 7), implying that this is an early upstream event. Thus, FUS-NLS mutations also impair FUS recruitment to DDS in patient-derived MNs.

We next asked whether interfering with nucleo-cytoplasmic shuttling of FUS is sufficient to impair DNA damage sensing by FUS. Earlier work has shown that FUS mislocalization depends on nucleo-cytoplasmic shuttling<sup>4</sup> which in turn depends on two main pathways: Transportin (TRN)-mediated nuclear import of

FUS, known to be disrupted in FUS-NLS mutations<sup>4-6</sup>, and DNA-PK mediated nuclear export secondary to DNA damage induction<sup>8</sup>. Arginine methylation of the PY-NLS domain modulates TRN binding to FUS and its nuclear import and inhibition of arginine methylation is known to restore TRN-mediated nuclear import in FUS-NLS mutant HeLa models<sup>5</sup>. FUS<sup>+</sup> aggregates in ALS postmortem specimens were reported to contain methylated FUS<sup>5</sup>, consistent with our iPSC-derived MNs (Fig. 1f). To test whether restoration of nuclear import of FUS can rescue its impaired recruitment to DDS, we

performed chemical inhibition of arginine methylation using adenosine-2,3-dialdehyde (AdOx)<sup>5</sup>. Indeed, AdOx rescued FUS mislocalization (Fig. 6e, f) and recruitment to DDS (Fig. 6c, d, Supplementary Movie 6), but also distal axon trafficking (Fig. 6g–l,

Supplementary Movies 8 and 9). Nuclear export of FUS depends on DNA-damage-induced FUS phosphorylation by DNA-PK<sup>8</sup>. Consistently, inhibition of DNA-PK (NU7441) also restored FUS cytosolic mislocalization (Fig. 6e, f), recruitment to DDS (Fig. 6c,





d, Supplementary Movie 6) and distal axon trafficking (Fig. 6g–l, Supplementary Movies 8 and 9). Taken together, these results provide strong evidence that impairment of nucleo-cytoplasmic shuttling is responsible for aggregate formation, the impairment of FUS-dependent DDR and neurodegeneration.

**FUS NLS pathology relies on PARP-dependent FUS-mediated DDR.** We next asked whether induction of DNA damage is sufficient to induce cytoplasmic mislocalization of FUS. Chemically inducing or increasing DNA damage by either by etoposide or arsenite (the latter known as a ROS-mediated DNA damage inducer) in untagged (Fig. 5b, d) or GFP-tagged human MNs (Fig. 6e, f) actually augmented cytoplasmic FUS mislocalization consistent with our above observations. These findings also correspond with recent data on murine cells showing an accumulation of FUS in the cytoplasm after DNA damage induction due to activation of DNA-PK<sup>8</sup>. Consistently, we also observed inhibition of FUS recruitment to DDS due to etoposide/arsenite treatment of control MNs (Fig. 6c, d, Supplementary Movie 6). PARylation is a crucial event in DNA repair. DNA damage is the primary activator of PARP1 that catalyzes the reaction of poly (ADP-ribosylation) (for review see ref. <sup>15</sup>). We thus investigated if the observed FUS NLS phenotypes rely on the PARP-dependent DDR signaling<sup>12–14,17</sup>. Indeed, PARP1 inhibition caused a reduction of FUS recruitment to DDS in control cells (Fig. 6c, d, Supplementary Movie 6) as previously reported for HeLa cells<sup>17</sup>. Furthermore, PARP1 inhibition also led to cytoplasmic FUS aggregation (Fig. 6e, f) and defects in distal axonal trafficking (Fig. 5g–l, Supplementary Movies 8 and 9), thereby faithfully mimicking FUS-NLS-mutant phenotypes.

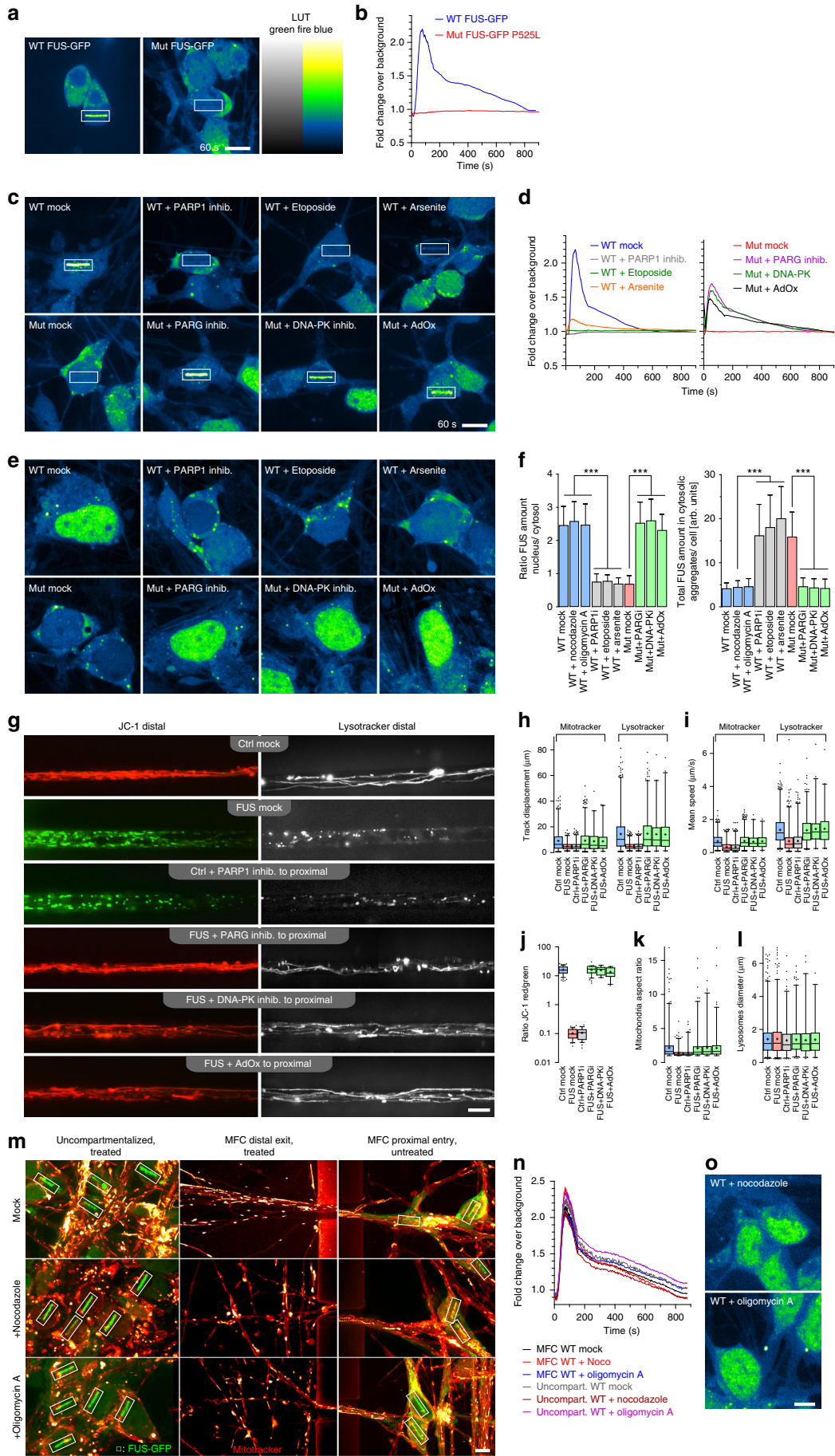
PAR is degraded by poly(ADP-ribose) glycohydrolase (PARG)<sup>18</sup> and PARG inhibition leads to prolonged persistence of FUS at DDS<sup>17</sup>. In our experimental setup, PARG inhibition restored FUS recruitment to DDS in FUSmt MN (Fig. 6c, d, Supplementary Movie 6). Moreover, PARG inhibition was sufficient to prevent FUS aggregate formation (Fig. 6e, f) and completely restored the defective distal axon trafficking phenotype (Fig. 6g–l, Supplementary Movies 8 and 9). It is unlikely that NLS mutations impair binding to PAR since the RGG domain was recently identified as being responsible for PAR binding to FUS<sup>13,25</sup>. We confirmed these findings and showed that prolonged PAR activity by PARG inhibition restored the NLS mutant phenotypes (Fig. 6g–l). These results are consistent with the idea that the FUS NLS pathophysiology actually relies on the PAR-dependent FUS-mediated DDR signaling subsequently leading to cytoplasmic FUS aggregation and neurodegeneration.

Only treatment (PARP1-, PARG inhibitor, etoposide, arsenite) at the proximal soma site, and not at the distal axon, induced or reversed the defective distal trafficking phenotype (Supplementary Figs. 3–9, Supplementary Movies 4, 5, 8 and 9). Compounds added exclusively to the proximal site cannot migrate to the distal site because the microflow in the microfluidic chambers is directed from distal to proximal (due to the higher distal liquid level, Fig. 2a and Methods). Therefore, the impact of the proximal treatments on distal axon trafficking occurred in the physical absence of these compounds, thereby excluding the possibilities of a local mode of action.

To further strengthen these observations, we tried to induce local (distal) axonal trafficking inhibition by either nocodazole (known to depolymerize microtubules) or oligomycin A treatment (complex 5 inhibitor). Both treatments caused local axonal trafficking arrest and axonal swelling (Fig. 6m, Supplementary Movies 10 and 11), but neither of them leads to deficits in FUS recruitment to DDS nor FUS cytoplasmic mislocalization and aggregation formation (Fig. 6n, o). In conclusion, the mimic/rescue of distal axonal phenotypes must be due to remote, upstream manipulation of DNA repair mechanisms, arguing against a pure axonopathy and in favor of a neuronopathy with prominent and early axonal degeneration (see also Figs. 2c–i and 4a–c) as starting point of the neurodegenerative disease process.

**DNA damage enhances FUS mislocalization and neurodegeneration.** Given that DNA damage recruits FUS and that FUS mislocalization disrupts DDR signaling, we hypothesized that FUS-NLS mutations induce a vicious cycle whereby DNA damage subsequently induces additional cytoplasmic FUS mislocalization which in turn results in aggravated DDR signaling through a consecutive loss of nuclear function. Time lapse experiments showed time-dependent cytosolic FUS mislocalization and appearance of cytoplasmic FUS inclusions after interference with DDR signaling (PARP1 inhib.) or DNA damage induction (etoposide) (Fig. 7a). While recruitment to DDS was blocked before the appearance of cytosolic FUS mislocalization by PARP1 inhibition in FUSwt MNs (Fig. 7a–c, Supplementary Movie 12), this was seen by etoposide treatment only after the appearance of cytosolic FUS mislocalization (Fig. 7a–c, Supplementary Movie 12). To further test the vicious cycle hypothesis, we performed several co-treatments. While DNA-PK inhibition or AdOX was able to restore the lack of FUS recruitment to DDS and FUS mislocalization by etoposide or arsenite (Fig. 7d, e, Supplementary Movie 13), DNA-PK inhibition did not rescue FUS recruitment to DDS during PARP1 inhibition (Fig. 7d, e) but did completely restore cytoplasmic mislocalization (Fig. 7f). This

**Fig. 5** DDR signaling is involved in FUS-NLS pathophysiology. **a** IF of SOX2 staining (green) validated NPC identity for DSB counting (by  $\gamma$ H2AX, red) in **(c)**. **b** DNA DSBs in iPSC-derived FUS R521C spinal MNs (right) versus WT control cells (Ctrl1 left, Table 1) by ICC for nuclear  $\gamma$ H2AX foci (red) at 14 and 30 DIV, bar: 10  $\mu$ m. More DSB foci (white arrowheads) were observed in FUS mutants (right) already at 14 DIV and increased in controls (left) and FUS mutants after Etoposide treatment. In addition, cytoplasmic FUS inclusions in FUS mutants increased after etoposide treatment (green, hollow arrowheads). **c, d** Both, FUS-NPCs **(c)** and mature-MNs **(d)** showed more DSBs per nucleus over controls ( $N = 3$ ). **e** Untreated mature FUS-GFP P525L (FUS) MN showed increased nuclear DSB foci over isogenic control cells, consistent with untagged FUS lines in **(d)**. 1 h etoposide treatment and 24 h withdrawal led to a similar response compared to control cells (i.e. transient increase of DSB foci and reversion to basal levels indicative of successful DSB repair). **f** Same as **e** but expressed as fold change over respective untreated control ( $N = 4$ ). Statistics **c–f**: data are plotted as mean, unpaired  $t$ -test (only **c**) or one-way ANOVA (**d–f**) with post-hoc Bonferroni test (\*, \*\*, \*\*\* $P$  values of 0.05, 0.01, and 0.001, respectively, error bars = STDEV). **g** Validation of the anti- $\gamma$ H2AX antibody in FUS-GFP P525L MNs (without etoposide) by costaining with anti-53BP1, a second marker for DSBs. Note the prominent colocalization (merge, yellow overlapping). **h** Live imaging of MN at 21 DIV shown as maximum intensity projections: distal loss of organelle motility and mitochondrial membrane potential in FUS mimicked through proximal etoposide or arsenite addition to control, bar: 10  $\mu$ m (Supplementary Movies 4, 5). **i–m** Organelle tracking **(i, j)**, mitochondrial membrane potential **(k)** and shape **(l, m)** analyses of **(h)** as box plots, batch analysis of Ctrl1–3 (Ctrl) and FUS R521C, R521L, R495QfsX527 (FUS) as described in Table 1, exception: arsenite treatment only on FUS corrected R521C (FUS-GFP WT). **n** ICC showing augmented DSBs ( $\gamma$ H2AX) in ALS-FUS case over healthy control person, bar: 20  $\mu$ m. **o** ICC showing FUS aggregation in the cytoplasm (white arrows) of a typical ALS-FUS case with R521C mutation (mid gallery row) in the NLS along with augmented  $\gamma$ H2AX occurrence in the nucleus (gray arrows) as opposed to an atypical, peculiar case (Y526C, bottom gallery row) with cytoplasmic co-aggregation of FUS and  $\gamma$ H2AX (yellow arrow), bar: 20  $\mu$ m



shows that DNA-PK is downstream of DNA damage response signaling induction. It further suggests that DNA-PK's strongest effect in FUS-ALS is the regulation of FUS nucleo-cytoplasmic shuttling<sup>8</sup>.

To gain further insights into possible downstream mechanisms in DDR by FUS we analyzed the two major pathways of DDR in postmitotic cells, namely classical non-homologous end joining (c-NHEJ) and alternative non-homologous end joining (a-NHEJ). While c-NHEJ depends on DNA-PK activation, a-NHEJ pathway is downstream of PARP1<sup>31</sup>. Within the c-NHEJ pathway, we found significant higher levels of total DNA-PK consistent with increased basal DDS in FUSmt MNs with no changes in phospho/total-DNA-PK, and no differences in KU70/KU80 (Fig. 7g, h, Supplementary Fig. 12). There was also no significant difference in the levels of a-NHEJ proteins (LIG1, PARP1) (Fig. 7g, h, Supplementary Fig. 12). DNA damage induction (etoposide) in FUSwt and FUSmt MNs resulted in a similar increase of phospho-/total DNA-PK and cleaved /full-length PARP1 ratio (Fig. 7g, i, Supplementary Fig. 12) suggesting no major disturbance of the downstream DNA damage response machinery in FUSmts (Fig. 5d, e). In turn, DNA-PK inhibition led to decreased phospho/total DNA-PK ratio but increased full length PARP1 (Fig. 7g, i, Supplementary Fig. 12), consistent with more active PARP1 in FUSmt MNs as if treated with PARG inhibition. These data underpin that DNA-PK serves mainly in FUS nucleo-cytoplasmic shuttling and that DDR mainly relies on poly(ADP-ribose) dependent a-NHEJ. In summary, we show that DNA damage is a key event in FUS-ALS which leads to DNA-PK activation. In turn, DNA-PK activation enhances cytoplasmic localization of FUS, thereby closing the vicious cycle by additionally depleting nuclear FUS, which is already the case in ALS-causing FUS-NLS mutations by impaired TRN-mediated nuclear import.

## Discussion

Using human iPSC-derived MNs and human postmortem specimens we show that FUS-ALS is caused by impairment of proper DNA damage response signaling subsequently leading to neurodegeneration and aggregate formation. Currently, there is much attention given to mechanisms of protein aggregation and to their clearance<sup>17,23,24</sup>. In contrast, our work suggests the need of novel therapeutic pathways upstream of aggregate formation involving modulation of DNA damage pathways. Some of these compounds

modulating DDR are already in clinical trials for cancer therapy and could thus rapidly be adapted to ALS.

There have been hints that DNA damage is apparent in FUS-ALS and that FUS-NLS mutations impair recruitment of FUS to DNA damage sites<sup>12</sup>, while others report only marginal<sup>13</sup> or no obvious phenotype<sup>14</sup> in DNA damage recruitment by NLS mutations. These differences most likely arise from the different cell types used in the respective studies (hiPSC-derived MNs were only used in our study) but might also be due to the technique of FUS expression (ectopic expression compared to endogenous expression, the latter used for the first time in the current study), although the expression levels were carefully controlled in the previous studies<sup>14</sup>.

Furthermore, PARP is involved in forming liquid compartments of FUS at sites of DNA damage, and aberrant phase transition of the liquid compartments to solid-like aggregates could be involved in the onset of the disease<sup>17,23,24</sup>. However, the exact relationship between DNA damage and the formation of cytoplasmic aggregates as well as neurodegeneration was lacking. Here, we show that DNA damage enhances cytoplasmic FUS mislocalization, thereby inducing a vicious cycle, in which failure of DNA damage repair signaling further enhances FUS mislocalization and induces aggregation and neurodegeneration.

Our study thus adds FUS-ALS to the class of neurodegenerative diseases with impaired DDR signaling, such as Ataxia telangiectatica, AOA1 and SCA3. Interestingly, FUS<sup>-/-</sup> mice suffer from genomic instability<sup>22</sup> and enhanced radiation sensitivity<sup>32</sup>. Whether this holds true for FUS-ALS patients is currently unknown. Furthermore, Parp1<sup>-/-</sup> mice were reported to suffer from high energy expenditure and decreased body fat mass similar to ALS patients (for review see ref. 33). This might be clinically relevant in many respects. For example, PARP1 inhibition has recently been suggested as a therapeutic strategy for neurodegenerative diseases (for review see ref. 15). In contrast, our data strongly argue against PARP1 inhibition in FUS-ALS, but suggest PARG or DNA-PK inhibition as promising treatment strategies.

Another link connecting FUS and DDR came from two reports on the interaction of FUS and HDAC1. Both reports showed that FUS directly interacted with HDAC1 and that this interaction is important for proper DDR. Consistently, FUS-NLS mutations showed a diminished interaction with HDAC1<sup>14,19</sup>. Furthermore, FUS-NLS mutant mice showed shortened dendrites at least in part due to BDNF signaling deficiency mediated by DNA damage

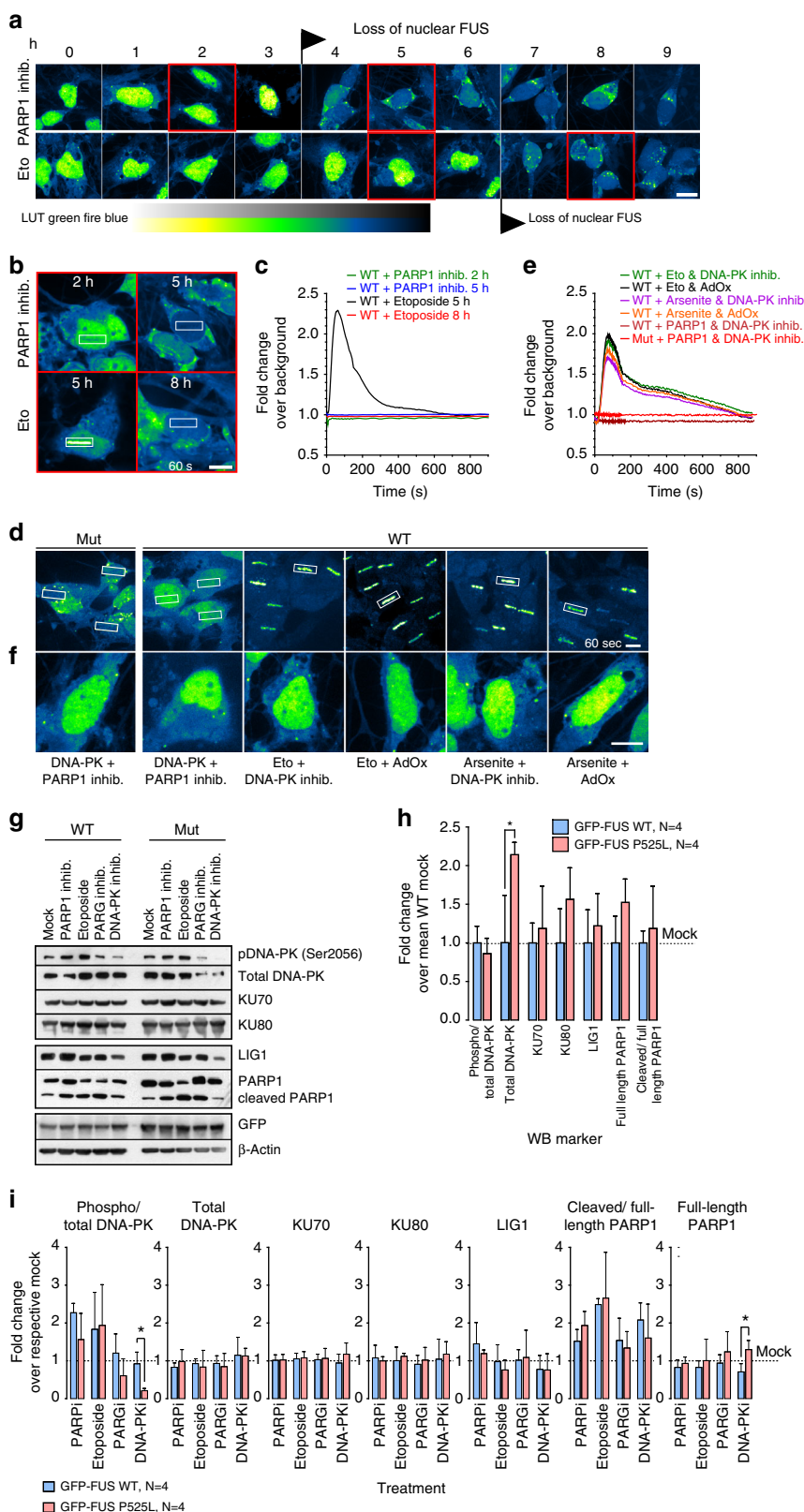
**Fig. 6** DDR signaling impairment in FUS-NLS mutations is upstream of neurodegeneration and aggregation formation. **a** Mutant P525L FUS failed to be recruited to DNA damage sites. Recruitment-withdrawal to Laser cuts in MN nuclei (boxed area) expressing normal (WT) or mutant P525L (Mut) FUS-GFP was imaged live at 21 DIV (Supplementary Movie 6). **b** Quantification of **a**, FUS-GFP at cut over time. **c** Chemical modulation of nuclear FUS impacted on recruitment of FUS-GFP to cuts in WT cells (top gallery) treated 24 h mock, with PARP1 inhib., etoposide or arsenite or in mutant cells (bottom gallery) treated 24 h mock, with PARG, DNA-PK inhibitors or AdOx (Supplementary Movie 6). **d** Quantification of **c**. **e** Compounds impacted on nuclear FUS-GFP levels in MNs: treatments WT versus Mut as for **c**, bars: 10  $\mu$ m. **f** Quantification of **e**, ratio FUS-GFP amount nucleus/cytosol (left) or total FUS amount in cytoplasmic aggregates (right). Data are plotted as mean, error bars = STDEV, one-way ANOVA with post-hoc Bonferroni test (\*, \*\*, \*\*\*P values of 0.05, 0.01, and 0.001, respectively, N = 3). **g** Proximal compound addition impacted on distal axonal trafficking at 21 DIV depicted as maximum intensity projections: PAPR1 inhib. mimicked mtFUS-phenotype whereas PARG, DNA-PK inhibitors and AdOx rescued mtFUS phenotype (Supplementary Movies 8, 9). Shown are representative examples of Ctrl1 and R521L, see Table 1. **h–i** Organelle tracking (**h**, **i**), mitochondrial membrane potential (**j**) and shape (**k**, **l**) analyses of G as box plots, batch analysis of Ctrl1–3 (Ctrl: Mock, PARP1 inhib.) and FUS R521C, R521L, R495QfsX527 (FUS: PARG inhib.) as described in Table 1, exception: DNA-PK and AdOx inhib. only on FUS R521L. **m** Left column: impact of microtubule disruption (24 h nocodazole, 5  $\mu$ M, mid) or respiratory inhibition (24 h oligomycin A, 10  $\mu$ M, bottom) on the recruitment of WT FUS-GFP to the Laser cut in nuclei (boxed areas) in uncompartmentalized MN at 21 DIV (Supplementary Movie 10). Note the unaltered FUS recruitment (green) despite the severe disruption of the mitochondria network (mitotracker deep red FM, LUT red hot) along with loss of processive motility in the treated cells (maximum intensity projection of movies). Mid and right column: ditto for treatment exclusively at the distal exit site of 900  $\mu$ m-MFCs (Supplementary Movie 11). Note the unaltered FUS recruitment (proximal entry, boxed areas) despite the severe disruption of the mitochondria network along with loss of processive motility at the distal site, bar: 10  $\mu$ m. **n** Quantification of FUS-GFP recruitment in **m**. **o** Nocodazole or oligomycin A treatment in **m** did not alter the normal nuclear FUS-GFP localization



induction<sup>19</sup>. FUS-NLS mutations most likely do not cause a complete loss of function of FUS protein since treatment with PARG is sufficient to restore FUS recruitment to DNA damage sites, cytoplasmic mislocalization and axon trafficking phenotypes (Fig. 6c, e, g). These findings are actually consistent with the study

by Wang et al. showing that mutant FUS proteins are still—at least in part—recruited to DDS, but were also impaired in the later steps of assembly or stabilization of the repair complex<sup>14</sup>.

FUS was shown to be required for DSB repair by homologous recombination (HR) or non-homologous end joining (NHEJ) and



FUS knockdown reduced both HR and NHEJ efficacy<sup>13,14</sup>. Furthermore, NHEJ efficacy was reduced by overexpression of FUS R521C but not by wtFUS protein in murine primary cortical neurons<sup>14</sup>. Interestingly, FUS knockdown affected neither the c-NHEJ factors KU70 and DNA-PK nor ATM substrates, such as 53BP1<sup>13</sup>, consistent with our data suggesting poly(ADP-ribose) mediated a-NHEJ as the DDR pathway downstream of FUS. Moreover, FUS was reported to directly interact with PAR<sup>13</sup> and PARylation was shown to induce additional PARP1 recruitment to DDS<sup>20</sup>. Thus, it might be possible that FUS mutations interfere with this interaction and might impair this feed-forward loop. However, the detailed downstream pathways for FUS mediated DDR signaling and its possible disturbance by FUS mutations needs further examination.

FUS was initially characterized as an oncogene (fused in sarcoma)<sup>34</sup>. FUS-CHOP fusion proteins lacks the c-terminal region, including RGG and NLS domain<sup>13</sup> and are responsible for PAR binding<sup>13</sup> and DNA DSB repair<sup>(14,19 and our study)</sup>. Interestingly enough, FUS-CHOP-positive myxoid liposarcoma are radiosensitive<sup>35</sup> and FUS knockdown increases radiosensitivity<sup>13</sup>. Furthermore, *Ews-/-* mice, another protein of the FET family (of which FUS is a member), are also highly sensitive to irradiation<sup>36</sup>. This is of immense clinical impact; currently, radiation is used on salivary glands as a treatment of pseudohypersalivation in ALS patients.

For dynamic measurement of FUS mislocalization, DNA recruitment and protein aggregation we generated isogenic iPSC lines with GFP-tags of the endogenous FUS protein using CRISPR/Cas9n. Thus, the results obtained herein are clearly due to underlying FUS mutations. Furthermore, by using both GFP-tagged and untagged isogenic lines, there is currently no evidence that the GFP-tagging biased the observed phenotypes.

We show a stepwise acquirement of degenerative phenotypes starting with impaired distal axonal organelle trafficking followed by distal axon degeneration and finally motor neuron cell death (Figs. 2 and 4). While post mortem analysis revealed clear motor neuron loss in the spinal cord of the advanced FUS-ALS cases studied (Fig. 3a, b), the *in vitro* data showed only minor signs of neuronal cell body degeneration at time points of severe distal axon degeneration (Fig. 2g–i), suggesting a dying-back process as typically seen in a distal axonopathy<sup>37</sup>. hiPSC-derived motor neuron cultures are the only way to monitor early disease course in human and could explain the differences with the post mortem results. However, while DNA damage induction always led to distal axonal phenotypes and FUS cytoplasmic mislocalization, this was not seen when inducing a solely axonal degeneration by nocodazole treatment or ATP depletion

(Fig. 6m–o). This suggests that FUS-ALS is a neuronopathy rather than a pure distal axonopathy, but one with prominent and especially early distal axonal degeneration.

One of the most intriguing questions of age-related neurodegenerative diseases is how a somatic mutation causes neurodegeneration specifically in aged individuals. Evidently, DNA damage accumulates during aging (for review see ref. 30). Of note, age-related motor neuron degeneration has been observed in mice lacking the DNA repair protein ERCC excision repair 1, endonuclease non-catalytic subunit<sup>38,39</sup>. However, whether mutation severity, age of onset, amount of DNA DSBs, appearance of neurodegenerative phenotypes and FUS aggregation do correlate remains to be shown in future studies.

## Methods

**Patient characteristics.** We included cell lines carrying “benign” (R521C, L) and “malign” (R495QfsX527, P525L) FUS mutations and systematically compared them to three control iPSC lines from healthy volunteers and to isogenic lines (Table 1). All procedures were in accordance with the Helsinki convention and approved by the Ethical Committee of the Technische Universität Dresden (EK45022009, EK393122012) and by the ethical committee of the University of Ulm (Nr. 0148/2009) and patients and controls gave their written consent prior to skin biopsy.

**Generation and expansion of iPSC lines.** Fibroblast or keratinocytes lines were established from skin biopsies or hair follicle cells obtained from familial ALS patients and healthy controls<sup>28</sup>. The generation and characterization of control iPSC lines was reported previously<sup>28,40</sup>. Fibroblast lines were reprogrammed as previously described<sup>28,40,41</sup>. Briefly, patient fibroblasts were reprogrammed using pMX-based retroviral vectors encoding the human cDNAs of *OCT4*, *SOX2*, *KLF4* and *cMYC* (pMX vectors). Vectors were co-transfected with packaging-defective helper plasmids into 293T cells using Fugene 6 transfection reagent (Roche). Fibroblasts were plated at a density of 50,000 cells/well on 0.1% gelatin-coated 6-well plates and infected three times with a viral cocktail containing vectors expressing *OCT4:SOX2:KLF4:cMYC* in a 2:1:1:1 ratio in the presence of 6 µg/ml protamine sulfate (Sigma Aldrich) and 5 ng/ml FGF2 (Peprotech). Infected fibroblasts were plated onto mitomycin C (MMC, Tocris) inactivated CF-1 mouse embryonic fibroblasts (in-lab preparation) at a density of 900 cells/cm<sup>2</sup> in fibroblast media. The next day media was exchanged to ES medium containing 78% Knock-out DMEM, 20% Knock-out serum replacement, 1% non-essential amino acids, 1% penicillin/streptomycin/glutamine and 50 µM β-Mercaptoethanol (all from Invitrogen) supplemented with 5 ng/ml FGF2 and 1 mM valproic acid (Sigma Aldrich). Media was changed every day to the same conditions. iPSC-like clusters started to appear at day 7 post infection, were manually picked 14 days post-infection and plated onto CF-1 feeder cells in regular ES-Media containing 5 ng/ml FGF2. Stable clones were routinely passaged onto MMC-treated CF-1 feeder cells (Globalstem) using 1 mg/ml collagenase type IV (Invitrogen) and addition of 10 µM Y-27632 (Ascent Scientific) for the first 48 h after passaging. Media change with addition of fresh FGF2 was performed every day.

iPSC lines from human hair keratinocytes were generated as described in refs. 42–44 by a lentivirus containing a polycistronic expression cassette encoding for *Oct4*, *Sox2*, *Klf4*, and *c-Myc* PMID19096035 produced in 70% confluent 10 cm dishes with Lenti-X 293T cells (Clontech, Mountain View, CA) by cotransfection of

**Fig. 7** Impairment of nucleo-cytoplasmic FUS shuttling leads to DNA damage, neurodegeneration and aggregate formation. **a** Time course of nuclear FUS withdrawal after addition of PARP1 inhib. (top gallery) or etoposide (eto, bottom gallery) in WT FUS-GFP MNs at 21 DIV. **b** Distinct inhibitory kinetics of FUS-dependent DNA repair through etoposide and PARP1 inhib: recruitment-withdrawal of FUS-GFP to nuclear laser cuts as for Fig. 6a on WT FUS-GFP MNs after PARP1 inhibitor (top) or etoposide (bottom) addition at indicated time points, i.e. before and after loss of nuclear FUS (corresponding red boxes in **a**), bars: 10 µm (Supplementary Movie 12). **c** Quantification of **b**. **d** FUS-GFP recruited to Laser cut in MNs double-treated 24 h with compounds as indicated (Supplementary Movie 13). Note the inhibition of recruitment to the cut (boxed areas) in mutant FUS-GFP P525L cells (far left) through double treatment with DNA-PKi and PARPi whereas DNA-PKi alone led to a rescue (Fig. 6c, Supplementary Movie 6), suggesting that PARP1 functions upstream of DNA-PK in DNA damage response. Furthermore, note that inhibition of recruitment through etoposide or arsenite in WT FUS-GFP (Fig. 6c, Supplementary Movie 6) was reverted through double treatment with either DNA-PKi or AdOx, suggesting a potent counterbalancing of etoposide/arsenite-driven displacement of FUS from the nucleus, thereby rescuing FUS recruitment to the cut (boxed areas). **e** Quantification of **d**. **f** Compounds impacted on nuclear FUS-GFP levels in MNs: double treatments Mut versus WT as for **d**. Note how DNA-PK inhib. or AdOx drove FUS-GFP back into the nucleus under conditions that normally lead to nuclear export of FUS (i.e. PARP1, etoposide or arsenite treatment, Fig. 6e). **g** Western blot (WB) analysis of markers for c-NHEJ DNA damage response (phospho and total DNA-PK, KU70 & KU80) and a-NHEJ (LIG1, PARP1 total and cleaved) on total lysates of MNs treated for 72 h as indicated. GFP, β-actin served as loading controls. **h** Densitometric quantification of **g**, WT (blue) versus FUS (red), mock only. Graphs show fold change over mean WT (mock baseline = 1) to reveal phenotypic differences of quasi untreated FUS over WT. **i** Densitometric quantification of **g** for all treatments. Graphs show fold change over respective cell line mock to reveal the compound response of each line (WT, blue, versus FUS, red) over its respective mock baseline (= 1). Statistics (**h**, **i**): data are plotted as mean, error bars = STDEV, one-way ANOVA with post-hoc Bonferroni test (\*, \*\*, \*\*\*P values of 0.05, 0.01, and 0.001, respectively, N = 4)



the polycistronic vector (8 mg), the pMD2 vector (2 mg), and the psPAX2 (5.5 mg) vector (both Addgene, Cambridge, MA) using 100 mL of the PolyFect transfection reagent (Qiagen, Hilden, Germany; [www.qiagen.com](http://www.qiagen.com)). Viral supernatant was collected at 48 and 96 h after transfection, concentrated using the Lenti-X Concentrator Kit (Clontech), resuspended in EpiLife medium, and stored in aliquots at  $-80^{\circ}\text{C}$ . For infection, up to  $3 \times 10^5$  keratinocytes per well of a 6-well plate were infected with  $5 \times 10^7$  proviral genome copies in EpiLife medium containing 8 mg/mL Polybrene (Sigma- Aldrich) at 2 sequent days. After another 24 h cells were detached using TrypLE Express (Invitrogen) and distributed onto 3 wells of a 6-well plate with already attached irradiated feeder cells ( $3 \times 10^5$  cells per well irradiated with 30 Gy) in hiPS cell medium. Further on the cells were cultured in a 5%  $\text{O}_2$  incubator. The medium was changed daily until arising colonies were large enough for mechanical passaging at about 2–3 weeks after transduction. Colonies displaying a clear stem cell morphology were picked and transferred onto irradiated MEFs or Matrigel-coated plates for further passage.

Stable clones were analyzed by qRT-PCR for silencing of viral transgenes prior to further experimental procedures.

**CRISPR/Cas9 genome editing.** To generate the two isogenic cell lines FUS WT-GFP and P525L-GFP, a patient-derived iPSC clone from a female patient carrying a heterozygous FUS R521C mutation was used (Table 1). The patient-specific FUS mutation was corrected at its mutation site and simultaneously C-terminal tagged with EGFP by CRISPR/Cas9-mediated genome editing via homology directed repair (HDR)<sup>45</sup>. For that a CRISPR/Cas9D10A vector (pX335B) containing the D10A mutant nickase version of Cas9 (Cas9n) and a pair of guide RNAs (gRNA) were used to create a double strand break (DSB) at the target site. The pX335B vector, containing Cas9n, was provided by the laboratory of Dr. Boris Greber, (Max Planck Institute for Molecular Biomedicine, 48149 Münster, Germany). As a HDR template a plasmid (pEX-K4) containing the FUS correction sequence (WT or P525L) plus EGFP-Tag was used (Eurofins Genomics).

To target the FUS R521C mutation site, two gRNA cassettes were designed. The gRNAs were manually selected by screening of the coding strand for suitable gRNA target sequences upstream of R521C mutation. DNA motifs screened for were CCN(N)19C or CCN(N)20C for target one (T1) and G(N)19NGG or G(N)20NGG for target two (T2). Target specific gRNAs (T1- gcgagtactctatctcaagt; T2- gtttagtagggagggcagat) then were cloned into the pX335B vector in two cloning steps. Successfully cloned vectors were identified via colony PCR after each ligation step. Positive clones were amplified, sequenced and used for transfection. The FUS correction sequences were designed according to the WT sequence of FUS (NCBI Ref. Seq. NC\_000016.10). Homology arms covering the mutation site, and in a size of 500 bp upstream and 400 bp downstream of the induced DSB were used. The EGFP-Tag was added to the last exon of FUS with a 9 bp linker-DNA sequence. The sequences for WT-EGFP and P525L-EGFP were synthesized de novo and cloned into the pEX-K4 from Eurofins Genomics.

For gene targeting of human iPSCs, feeder-free iPSCs cultured in TeSR-E8 medium (Stemcell Technologies) were co-transfected with pX335B vector (containing the Cas9n cassette, two gRNAs and a puromycin selection cassette) and pEX-K4 vector (containing the FUS WT-EGFP or P525L-EGFP sequence) using FuGENE HD transfection reagent (Promega). 24 h after transfection, cells containing the pX335B vector were selected by treatment with 0.4  $\mu\text{g}/\mu\text{l}$  Puromycin (InvivoGen) for another 24 h. After selection, cells were allowed to recover for 3–7 days and then passaged onto a new plate (2000 cells per 6-well). After 10–14 days EGFP-positive clones were picked and further cultured for characterization.

To identify successful homologous recombined clones, DNA was isolated (DNeasy Blood&Tissue Kit, Qiagen) from these cells and PCR was performed to confirm the presence of the EGFP-Tag within the genomic sequence of FUS. For this a forward primer (AGTTACCAGCCTCTCCAAGC) targeting FUS upstream of the used homology arms, and a reverse primer (CGGTGGTGCAGATGAACCTT) targeting EGFP were used. After successful PCR the genotype of clones positive for FUS-EGFP was determined by PCR and sequencing. For the genotyping PCR, the forward primer (CAGTTGAACAGAGGCCATAGG) and reverse primer (CAGTTGAACAGAGGCCATAGG) were used targeting FUS up- and downstream of EGFP, including the mutation site. Amplification results in two PCR products (1257 bp for FUS with EGFP and 528 bp for FUS without EGFP), if cells are heterozygous for the introduced modification. Additionally, gDNA of non-transfected cells was amplified as negative control, resulting in the amplification of only one PCR product (528 bp for FUS without EGFP). To confirm the genotype by sequencing, PCR products were analyzed on a 1% agarose gel and the two different sized bands were purified from the gel (QIAquick Gel Extraction Kit, Qiagen). In order to identify if correction of FUS occurred on the originally mutated allele and not on the WT allele, both purified PCR products were sequenced (Supplementary Fig. 1d, e). The PCR product containing FUS with EGFP (Allele A) was sequenced using the reverse primer (CGGTGGTGCAGATGAACCTT). The smaller PCR product containing FUS without EGFP (Allele B) was sequenced using the reverse primer (TGGGTGATCAGGAATTGGAAGG). The original genotype of the used patient-derived iPSC line was FUS-R521C/FUS-WT. The genotype of successfully modified clones WT-GFP and P525L-GFP is FUS-WT-EGFP/FUS-WT and FUS-P525L-EGFP/FUS-WT, respectively (Supplementary Fig. 1d, e).

To check for possible off-target effects of Cas9n both target specific gRNAs (T1 and T2) were checked via the “CRISPR Design” online tool from Zhang laboratory (<http://crispr.mit.edu>) and the “Off-spotter” tool from Pliatsika et al.<sup>46</sup>. The online tools confirmed that there are no genomic off-targets that are targeted from both gRNAs in combination, which could result in the introduction of a DSB at any untargeted site.

**Mycoplasma testing.** We checked every new cell line when entering the lab and after reprogramming, afterwards routinely check for mycoplasma every three to six months. We used the Mycoplasma Detection kits for conventional PCR according to manufacturer’s instructions (Venor Gem, No 11–1025).

**In vitro differentiation of embryoid bodies.** iPSC colonies were grown under standard conditions, cleaned and treated with collagenase type IV (2 mg/ml, Invitrogen). Floating aggregates were collected and transferred into ultra-low attachment plates (NUNC) in regular ES-Media containing 5  $\mu\text{M}$  Y-27632 (Ascent Scientific) for meso-/endodermal differentiation or ES-Media containing 5  $\mu\text{M}$  Y-27632, 10  $\mu\text{M}$  SB431542 (Tocris) and 1  $\mu\text{M}$  Dorsomorphin (Tocris) for ectodermal differentiation. Two days later the medium was changed to the same conditions leaving out the Y-27632. After four days of EB formation, aggregates were plated onto gelatin (0.1%, Millipore) coated wells for meso-/endodermal differentiation or onto plates coated with Matrigel<sup>TM</sup> (BD Bioscience) for ectodermal differentiation. EBs were differentiated for two weeks using 77.9% DMEM (high glucose, Invitrogen), 20% FCS (PAA), 1% non-essential amino acids (Invitrogen), 1% penicillin/streptomycin/glutamine (Invitrogen) and 0.1%  $\beta$ -Mercaptoethanol (Invitrogen) for the meso-/endodermal lineage and 50% DMEM/F12 (Invitrogen), 50% Neurobasal (Invitrogen) containing 1:200  $\text{N}_2$  supplement (Invitrogen), 1:100 B27 supplement without vitamin A (Invitrogen), 1% penicillin/streptomycin/glutamine, 0.1%  $\beta$ -Mercaptoethanol and 1:500 BSA Fraction V (Invitrogen) for ectodermal differentiation.

**AP staining and immunofluorescence on iPSC colonies.** For pluripotency marker stainings, iPSC colonies were passaged as described above and grown on Matrigel<sup>TM</sup>-coated coverslips in ES medium containing, 50% MEF-conditioned media (own preparation) supplemented with 5 ng/ml FGF2 (Sigma). Colonies were then stained for alkaline phosphatase according to the manufacturer’s protocol (Millipore) or were fixed with 4% paraformaldehyde (PFA) in PBS for 10 min at RT for analysis of pluripotency markers by immunofluorescence. Fixed colonies were incubated for 2 h in blocking solution (3% normal horse serum and 0.05–0.2% Triton-X100 in PBS). Plates were incubated over night at 4  $^{\circ}\text{C}$  using the following primary antibodies: rabbit anti-Nanog (1:500), rabbit anti-Oct4 (1:1000), mouse anti-SSEA4 (1:500), mouse anti TRA-1-60 (1:500) (all from Abcam) and mouse anti-Sox2 (1:500, R&D Systems). Differentiated EBs were stained with rabbit anti- $\alpha$ -SMA (1:500, Sigma Aldrich), mouse anti- $\alpha$ -Fetoprotein (1:500, Abcam), rabbit anti-GATA4 (1:500, Abcam), and mouse anti-TUJ1 (1:1000, Covance), mouse anti-Actinin (Sigma, 1:200) and mouse anti Beta-Catenin (BD Bioscience 1:500).

**Karyotyping.** FUS iPSC and control cell lines were karyotyped using the HumanCytoSNP-12v array. All clones showing pathological SNPs were excluded (data not shown).

**Genotyping.** FUS iPSC lines were genotyped after all other characterization had been finished. This was done by a diagnostic human genetic laboratory (CEGAT, Tübingen, Germany) using diagnostic standards.

**Differentiation of human NPCs to spinal MNs.** The generation of human NPCs and MNs was accomplished following the protocol from Reinhardt et al.<sup>26</sup>.

In brief, colonies of iPSCs were collected and stem cell medium, containing 10  $\mu\text{M}$  SB-431542, 1  $\mu\text{M}$  Dorsomorphin, 3  $\mu\text{M}$  CHIR 99021 and 0.5  $\mu\text{M}$  pumorphamine (PMA), was added. After 2 days hESC medium was replaced with N2B27 consisting of the aforementioned factors and DMEM-F12/Neurobasal 50:50 with 1:200  $\text{N}_2$  Supplement, 1:100 B27 lacking Vitamin A and 1% penicillin / streptomycin / glutamine. On day 4 150  $\mu\text{M}$  ascorbic acid was added while Dorsomorphin and SB-431542 were withdrawn. 2 Days later the EBs were mechanically separated and replated on Matrigel coated dishes. For this purpose Matrigel was diluted (1:100) in DMEM-F12 and kept on the dishes over night at room temperature. Possessing a ventralized and caudalized character the arising so called small molecule NPCs (smNPC) formed homogenous colonies during the course of further cultivation. It was necessary to split them at a ratio of 1:10–1:20 once a week using Accutase for 10 min at 37  $^{\circ}\text{C}$ .

Final MN differentiation was induced by treatment with 1  $\mu\text{M}$  PMA in N2B27 exclusively. After 2 days 1  $\mu\text{M}$  retinoic acid (RA) was added. On day 9 another split step was performed to seed them on a desired cell culture system. Furthermore the medium was modified to induce neural maturation. For this purpose the developing neurons were treated with N2B27 containing 10 ng/ $\mu\text{l}$  BDNF, 500  $\mu\text{M}$  dbcAMP and 10 ng/ $\mu\text{l}$  GDNF. Following this protocol it was possible to keep the cells in culture for over 2 months.

**Treatments and inhibitors.** Adenosine-2',3'-dialdehyde (AdOX, arginine methyltransferase inhibitor, Sigma-Aldrich A7154) was dissolved in water and traces of HCl to obtain a 10 mM stock, DNA-PK inhibitor NU7441 (Tocris Cat. No. 3712) was dissolved in DMSO to obtain a 5 mM stock, Sodium Arsenite (Sigma-Aldrich S7400) was dissolved in water to obtain a 5 mM stock, Etoposide (Sigma-Aldrich E1383) was dissolved in DMSO to obtain a 500  $\mu$ M stock, Gallo-tannin (PARG inhibitor, Santa Cruz Biotechnology sc-202619) was dissolved in water to obtain a 30 mM stock and ABT-888 (PARP1 inhibitor, Santa Cruz Biotechnology sc-202901) was dissolved in DMSO to obtain a 20 mg/ml stock. For treatment of hiPSC-derived spinal MNs in Xona Microfluidic chambers (see below), compounds were added either exclusively to the proximal or distal site for locally restricted application in compartmentalized cultures, thereby allowing to distinguish between local versus remote compound action at the distal and proximal readout positions (refer also to 'Life cell imaging' below). Cells were incubated for 72 h before live imaging and final concentrations were as follows: 10  $\mu$ M for AdOX, 2  $\mu$ M for DNA-PK, 30  $\mu$ M for PARG inhibitor, 2  $\mu$ g/ml for PARP1 inhibitor and 2  $\mu$ M for Etoposide.

For un-compartmentalized cell cultures, all compounds were added only 24 h before imaging (e.g. for the Laser cutter experiments, if not otherwise stated in time course experiments) with final concentrations as follows: 5  $\mu$ M for AdOX, 5  $\mu$ M for DNA-PK, 300  $\mu$ M for PARG inhibitor, 20  $\mu$ g/ml for PARP1 inhibitor, 5  $\mu$ M Sodium Arsenite and 5  $\mu$ M for Etoposide. DMSO was used for Mock controls.

**Microfluidic chambers.** The MFCs were purchased from Xona (RD900). At first, Nunc glass bottom dishes with an inner diameter of 27 mm were coated with Poly-L-Ornithine (Sigma-Aldrich P4957, 0.01% stock diluted 1:3 in PBS) overnight at 37 °C. After 3 steps of washing with sterile water, they were kept under the sterile hood for air drying. MFCs were sterilized with 70% Ethanol and also left drying. Next, the MFCs were dropped onto the dishes and carefully pressed on the glass surface for firm adherence. The system was then perfused with Laminin (Roche 11243217001, 0.5 mg/ml stock diluted 1:50 in PBS) for 3 h at 37 °C. For seeding cells, the system was once washed with medium and then 10  $\mu$ l containing a high concentration of cells ( $3 \times 10^7$  cells/ml) were directly injected into the main channel connecting two wells. After allowing for cell attachment over 30–60 min in the incubator, the still empty wells were filled up with maturation medium. This method had the advantage of increasing the density of neurons in direct juxtaposition to microchannel entries whereas the wells remained cell-free, thereby reducing the medium turnover to a minimum. To avoid drying out, PBS was added around the MFCs. Two days after seeding, the medium was replaced in a manner which gave the neurons a guidance cue for growing through the microchannels. Specifically, a growth factor gradient was established by adding 100  $\mu$ l N2B27 with 500  $\mu$ M dbcAMP to the proximal seeding site and 200  $\mu$ l N2B27 with 500  $\mu$ M dbcAMP, 10 ng/ $\mu$ l BDNF, 10 ng/ $\mu$ l GDNF and 100 ng/ $\mu$ l NGF to the distal exit site. The medium was replaced in this manner every third day. After 7 days, the first axons began spreading out at the exit site and cells were typically maintained for up to six weeks.

**Immunofluorescence stainings.** For immunofluorescence staining, cells were washed twice with PBS without  $\text{Ca}^{2+}/\text{Mg}^{2+}$  (LifeTechnologies) and fixed with 4% PFA in PBS for 10 min at room temperature. PFA was aspirated and cells were washed three times with PBS. Fixed cells were first permeabilized for 10 min in 0.2% Triton X solution and subsequently incubated for 1 h at RT in blocking solution (1% BSA, 5% donkey serum, 0.3 M glycine and 0.02% Triton X in PBS). Following blocking, primary antibodies were diluted in blocking solution and cells were incubated with primary antibody solution overnight at 4 °C except for the  $\gamma$ H2A.X antibody which was kept for only 2 h at room temperature on the fixed material. The following primary antibodies were used: chicken anti-SMI32 (1:10,000, Covance), mouse anti-FUS (1:5000, Sigma-Aldrich), rat anti-meFUS (1:100<sup>5</sup>), rabbit anti-beta-III-Tubulin (1:3000, Covance), mouse anti-Hb9 (1:100 Development studies Hybridoma Bank), rabbit anti-Islet (1:500, Abcam), mouse anti- $\gamma$ H2A.X (1:500 Millipore), rabbit anti-ChAt (1:500, Chemicon), rabbit anti-53BP1 (1:1000, Novusbio). Nuclei were counter stained using Hoechst (LifeTechnologies).

**Western blotting.** Western blot analysis (FUS) was performed as described in Prause et al.<sup>47</sup>. DNA damage pathway was analyzed as follows. Lysates of neuronal cell cultures were prepared as described<sup>48</sup> with modified RIPA buffer consisting of 50 mM Tris-HCl (pH 7.4), 1% Nonidet-P40, 0.25% sodium deoxycholate, 150 mM NaCl, 1 mM EDTA, 1 mM  $\text{NaVO}_3$ , 2 mM NaF (all Sigma-Aldrich), Complete protease inhibitor cocktail (Roche). Protein amount was measured by BCA assay (Thermo Fisher Scientific). After SDS-PAGE and transfer of proteins onto nitrocellulose membranes (GE Healthcare), specific proteins were detected using the indicated primary antibodies and horseradish peroxidase-conjugated donkey anti-rabbit and sheep anti-mouse antibodies (GE Healthcare). Detection of proteins on X-ray films (GE Healthcare) was accomplished with enhanced chemiluminescent reagent (Amersham). Antibodies were purchased as indicated: DNA-PK (#4602), PARP1 (#9542), KU80 (#2180, Cell Signaling Technology),  $\beta$ -actin (A5441, Sigma), phospho-DNA-PK S2056 (ab18192), phospho-DNA-PK S2056 (ab18192, Abcam), LIG1 (ab177946), KU70 (ab3114), GFP (ab290, Abcam).

**Live cell imaging and tracking analyses.** For tracking of lysosomes and mitochondria, cells were double-stained live with 50 nM LysoTracker Red DND-99 (Molecular Probes Cat. No. L-7528) and 50 nM Mitotracker Deep Red FM (Molecular Probes Cat. No. M22426). For measuring mitochondrial membrane potential (and tracking as well), cells were stained with 200 nM Mitotracker JC-1 (Molecular Probes Cat. No. M34152). Trackers were added directly to culture supernatants and incubated for 1 h at 37 °C. Imaging was then performed without further washing of cells. Live imaging of compartmentalized axons in Xona Microfluidic Chambers (MFC) was performed with a Leica HC PL APO 100  $\times$  1.46 oil immersion objective on an inverted fluorescent Leica DMI6000 microscope enclosed in an incubator chamber (37 °C, 5%  $\text{CO}_2$ , humid air) and fitted with a 12-bit Andor iXON 897 EMCCD camera (512 $\times$ 512, 16  $\mu$ m pixels, 229.55 nm/pixel at 100X magnification). For more details, refer to [https://www.biodip.de/wiki/Bioz06\\_-\\_Leica\\_AFLX6000\\_TIRF](https://www.biodip.de/wiki/Bioz06_-_Leica_AFLX6000_TIRF). Excitation was performed with a TIRF Laser module in epifluorescence (widefield) mode with lines at 488, 561 and 633 nm. Fast dual color movies were recorded at 3.3 frames per second (fps) per channel over 2 min (400 frames in total per channel) with 115 ms exposure time as follows: LysoTracker Red (excitation: 561 nm, emission filter TRITC 605/65 nm) and Mitotracker Deep Red (excitation: 633 nm, emission filter Cy5 720/60 nm) or for Mitotracker JC-1 with excitation at 488 nm and fast switching between emission filter FITC 527/30 nm (green channel for compromised membrane potential) and TRITC 605/65 nm (red channel for intact membrane potential). Movie acquisition was performed at strictly standardized readout positions within the micro channels of the micro groove barrier that separated the proximal seeding site from the distal axonal exit as illustrated in Fig. 2a. Specifically, the readout windows were located either just adjacent to the channel exit (distal readout) or the channel entry (proximal readout).

**Tracking analysis.** Movies were analyzed with FIJI software using the TrackMate v2.7.4 plugin for object (lysosomes and mitochondria) recognition and tracking. Settings were as follows: pixel width: 0.23  $\mu$ m, pixel height: 0.23  $\mu$ m, voxel depth: 1  $\mu$ m, crop settings: not applied, select a detector: DoG detector with estimated blob size: 1.6  $\mu$ m, threshold: 45, median filter: no, subpixel localization: yes, initial thresholding: none, select view: HyperStack Displayer, set filters on spots: quality above 45, select a tracker: linear motion LAP tracker, initial search radius: 2  $\mu$ m, search radius: 2  $\mu$ m, Max. frame gap: 2, set filters on tracks: track duration  $\geq$  3 s. Typically, 200–500 tracks per movie were obtained and analyzed with respect to track displacement (measure for processive, i.e. straight, motility as opposed to undirected random walks) and mean speed. Tracking is illustrated in Supplementary Movie 5. Results were assembled and post-filtered (threshold for track displacement  $\geq$  1.2  $\mu$ m) in KNIME and MS Excel and bulk statistics analyzed and displayed as box plots in GraphPad Prism 5 software (Figs. 3b, c, e–i, 4i–m and 5f–j). Box plot statistics are provided in Supplementary Tables 1–17. Box plot settings: whiskers from 1–99%, outliers as dots, boxes from 25–75 percentile, median as horizontal center line, mean as cross. Significant differences between conditions (i.e. cell lines, compound treatments, etc.) were revealed with the nonparametric Kruskal-Wallis test for non-Gaussian distributions and Dunns post hoc test with significance level  $P \leq 0.05$  and 95% confidence interval. Box plots represent batch results merged from all apparently healthy control lines (Ctrl 1–3) or mutant ALS-FUS lines (R521C, R521L, R495QsfX527), respectively, and three independent experiments (i.e. differentiations, refer to Fig. 1a). A minimum of 5 movies (showing 2 micro channels each) was acquired at each readout positions (distal versus proximal) per line, condition and experiment resulting in a minimum of 15 movies in total for the batch analysis. We confirmed that all control and FUS lines were phenotypically indistinguishable, thereby validating our batch analysis (Supplementary Figs. 2–9).

**Static analysis of cell organelles.** For analysis of organelle count and morphology (mitochondria: elongation; lysosomes: diameter), object segmentation, thresholding and shape analysis was performed with a sequence of commands in FIJI software executed with Macro1 for mitochondria:

```
run("Slice Keeper", "first=1 last=1 increment=1");
run("Grays");
run("Subtract Background...", "rolling=3");
setAutoThreshold("IsoData dark");
//run("Threshold...");
run("Convert to Mask");
run("Set Measurements...", "area fit shape feret's redirect=None decimal=5");
run("Analyze Particles...", "size=4-Infinity pixel
circularity=0.00-1.00 show=Ellipses display summarize");
and Marco2 for lysosomes:
run("Slice Keeper", "first=1 last=1 increment=1");
run("Grays");
run("Enhance Contrast...", "saturated=0.1 normalize");
run("Subtract Background...", "rolling=5");
setAutoThreshold("Yen dark");
run("Convert to Mask");
run("Set Measurements...", "area fit shape feret's redirect=None decimal=5");
run("Analyze Particles...", "size=3-Infinity pixel
circularity=0.40-1.00 show=Ellipses display summarize");
```

These macros returned result tables containing the aspect ratio of fitted ellipses (long:short radius) that was taken as the measure for mitochondrial elongation as well as the outer Feret's diameter that was taken as lysosomal diameter. The same set of movies as for the tracking analysis (see above) was used (first frame only). Typically, hundreds of organelles were analyzed per movie. For bulk statistics, the same batch analysis as for the tracking analysis was performed with resultant distributions displayed as box plots (Figs. 3h, i, 4l, m and 5i, j).

For analysis of mitochondrial membrane potential (ratio JC-1 red:green channel), object segmentation was performed with the channel of higher intensity (mostly the red) to generate a selection limited to mitochondria using Macro3:

```
resetMinAndMax();
title=getTitle();
run("Slice Keeper", "first=1 last=1 increment=1");
run("Subtract Background...", "rolling=10");
setAutoThreshold("Default dark");
//run("Threshold...");
run("Convert to Mask");
run("Create Selection");
```

The resultant selection was saved as region of interest (ROI) and applied on both channels to reveal the total integral intensity and area of mitochondria and background in both channels using the "Measure" command. After area normalization and background subtraction, ratios of integral intensity red:green were taken as mean membrane potential per movie (first frame only) and batch-analyzed as for the tracking analysis (see above). The resultant distributions were displayed as box plots on a log scale (Figs. 3g, 4k and 5h).

**DNA damage laser cutting assay.** The UV laser cutter setup utilized a passively Q-switched solid-state 355 nm UV-A laser (Powerchip, Teem Photonics) with a pulse energy of 15  $\mu$ J at a repetition rate of 1 kHz. With a pulse length of <350 ps this resulted in a peak-power of 40 kW, of which typically less than 5% was used to cut tissues. The power was modulated using an acousto-optic modulator (AOM, AA.MQI 10-43-UV, Pegasus Optik). The laser-beam diameter was matched to the size of the back-aperture of the objectives by means of a variable zoom beam expander (Sill Optics). This enabled diffraction-limited focusing while maintaining high transmission for objectives with magnifications in the range of 20–100X. Point-scanning was realized with a pair of high-speed galvanometric mirrors (Lightning DS, Cambridge Technology). To this end, the scanning mirrors were imaged into the image-plane of the rear port of a conventional inverted microscope (Axio Observer Z1, Zeiss) with a telecentric f-theta objective (Jenoptik). In order to ease adjusting parfocality between the cutter and the spinning disk and to compensate for the offset between the positions of the back-planes of different objectives, the scan-mirrors and the scan-optics were mounted on a common translation stage. In the microscope reflector cube, a dichroic mirror reflected the UV light onto the sample and transmitted the fluorescence excitation and emission light. A UV-blocking filter in the emission path protects the camera and enables simultaneous imaging and ablating. The AOM, the galvanometric mirrors as well as a motorized stage (MS 2000, ASI) with a piezo-electric actuator, on which the sample is mounted, were computer-controlled using custom-built software (LabView, National Instruments) enabling cutting in 3D. Diffraction-limited cutting with little geometric distortion, high homogeneity of the intensity and good field flatness was possible in the entire field of view of the spinning disk. The maximum depth is limited by the free working distance of the objective used and the travel of the piezo-actuator (100  $\mu$ m). A Zeiss alpha Plan-Fluar 100  $\times$  1.45 oil immersion objective was used and 24 laser shots in 0.5  $\mu$ m-steps were administered over a 12  $\mu$ m linear cut.

**Imaging and quantification of cytosolic FUS aggregation in FUS-GFP tagged lines.** Untreated, Mock- or compound-treated cells were fixed and a Z-stack of 20 images in 0.5  $\mu$ m-steps was acquired with standard filter settings for GFP fluorescence. The Z-stack covered the full range from the bottom cytosolic to the top nuclear focal plane to capture all FUS protein. For quantification of resultant maximum intensity projections, the total integral GFP intensity in the nucleus, total cytosol as well as in cytosolic aggregates only was analyzed with FIJI software.

**Quantification and statistics.** Randomly assigned images of different experiments were quantified on day 14 of neuronal differentiation to evaluate MN differentiation capacity. To analyze DNA damage, images of NPCs and of mature MN 30 days after differentiation initiation were examined and the mean number of  $\gamma$ H2AX foci representing DSBs per nucleus was determined.

A minimum of three independent experiments based on three different differentiation pipelines were always performed. Statistical analysis was performed using GraphPad Prism version 5.0. If not otherwise stated, one-way ANOVA was used for all experiments with post-hoc Bonferroni post test to determine statistical differences between groups. \* $P < 0.05$ , \*\* $P < 0.01$ , \*\*\* $P < 0.001$ , \*\*\*\* $P < 0.0001$  were considered significant. Data values represent mean  $\pm$  SDTEV unless indicated otherwise.

**Electrophysiology.** Patch-clamp recordings were performed as described previously<sup>28</sup>. To perform electrophysiological experiments during week 7 of total

differentiation, we seeded 300,000 cells per Matrigel-coated coverslip in a 24 well plate on day 25. To ensure recording of MNs we selected large (>20 pF) multipolar neurons only. Furthermore, the internal patch solution was filled with secondary antibody alexa 488 to allow MN identification after an additional immunostaining step using alexa 555 against SMI32 primary antibody.

**Histology.** Human post mortem samples (spinal cords,  $n = 3$  of FUS mutations (NLS mutation) and 4 for controls), were obtained from the Amsterdam Academic Medical Center (AMC), Division of Neuropathology, Department of Pathology ALS Bank following the guidelines of the local ethics committee. The spinal cords of these clinically confirmed FUS-ALS patients, as well as age-matched controls had been obtained within 6–12 h after death. Tissues were used in compliance with the Declaration of Helsinki. All FUS-ALS patients suffered from clinical signs and symptoms of lower and upper MN disease with the eventual involvement of Cortex, brain stem motor nuclei. Age-matched control patients did not show any neuropathological anomalies. Transverse paraffin sections (3–4  $\mu$ m in thickness) of human (lumbar, thoracic, cervical) spinal cord were cut on a microtome. Sections were placed on silane-coated slides, de-waxed, rehydrated and heated in citrate buffer for antigen retrieval. Processed sections were incubated with primary antibodies (Mouse anti H2AX (Millipore), rabbit anti-FUS- (NOVUS)), each (1:100) for 1 h at room temperature. Appropriate HRP secondary antibodies were used (1:200, Vector Laboratories, USA) for 1 h, followed by DAB visualization (DAKO, Denmark). For immunofluorescence secondary antibodies conjugated with Alexa fluorophore (Invitrogen) were used. Staining patterns were visualized using a Zeiss LSM 700 confocal microscope. The resulting confocal images were processed using the Zeiss LSM software and Adobe Photoshop CS5. DAB immunohistochemical sections were photographed using an Axioplan microscope (Zeiss) with an Axio Cam HR camera using 63X oil immersion lens (Zeiss).

**Data availability.** All data related to the manuscript is included in the main text or Supplementary Files, or available from the authors upon reasonable request.

Received: 2 November 2016 Accepted: 20 November 2017

Published online: 23 January 2018

## References

- Vance, C. et al. Mutations in FUS, an RNA processing protein, cause familial amyotrophic lateral sclerosis type 6. *Science* **323**, 1208–1211 (2009).
- Kwiatkowski, T. J. Jr et al. Mutations in the FUS/TLS gene on chromosome 16 cause familial amyotrophic lateral sclerosis. *Science* **323**, 1205–1208 (2009).
- Mackenzie, I. R., Rademakers, R. & Neumann, M. TDP-43 and FUS in amyotrophic lateral sclerosis and frontotemporal dementia. *Lancet Neurol.* **9**, 995–1007 (2010).
- Dormann, D. et al. ALS-associated fused in sarcoma (FUS) mutations disrupt transportin-mediated nuclear import. *EMBO J.* **29**, 2841–2857 (2010).
- Dormann, D. et al. Arginine methylation next to the PY-NLS modulates transportin binding and nuclear import of FUS. *EMBO J.* **31**, 4258–4275 (2012).
- Dormann, D. & Haass, C. Fused in sarcoma (FUS): an oncogene goes awry in neurodegeneration. *Mol. Cell. Neurosci.* **56**, 475–486 (2013).
- Japtok, J. et al. Stepwise acquirement of hallmark neuropathology in FUS-ALS iPSC models depends on mutation type and neuronal aging. *Neurobiol. Dis.* **82**, 420–429 (2015).
- Deng, Q. et al. FUS is phosphorylated by DNA-PK and accumulates in the cytoplasm after DNA damage. *J. Neurosci.* **34**, 7802–7813 (2014).
- Lim, S. M. et al. Directly converted patient-specific induced neurons mirror the neuropathology of FUS with disrupted nuclear localization in amyotrophic lateral sclerosis. *Mol. Neurodegener.* **11**, 8 (2016).
- Ichiyanagi, N. et al. Establishment of in vitro FUS-associated familial amyotrophic lateral sclerosis model using human induced pluripotent stem cells. *Stem Cell Rep.* **6**, 496–510 (2016).
- Lenzi, J. et al. ALS mutant FUS proteins are recruited into stress granules in induced pluripotent stem cell-derived motoneurons. *Dis. Model Mech.* **8**, 755–766 (2015).
- Rulten, S. L. et al. PARP-1 dependent recruitment of the amyotrophic lateral sclerosis-associated protein FUS/TLS to sites of oxidative DNA damage. *Nucl. Acid. Res.* **42**, 307–314 (2014).
- Mastrocola, A. S., Kim, S. H., Trinh, A. T., Rodenkirch, L. A. & Tibbetts, R. S. The RNA-binding protein fused in sarcoma (FUS) functions downstream of poly(ADP-ribose) polymerase (PARP) in response to DNA damage. *J. Biol. Chem.* **288**, 24731–24741 (2013).
- Wang, W. Y. et al. Interaction of FUS and HDAC1 regulates DNA damage response and repair in neurons. *Nat. Neurosci.* **16**, 1383–1391 (2013).
- Martire, S., Mosca, L. & d'Erme, M. PARP-1 involvement in neurodegeneration: a focus on Alzheimer's and Parkinson's diseases. *Mech. Ageing Dev.* **146–148**, 53–64 (2015).



16. Britton, S. et al. DNA damage triggers SAF-A and RNA biogenesis factors exclusion from chromatin coupled to R-loops removal. *Nucl. Acid. Res.* **42**, 9047–9062 (2014).
17. Patel, A. et al. A liquid-to-solid phase transition of the ALS protein FUS accelerated by disease mutation. *Cell* **162**, 1066–1077 (2015).
18. D'Amours, D., Desnoyers, S., D'Silva, I. & Poirier, G. G. Poly(ADP-ribosylation) reactions in the regulation of nuclear functions. *Biochem. J.* **342**, 249–268 (1999).
19. Qiu, H. et al. ALS-associated mutation FUS-R521C causes DNA damage and RNA splicing defects. *J. Clin. Invest.* **124**, 981–999 (2014).
20. Mortusewicz, O., Ame, J. C., Schreiber, V. & Leonhardt, H. Feedback-regulated poly(ADP-ribosylation) by PARP-1 is required for rapid response to DNA damage in living cells. *Nucl. Acid. Res.* **35**, 7665–7675 (2007).
21. Ferrante, R. J. et al. Evidence of increased oxidative damage in both sporadic and familial amyotrophic lateral sclerosis. *J. Neurochem.* **69**, 2064–2074 (1997).
22. Hicks, G. G. et al. Fus deficiency in mice results in defective B-lymphocyte development and activation, high levels of chromosomal instability and perinatal death. *Nat. Genet.* **24**, 175–179 (2000).
23. Murakami, T. et al. ALS/FTD mutation-induced phase transition of FUS liquid droplets and reversible hydrogels into irreversible hydrogels impairs RNP granule function. *Neuron* **88**, 678–690 (2015).
24. Burke, K. A., Janke, A. M., Rhine, C. L. & Fawzi, N. L. Residue-by-residue view of in vitro FUS granules that bind the C-terminal domain of RNA polymerase II. *Mol. Cell* **60**, 231–241 (2015).
25. Altmeyer, M. et al. Liquid demixing of intrinsically disordered proteins is seeded by poly(ADP-ribose). *Nat. Commun.* **6**, 8088 (2015).
26. Reinhardt, P. et al. Derivation and expansion using only small molecules of human neural progenitors for neurodegenerative disease modeling. *PLoS ONE* **8**, e59252 (2013).
27. Stockmann, M. et al. Developmental and functional nature of human iPSC derived motoneurons. *Stem Cell Rev.* **9**, 475–492 (2013).
28. Naujock, M. et al. 4-aminopyridine induced activity rescues hypoexcitable motor neurons from ALS patient-derived induced pluripotent stem cells. *Stem cells* **34**, 1563–1575 (2016).
29. Deng, J. et al. FUS interacts with HSP60 to promote mitochondrial damage. *PLoS Genet.* **11**, e1005357 (2015).
30. Madabhushi, R., Pan, L. & Tsai, L. H. DNA damage and its links to neurodegeneration. *Neuron* **83**, 266–282 (2014).
31. Iliakis, G., Murmann, T. & Soni, A. Alternative end-joining repair pathways are the ultimate backup for abrogated classical non-homologous end-joining and homologous recombination repair: implications for the formation of chromosome translocations. *Mutat. Res. Genet. Toxicol. Environ. Mutagen* **793**, 166–175 (2015).
32. Kuroda, M. et al. Male sterility and enhanced radiation sensitivity in TLS(–/–) mice. *EMBO J.* **19**, 453–462 (2000).
33. Dupuis, L., Pradat, P. F., Ludolph, A. C. & Loeffler, J. P. Energy metabolism in amyotrophic lateral sclerosis. *Lancet Neurol.* **10**, 75–82 (2011).
34. Rabbitts, T. H., Forster, A., Larson, R. & Nathan, P. Fusion of the dominant negative transcription regulator CHOP with a novel gene FUS by translocation t(12;16) in malignant liposarcoma. *Nat. Genet.* **4**, 175–180 (1993).
35. Pitson, G. et al. Radiation response: an additional unique signature of myxoid liposarcoma. *Int. J. Radiat. Oncol. Biol. Phys.* **60**, 522–526 (2004).
36. Li, H. et al. Ewing sarcoma gene EWS is essential for meiosis and B lymphocyte development. *J. Clin. Invest.* **117**, 1314–1323 (2007).
37. Fischer, L. R. et al. Amyotrophic lateral sclerosis is a distal axonopathy: evidence in mice and man. *Exp. Neurol.* **185**, 232–240 (2004).
38. Borgesius, N. Z. et al. Accelerated age-related cognitive decline and neurodegeneration, caused by deficient DNA repair. *J. Neurosci.* **31**, 12543–12553 (2011).
39. de Waard, M. C. et al. Age-related motor neuron degeneration in DNA repair-deficient Ercc1 mice. *Acta Neuropathol.* **120**, 461–475 (2010).
40. Reinhardt, P. et al. Genetic correction of a LRRK2 mutation in human iPSCs links parkinsonian neurodegeneration to ERK-dependent changes in gene expression. *Cell Stem Cell* **12**, 354–367 (2013).
41. Lojewski, X. et al. Human iPSC models of neuronal ceroid lipofuscinosis capture distinct effects of TPP1 and CLN3 mutations on the endocytic pathway. *Hum. Mol. Genet.* **23**, 2005–2022 (2014).
42. Stockmann, M. & Lock, J. F. How far is the development of 13C-liver-function breath tests? *Dig. Dis. Sci.* **58**, 1804–1805 (2013).
43. Linta, L. et al. Rat embryonic fibroblasts improve reprogramming of human keratinocytes into induced pluripotent stem cells. *Stem Cells Dev.* **21**, 965–976 (2012).
44. Illing, A. et al. Definitive endoderm formation from plucked human hair-derived induced pluripotent stem cells and SK channel regulation. *Stem Cells Int.* **2013**, 360573 (2013).
45. Ran, F. A. et al. Double nicking by RNA-guided CRISPR Cas9 for enhanced genome editing specificity. *Cell* **154**, 1380–1389 (2013).
46. Pliatsika, V. & Rigoutsos, I. “Off-Spotter”: very fast and exhaustive enumeration of genomic lookalikes for designing CRISPR/Cas guide RNAs. *Biol. Direct* **10**, 4 (2015).
47. Prause, J. et al. Altered localization, abnormal modification and loss of function of Sigma receptor-1 in amyotrophic lateral sclerosis. *Hum. Mol. Genet.* **22**, 1581–1600 (2013).
48. Vehlow, A. et al. Adhesion- and stress-related adaptation of glioma radiochemoresistance is circumvented by  $\beta 1$  integrin/JNK co-targeting. *Oncotarget* **25**, 49224–49237 (2017).
49. Corcia, P. et al. A novel mutation of the C-terminal amino acid of FUS (Y526C) strengthens FUS gene as the most frequent genetic factor in aggressive juvenile ALS. *Amyotroph. Lateral Scler Frontotemporal Degener.* **18**, 1–4 (2017).

## Acknowledgements

We acknowledge the great help in cell culture by Sylvia Kanzler, Anett Böhme and Katja Zoschke. Ronny Szczech helped with the tracking analysis. The Light Microscopy Facility (LMF) of CMCB (Center for Molecular and Cellular Bioengineering, Technische Universität Dresden) provided invaluable support for all live imaging experiments. The meFUS antibody was provided by D. Dormann. We sincerely thank Stichting ALS Nederland and ALS Centre Netherlands (E. Aronica) for ALS research support. This work was supported, in part, by the Else Kröner foundation to M.N., “Deutsche Gesellschaft für Muskelerkrankungen (He2/2)” to A.H., the Roland Ernst Stiftung Saxony to A.H., the MeDDrive program of the Medical Faculty at the Technische Universität Dresden to A.H., BIOCREA GMBH to A.H., the NOMIS foundation to A.H., grant No 281903 of the European Research Council to S.W.G., the Helmholtz Virtual Institute “RNA dysmetabolism in ALS and FTD (VH-VI-510)” to A.H., T.M.B., A.C.L., S.L. and A. S., an unrestricted grant by a family of a deceased ALS patient to A.H., the German Motor Neuron Disease Network (BMBF-MND-Net; Funds 360644) to J.W., the Interdisciplinary Centre for Clinical Research (IZKF Aachen, N7-4), the German Myopathy Society (DGM) and the Initiative Therapieforschung ALS e.V. to A.G. and J.W., the Frick Foundation for ALS research to E.S., the Minna-James-Heineman-Stiftung to E.S., Association Française contre les Myopathies (AFM) to E.S., the Muscular Dystrophy Association (MDA), the EU Joint Programme – Neurodegenerative Disease Research (JPND; grant numbers ZonMW 733051075 (TransNeuro) and ZonMW 733051073 (LocalNMD)) and an ERC consolidator grant (ERC-2017-COG 770244) to E.S. and the Max Planck Society to E.S.

## Author contributions

M.N., A.P. and A.H. designed all of the experiments. T.M.B., A.C.L., S.L., I.P., M.F., E. S., X.L., P.R., J.S., J.H.W., A.F., K.H., A.Hy, A.S. and A.H. generated and provided the study material. J.J. generated isogenic lines. M.N., N.S., F.W. and S.P. performed and analyzed the functional assays. M.N., A.P., S.W.G., A.Hy and A.H. designed, performed and analyzed the laser cutter experiments. M.N., A.P., F.P.-M. and A.H. designed, performed and analyzed all live cell imaging. M.N., A.P., J.J., F. P.-M., N.S., F.W., S.P., A.V., R.G. M.J., N.C. and A.H. designed, performed and analyzed all cell culture experiments. A.G., D.T. and J.W. did the neuropathology analysis. A.H. supervised the project, M.N., A.P. and A.H. wrote the manuscript and all other authors critically revised the manuscript.

## Additional information

**Supplementary Information** accompanies this paper at <https://doi.org/10.1038/s41467-017-02299-1>.

**Competing interests:** The authors declare no competing financial interests.

**Reprints and permission** information is available online at <http://npg.nature.com/reprintsandpermissions/>

**Publisher's note:** Springer Nature remains neutral with regard to jurisdictional claims in published maps and institutional affiliations.



**Open Access** This article is licensed under a Creative Commons Attribution 4.0 International License, which permits use, sharing, adaptation, distribution and reproduction in any medium or format, as long as you give appropriate credit to the original author(s) and the source, provide a link to the Creative Commons license, and indicate if changes were made. The images or other third party material in this article are included in the article's Creative Commons license, unless indicated otherwise in a credit line to the material. If material is not included in the article's Creative Commons license and your intended use is not permitted by statutory regulation or exceeds the permitted use, you will need to obtain permission directly from the copyright holder. To view a copy of this license, visit <http://creativecommons.org/licenses/by/4.0/>.

© The Author(s) 2018

### 3.3 Clinical Translation - Malignancy Rate and Further Clinical Aspects of FUS-ALS Patients

The following sections refer to the results of the second main publication of this dissertation:

**Naumann M**, Peikert K, Günther R, van der Kooi AJ, Aronica E, Hübers A, Danel V, Corcia P, Pan-Montojo F, Cirak S, Haliloglu G, Ludolph AC, Goswami A, Andersen PM, Prudlo J, Wegner F, Van Damme P, Weishaupt JH, Hermann A. Phenotypes and malignancy risk of different FUS mutations in genetic amyotrophic lateral sclerosis. *Ann Clin Transl Neurol.* 2019 Nov 4. doi: 10.1002/acn3.50930



In juvenile ALS patients in Germany, *FUS* mutations were demonstrated to be the most frequent among all ALS-associated gene mutations (Hübers et al., 2015). In contrast, others reported conspicuously old patients with evident *FUS* mutation (Akiyama et al., 2016; Shang & Huang, 2016), which makes individual disease prognosis an impossible task for the consulting physician.

Furthermore, if one considers the frequency of increased DNA damage, which could be demonstrated in the *in-vitro* cell model of this thesis, in connection with the fact that *FUS*-deficient mice showed increased radiation sensitivity and global genomic instability (Hicks et al., 2000; Kuroda et al., 2000), the question arose whether FUS-ALS patients are at risk of malignant diseases due to genomic instability/increased DNA damage. Therefore, a cross-sectional, multinational, and retrospective cohort study was conducted to learn more about genotype-phenotype relationships and to answer the question of a potentially increased risk of malignant tumours in FUS-ALS patients, which would have relevant clinical implications. A total of 40 FUS-ALS patients with available disease histories were identified. However, only one patient could be found who clearly suffered from a malignant disease. During his childhood, he was diagnosed with acute lymphoblastic leukaemia. Afterwards, he received prophylactic whole-brain radiation and later he was diagnosed with meningioma and at the age of 31 years with motor neuron disease. This case obviously suggests increased sensitivity to radiation and a tendency to develop neoplasms. However, the entire cohort had a lifetime prevalence of only 0.025. Statistical testing using Fisher's exact test against prevalence data from control cohorts of healthy individuals (Haberland, Bertz, Wolf, Ziese, & Kurth, 2010) and against retrospective lifetime prevalence data from sporadic ALS patients (F. Fang et al., 2013) revealed no significant differences, respectively. At least in this cohort, no significantly increased risk for malignancies in FUS-ALS patients was observed. In order to increase the statistical power for the genotype-phenotype correlation analysis, the data of all newly identified patients were combined with all available previously published FUS-ALS patients with evident clinical documentation. The combined cohort data confirmed previous single case

observations regarding the pathogenicity of individual genetic alterations. In particular, the modification of the amino acid P525L, which was also used in the cell culture experiments in the first part of this thesis, proved to be most severe and led to a mean age of onset of the disease below 20 years and survival time after first symptoms of 13 months. Similar but less drastic results were obtained for frameshift and truncating mutations leading to a complete structural or functional loss of the C-terminus of FUS (Figure 1 and Table 2; Naumann et al. 2019). Remarkably, patients with one of these three genetic alterations showed surprisingly frequent initial bulbar/brain stem symptoms such as slurred speech or dysphagia, which are known to have a negative impact on survival due to the increased risk of aspiration (Figure 4D; Naumann et al. 2019). On the other hand, the most common genetic modification found in the FUS-ALS patients was a mismatch mutation at position R521. This R521 cohort showed a broad range of symptom onset and survival, suggesting additional disease factors that play a role. Regardless of the latter, the clinical site of their initial symptoms was almost exclusively considered to be a spinal onset, which is much more common than is known in sporadic ALS. In contrast to sporadic ALS, FUS-ALS patients showed a positive correlation between the age of onset of the disease and survival time, suggesting that FUS-ALS might be a particularly serious sub-disease. Taken together, the overview of individual mutations and the respective clinical features will be helpful for physicians in diagnosing and counselling (FUS-) ALS patients.

## RESEARCH ARTICLE

# Phenotypes and malignancy risk of different *FUS* mutations in genetic amyotrophic lateral sclerosis

Marcel Naumann<sup>1,2,3</sup> , Kevin Peikert<sup>1,3</sup>, Rene Günther<sup>1,2</sup>, Anneke J. van der Kooij<sup>4</sup>, Eleonora Aronica<sup>5</sup>, Annemarie Hübers<sup>6</sup>, Veronique Danel<sup>7</sup>, Philippe Corcia<sup>7</sup>, Francisco Pan-Montojo<sup>8</sup>, Sebahattin Cirak<sup>9,10</sup>, Gökür Haliloglu<sup>11</sup>, Albert C. Ludolph<sup>6</sup>, Anand Goswami<sup>12</sup>, Peter M. Andersen<sup>13</sup>, Johannes Prudlo<sup>3,14,15</sup>, Florian Wegner<sup>16</sup>, Philip Van Damme<sup>17,18</sup>, Jochen H. Weishaupt<sup>6</sup> & Andreas Hermann<sup>1,2,3,14,19</sup> 

<sup>1</sup>Department of Neurology, Technische Universität Dresden, Dresden, Germany

<sup>2</sup>German Center for Neurodegenerative Diseases (DZNE), Dresden, Germany

<sup>3</sup>Translational Neurodegeneration Section "Albrecht-Kossel", Department of Neurology, University Medical Center Rostock, University of Rostock, Rostock, 18147, Germany

<sup>4</sup>Department of Neurology, Amsterdam UMC, Academic Medical Centre, Amsterdam Neuroscience, University of Amsterdam, Amsterdam, the Netherlands

<sup>5</sup>Amsterdam UMC, Department of (Neuro)Pathology, Amsterdam Neuroscience, University of Amsterdam, Amsterdam, The Netherlands

<sup>6</sup>Department of Neurology, German Center for Neurodegenerative Diseases, University of Ulm, Ulm, Germany

<sup>7</sup>Centre expert pour la SLA et les maladies du motoneurone hôpital SALENGRO, CHU, Lille, France

<sup>8</sup>Department of Neurology, Klinikum der Universität München, Munich Cluster for Systems Neurology, SyNergy, Munich, 81377, Germany

<sup>9</sup>Division of Pediatric Neurology, Department of Pediatrics, University Hospital Cologne, Cologne, Germany

<sup>10</sup>Center for Molecular Medicine, University of Cologne, Cologne, Germany

<sup>11</sup>Department of Pediatric Neurology, Hacettepe University Children's Hospital, Ankara, 06100, Turkey

<sup>12</sup>Institute of Neuropathology, RWTH Aachen University Hospital, Aachen, 3052074, Germany

<sup>13</sup>Institute of Pharmacology and Clinical Neuroscience, Umeå University, Umeå, SE-90185, Sweden

<sup>14</sup>German Center for Neurodegenerative Diseases (DZNE) Rostock/Greifswald, Rostock, 18147, Germany

<sup>15</sup>Department of Neurology, University of Rostock, Rostock, Germany

<sup>16</sup>Department of Neurology, Hannover Medical School, Hannover, Germany

<sup>17</sup>Department of Neurology, University Hospitals Leuven, Leuven, Belgium

<sup>18</sup>Department for Neuroscience, VIB-KU Leuven Center for Brain & Disease Research, Leuven, Belgium

<sup>19</sup>Center for Transdisciplinary Neurosciences Rostock (CTNR), University Medical Center Rostock, University of Rostock, Rostock, 18147, Germany

## Correspondence

Andreas Hermann, Translational Neurodegeneration Section "Albrecht Kossel", Department of Neurology, University Medical Center Rostock, Gehlsheimer Straße 20, 18147 Rostock, Germany.  
Tel: +49 (0)381 494-9511;  
Fax: +49381 4949542;  
E-mail: Andreas.Hermann@med.uni-rostock.de

## Funding Information

This work was supported in part by the NOMIS foundation to A.H., the Helmholtz Virtual Institute "RNA dysmetabolism in ALS and FTD (VH-VI-510)" to A.H., A.C.L., P.M.A., an unrestricted grant by a family of a deceased ALS patient to A.H., the Stiftung zur Förderung der Hochschulmedizin in Dresden and the Hermann und Lilly Schilling-Stiftung für medizinische Forschung im Stifterverband. This work was supported by the Deutsche Forschungsgemeinschaft, Germany grant (CI 218/1–1) to Dr.

## Abstract

**Objective:** Mutations in Fused in Sarcoma (*FUS* or *TLS*) are the fourth most prevalent in Western European familial amyotrophic lateral sclerosis (ALS) populations and have been associated with causing both early and very late disease onset. *FUS* aggregation, DNA repair deficiency, and genomic instability are contributors to the pathophysiology of *FUS*-ALS, but their clinical significance per se and their influence on the clinical variability have yet to be sufficiently investigated. The aim of this study was to analyze genotype–phenotype correlations and malignancy rates in a newly compiled *FUS*-ALS cohort. **Methods:** We cross-sectionally reviewed *FUS*-ALS patient histories in a multicenter cohort with 36 novel cases and did a meta-analysis of published *FUS*-ALS cases reporting the largest genotype–phenotype correlation of *FUS*-ALS. **Results:** The age of onset (median 39 years, range 11–80) was positively correlated with the disease duration. C-terminal domain mutations were found in 90%. Among all, P525L and truncating/ frameshift mutations most frequently caused juvenile onset, rapid disease progression, and atypical ALS often associated with negative family history while the R521 mutation site was associated with late disease onset and pure spinal phenotype. Malignancies were found in one of 40 patients. **Interpretation:** We report the largest genotype–phenotype correlation of *FUS*-ALS, which enables a careful prediction of the clinical course in newly

Sebahattin Cirak. KP is supported by Else-Kröner-Forschungskolleg Dresden. PVD holds a senior clinical investigatorship of FWO-Vlaanderen and is supported by the ALS Liga België and the KU Leuven funds “Een Hart voor ALS” and “Laeversfonds voor ALS Onderzoek”.

diagnosed patients. In this cohort, FUS-ALS patients did not have an increased risk for malignant diseases.

Received: 20 September 2019; Accepted: 29 September 2019

**Annals of Clinical and Translational Neurology** 2019; 6(12): 2384–2394

doi: 10.1002/acn3.50930

## Introduction

Amyotrophic lateral sclerosis (ALS) is recognized as one of the most severe neurodegenerative diseases. Progressive muscular paresis due to motor neuron (MN) demise leads to a rapid loss of autonomous mobility and usually culminates in death of patients after 3–5 years.<sup>1</sup> Approximately, 10% of all ALS patients self-report a familial predisposition. Mutations in more than 38 genes were identified to be implicated in the pathological MN degeneration.<sup>2</sup> In 1% of sporadic and up to 5% of familial ALS cases, mutations in *Fused in Sarcoma (FUS)* were found to be causative,<sup>3</sup> primarily located in the PY-nuclear localization sequence (NLS) of the protein and are often associated with a more severe course compared to patients with C9ORF72, TBK1, TARDBP, or SOD1 mutations. Furthermore, the severity of these genetic errors appears to positively correlate with disease onset<sup>4</sup> and recently, *FUS* mutations were shown to have the highest proportion of all ALS-related gene mutations in juvenile ALS patients in Germany.<sup>5</sup> Indeed, the youngest FUS-ALS patient reported a disease onset at 11 years of age<sup>6</sup> presenting with the P525L mutation. In smaller case series, bulbar disease onset was reported more often,<sup>7</sup> which is known to be a negative predictor for survival in sporadic ALS.<sup>8</sup> Others, however, reported on FUS-ALS patients with particularly late onset.<sup>7,9,10</sup> Altogether, the rarity and variations of individual disease courses make appropriate predictions about individual patient survival impossible.

*FUS* exerts its function as a DNA-/RNA-binding protein primarily in the nucleus and is centrally implicated in splicing regulation, stress granule formation, and DNA repair.<sup>11,12</sup> We and others recently reported on drastically increased DNA damage in various cell types with *FUS*-NLS mutations, which was shown to be associated with neuronal cell death.<sup>13–15</sup> It is, however, not known if other cells in FUS-ALS patients are also affected by accumulated DNA damage leading to genomic instability, which is the basis for the multistep process of cancer development. The fact

that *FUS* knock-out mouse embryonic fibroblasts display abundant chromosomal instability and enhanced radiation sensitivity would underline this reasoning.<sup>16,17</sup>

Neurodegenerative diseases in general were reported to correlate with an altered risk for malignant diseases. Evidence exists for a lower tumor risk in Alzheimer's, Huntington's, and Parkinson's diseases,<sup>18,19</sup> whereas no difference could be found in overall ALS patients compared to the general population.<sup>20</sup> However, due to the low prevalence of *FUS* mutations, a possible cancer hazard could be masked. Therefore, we identified via a multicenter approach 36 novel patients with *FUS* mutations and reviewed available medical records for the presence of malignancies. Furthermore, we analyzed individual disease parameters in context of previously reported FUS-ALS cases to deepen our knowledge of genotype–phenotype correlations in this rare disease.

## Materials & Methods

The study was performed according to the Declaration of Helsinki and approved by the local institutional review boards (EK 393122012, EK 49022016 at the Technische Universität Dresden). We performed a multicenter cross-sectional study to identify genetically proven FUS-ALS patients according to El-Escorial criteria<sup>21</sup> and surveyed all available medical records including postmortem ( $n = 8$ ) analysis for the occurrence of neoplasms (Table 1). If applicable, informed consent was obtained from the individuals. Documentation of benign hyperplasia or dysplasia was included into the table but otherwise disregarded because of mostly missing further pathological information. For statistical testing, we compared with the German cancer statistics from 2004<sup>22</sup> serving as a control group whilst taking the negligible amount of ALS patients therein into account.

Furthermore, all available demographic and disease-related data were obtained. To measure the individual disease course/survival more precisely, the term “onset to



**Table 1.** Demographic data of newly reported FUS-ALS cases (=cohort 1).

Sex	AoO (y)	Age at death (y)	Site of onset	Family history	Amino acid change	Tumor	Tumor in Autopsy	Onset to death (m)	OTSE (m)
female	22	alive	arms	positive	P525L	none reported	not applicable	not applicable	7
female	58	58	arms	positive	R521L	none reported	NA	7	7
female	24	26	bulbar	negative	Y526C	none reported	NA	22	9
female	NA	16	NA	negative	R495*	none reported	negative	10	10
female	33	35	dropped head	NA	Y526C	cystic tumor intraspinal	positive	16	16
female	39	40	right leg	positive	R521C	several benign tumors	positive	19	19
female	38	40	legs	NA	R521C	Focal nodular hyperplasia liver	positive	25	25
female	38	41	legs (right)	positive	R521H <sup>1</sup>	none reported	NA	31	31
female	46	49	arms	positive	R521H	none reported	NA	37	37
female <sup>4</sup>	60	63	arms (left)	positive	R521H <sup>2</sup>	none reported	NA	37	37
female	44	47	arms (left)	positive	R521H <sup>2</sup>	none reported	NA	38	38
female	61	66	arms	positive	R521C	none reported	NA	60	60
female <sup>4</sup>	33	39	legs (left)	positive	R521H <sup>2</sup>	none reported	NA	71	71
female	NA	NA	NA	NA	R521H	none reported	NA	NA	NA
female	NA	NA	NA	NA	R521H	none reported	NA	NA	NA
female	NA	NA	NA	NA	R521H	none reported	NA	NA	NA
female	NA	70	NA	NA	R521C	none reported	NA	NA	NA
female	NA	70	NA	NA	R521C	several benign tumors	positive	NA	NA
female	17	18	bulbar	negative	P525L	none reported	NA	24	24
male	17	18	legs	negative	P525L	none reported	NA	15	15
male	31	32	bulbar	positive	R495Qfs*527	Acute lymphoblastic leukemia (ALL)	NA	18	18
male	23	25	Legs right	positive	G478Lfs*23	none reported	not applicable	19	19
male	39	40	right arm	positive	R521C	none reported	negative	20	20
male	39	41	bulbar	NA	R521C	none reported	negative	20	20
male	54	56	left (arm)	positive	R521C	none reported	negative	27	27
male	71	74	arms (left)	positive	R521H <sup>1</sup>	none reported	NA	29	29
male	62	65	legs (left)	positive	R521C	none reported	NA	48	48
male	43	alive	arms (right)	positive	R521H	none reported	not applicable	not applicable	61
male	63	alive	NA	positive	M254I	none reported	NA	NA	72
male <sup>4</sup>	65	73	arms	positive	R521H <sup>2</sup>	none reported	NA	86	86
male	35	49	right hand	negative	Q23L	none reported	negative	175	175
male	NA	NA	NA	NA	R521H	none reported	NA	NA	NA
male	NA	40	NA	NA	R521C	none reported	NA	NA	NA
male	27	28	arms/ shoulders	positive	R521C <sup>3</sup>	none reported	NA	13	13
male	40	41	arms (left)	positive	R521C <sup>3</sup>	none reported	NA	13	13
male	59	alive	legs (left)	positive	K510R	none reported	not applicable	not applicable	not applicable
male	40	alive	legs (right)	NA	R521H	none reported	not applicable	not applicable	not applicable
male	41	alive	legs	positive	G509D	none reported	not applicable	not applicable	not applicable
male	13	alive	arms	NA	Y526C	none reported	not applicable	not applicable	30

NA, not available, <sup>1,2,3</sup>indicate familial relation, <sup>4</sup>indicates single patients that have been already published,<sup>30</sup> but were included to demonstrate familial relation to others in the table.

severe event" (OTSE, months, m) was designed estimating the time from onset to the constant need for assisted ventilation, tube feeding, or death, which was also the censoring date for the Kaplan-Meier curve in Figure 3.

Additionally, 150 published ALS cases with *FUS* mutation (cohort 2) were collected by searching the pubmed

database for the terms "FUS," "ALS," and "FUS MUTATION." Only affected patients with both existing clinical data and known mutations status were included. Combined mean or median data were likewise excluded. Using this approach, a total of 186 patients from 44 studies were included in our analysis (Table S1).

## Statistics

Testing for statistical significance and general descriptive analysis was done using the IBM SPSS Statistics version 25 software. Individual tests are described beneath the respective figures, all were carried out as two-sided test and a  $P \leq 0.05$  was considered to indicate significant test results. The median was used as main data aggregation estimator with the median 95% confidence interval to indicate dispersion. Testing for normality distribution was carried out using the Shapiro-Wilk test. Normal distribution was found if not stated otherwise in the results section allowing the usage of student *t*-test. However, for all data depicted by boxplot diagrams, the null hypothesis was rejected, hence either the Kruskal-Wallis H or Mann-Whitney U test were used (Fig. 3A, 4B and C). Bonferroni correction was applied in Figure 3A. Following Kaplan-Meier plotting, the Log-rank test was used to estimate survival differences between FUS-ALS patient subgroups. Pearson's Chi-square test was carried out to evaluate the sex difference frequency. Fisher's exact test

was applied to compare the tumor prevalence data from different populations. Spearman rank correlation coefficients were used to examine correlations between age of onset (AoO) and OTSE with a correlation coefficient of  $\rho < 0.3$  considered as a weak,  $\rho = 0.3\text{--}0.59$  a moderate, and  $\rho \geq 0.6$  a strong correlation.

## Data Availability Statement

The authors state that all data are available upon individual request.

## Results

### Demographic and disease-related data of identified patients with *FUS* mutation

We included two cohorts of FUS-ALS patients in this study. First, we retrospectively analyzed case files in a cross-sectional multicentric study and identified 36 unpublished FUS-ALS cases (Table 1). Additionally, we

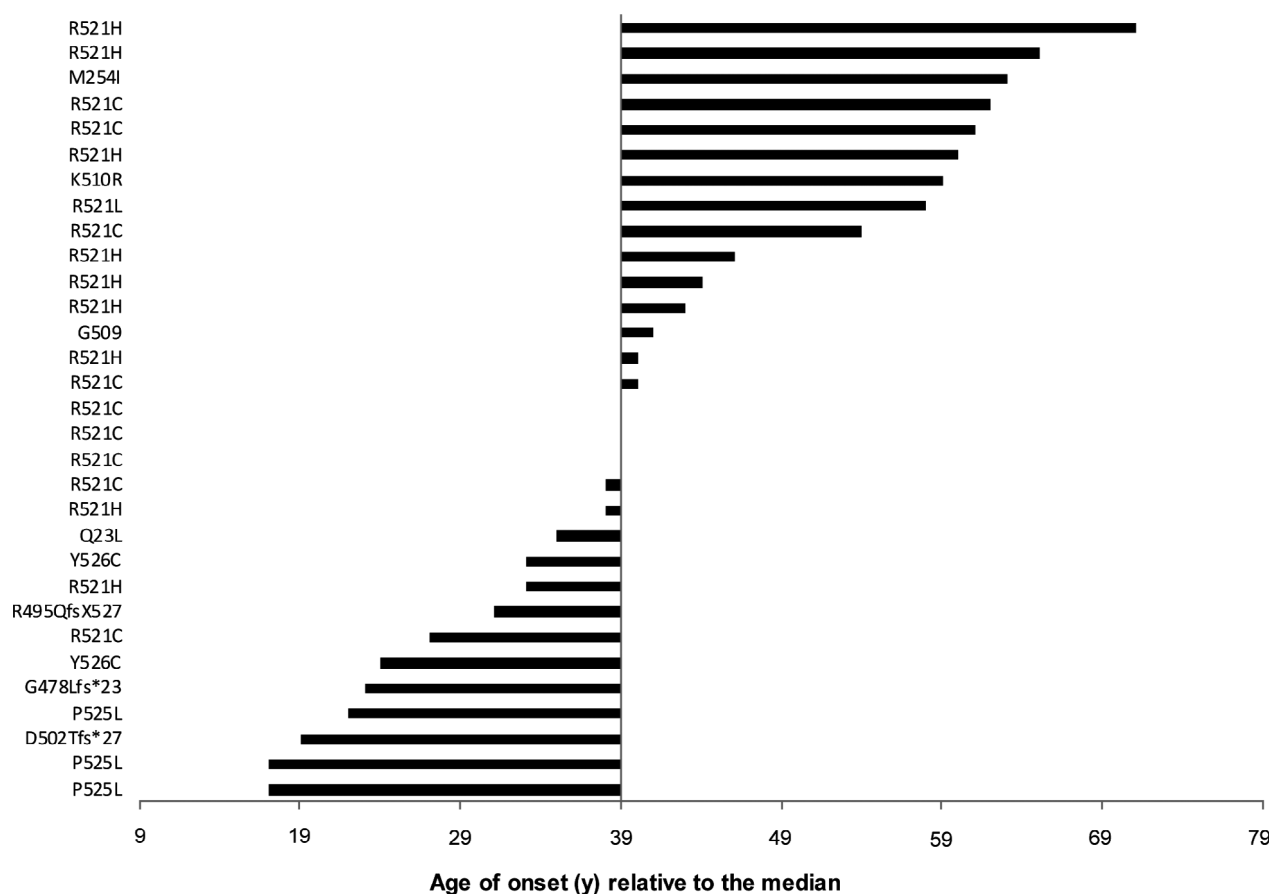


**Figure 1.** Age at onset of newly acquired patients (=cohort 1) depicted as bar diagram for every case starting from the median value,  $n = 30$ . Similarly, data of all patients (cohort 1 and 2) are shown in Figure S1.

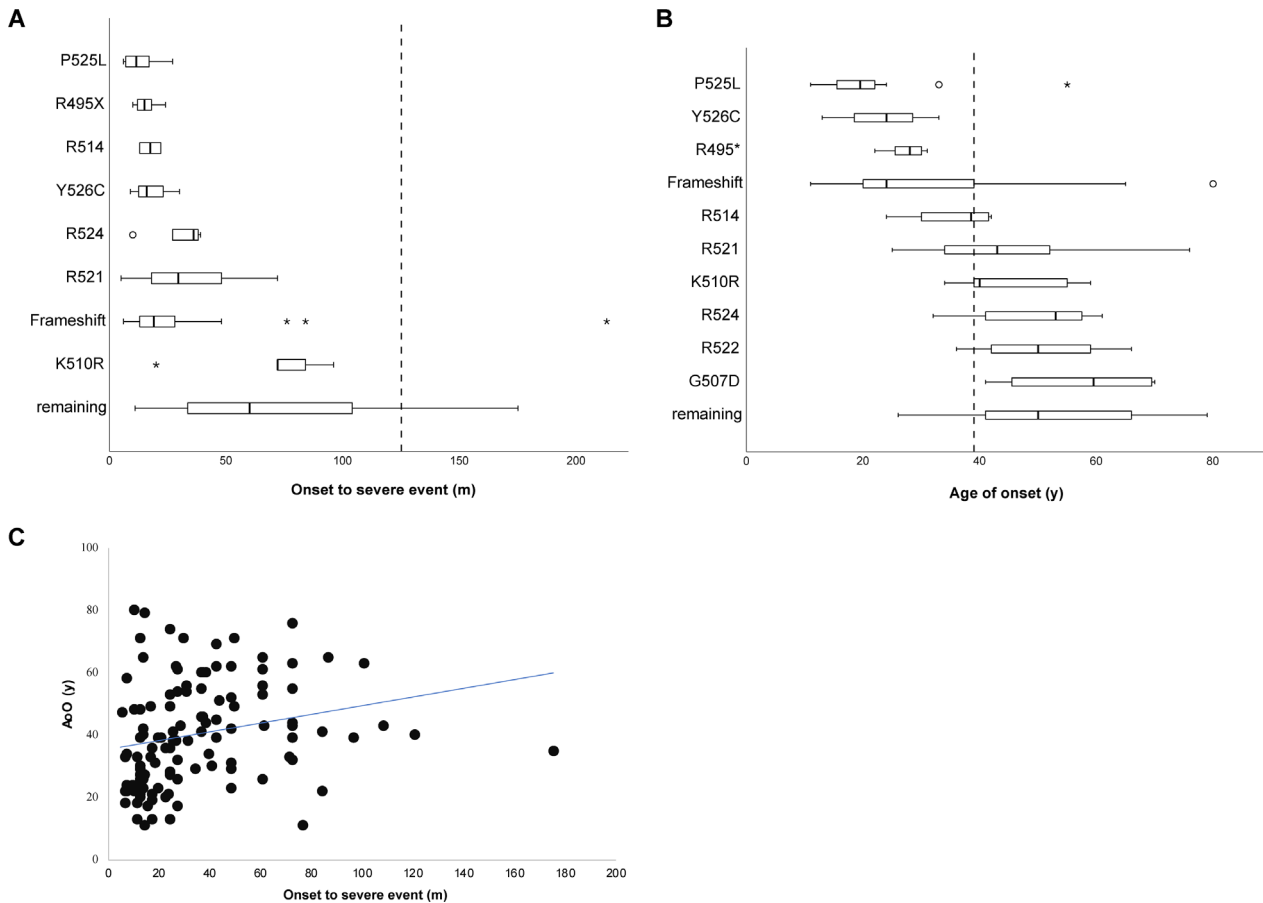


**Figure 2.** (A), (B) Boxplot diagrams of disease duration (onset to severe event, OTSE) and age of onset (AoO) depending on individual mutation sites in the combined group. The median value of the total group is drawn as broken line. Mutation sites were selected if information was available on  $\geq 2$  cases. (C) Scatter blots of AoO and OTSE indicating moderate positive correlation.

collected information on recently published FUS-ALS patients for whom both relevant clinical information and genetic testing were available (Table S1). Demographic data are shown in Tables S2–S4.

In cohort 1, 34 patients (94%) had a C-terminal mutation within the nuclear localization signal (NLS), whereas the two remaining patients showed mutations at position 23 in the Prion-like domain (PLD) or at 254 in the Glycine-rich repeats domain underlining the previously reported abundance of C-terminal mutations in FUS patients. Furthermore, our cohort included three cases with the P525L change, four patients were found to have a truncating mutation following inclusion of an early stop codon or frameshift alterations. Male sex was slightly more frequent with a ratio of 1.18:1 ( $P = 0.74$ , Chi-square test). The median AoO was 39 (CI 31–44) years and the median survival time from symptom onset until either permanent necessity for live-prolonging measures or death (OTSE) was

25 months (CI 18–31) months. Sex did neither influence AoO ( $P = 0.8$ , students *t*-test) nor OTSE ( $P = 0.26$ , students *t*-test). Bulbar disease onset was observed in 13.8% of patients.

Cohort 2 included recently published FUS-ALS cases for whom clinical information was available and genetic testing was done on the reported individual. By doing so, we collected 150 additional cases (Table S1). C-terminal domain mutations were found in 89% with the R521C amino acid change being the most prevalent mutation (17%). In general, the locus 521 had the highest abundance of different amino acid changes and was mutated most frequently (36%). Importantly, with regard to median AoO/OTSE, we observed almost identical values in cohort 2 (Table S3) compared to cohort 1 (Table S2), highlighting the validity of the data ( $P = 0.84$  and  $P = 0.61$ , students *t*-test, respectively). Due to lack of data availability, the sex influence could not be completely evaluated.

### Genotype–phenotype correlations

Figure 1 demonstrates the variability of the age at onset in cohort 1 (see Fig. S1/ DataS1 for all patients) implying that certain mutations do result in very different phenotypes.

As shown above, cohort 1 and 2 did not differ concerning AoO and OTSE (Tables S2–S4). Therefore, we combined the data for further analysis of genotype–phenotype correlations resulting in the so far largest reported cohort of 186 FUS-ALS patients (Table S1).

Table S4 summarizes descriptive data of the combined cohorts. Interestingly, we found a moderate but significant positive correlation between AoO and OTSE (Fig. 2C, Spearman  $\rho = 0.37$ ,  $P < 0.001$ ), which is contrary to sporadic ALS, in which late onset is associated with faster disease progression.<sup>23,24</sup>

Figure 2 implicates that certain mutations may result in distinct clinical disease parameters. In detail, P525L, Y526C, and R495X led to the most striking difference compared to the other groups listed in Table 2. One patient of the new cohort 1 had a particularly early onset at the age of 13 and subsequent genome sequencing revealed the Y526C missense mutation in his case. On examination, he showed weakness in all extremities without obvious clinical signs of upper MN impairment. Furthermore, he had a mild intellectual disability and a cerebellar nystagmus; however, there was no evidence for bulbar disease. His condition deteriorated rapidly resulting in the need for constant ventilation support and tube feeding 30 months after onset paralleled by locked-in syndrome.

Next, we grouped the most frequently reported amino acid changes at the loci P525L, R521, truncating/frame-shift mutations, and others for deeper investigation. Figure 3A demonstrates that carriers of a P525L (21 years, CI 15–22) or truncating/frameshift (27 years, CI 23–31) mutation had a significantly lower median age of onset compared to the remaining carriers (47 years, CI 39–55) and to the R521 carriers (43 years, CI 39–49, Kruskal-Wallis H test, post hoc Bonferroni correction,  $P < 0.001$ ). Interestingly, the cumulative survival of the individual mutation carriers was significantly different (Fig. 3B, Log-rank Test,  $df = 3$ ,  $P < 0.001$ ) as indicated by the Kaplan-Meier curves demonstrating the shortest survival for the P525L patients.

Further analysis of the data revealed that the initial site of disease onset is different for individual mutations (Fig. 4A). Whereas P525L (42%) and truncation/frame-shift (44%) carriers (44%) more frequently presented with initial bulbar disease, only 3% of R521 mutation carriers had such symptoms at onset. As expected, we observed a significantly shorter median OTSE in bulbar-onset FUS-ALS patients compared to patients with spinal onset

**Table 2.** Descriptive data of frequent FUS mutation carriers in the combined group.

	R521	R495*	Frameshift	R514	P525L	R524	G507D	K510R	R522	Y526C	Remaining	Total
AoO (y)	43 (39–48, N = 69)	28 (24–31, N = 8)	26 (22–31, N = 28)	39 (36–42, N = 4)	19.5 (13–22, N = 20)	55 (34–61, N = 7)	59.5 (34.7–80, N = 4)	40 (39–55, N = 8)	50 (30.8–70.2, N = 4)	28.5 (24–33, N = 3)	47 (34–72.5, N = 21)	39 (33.5–41, N = 176)
OTSE (m)	31 (25–40, N = 54)	18 (12–48, N = 6)	19 (12.5–26, N = 21)	17.5 (13–22, N = 2)	13 (10–20, N = 14)	36 (10–39, N = 5)	42 (N = 1)	78 (72–102, N = 6)	24 (N = 1)	19 (16–22, N = 3)	54.5 (24–108, N = 11)	24 (20–28.5, N = 124)

Median values (95% Confidence interval of the median) for the age of onset (AoO) and survival time until severe event (OTSE) are shown for patient groups with given mutation patterns.

(18 m, CI 13.8–22.3 vs. 30 m, CI 31.8–44.8,  $P = 0.002$ , Mann-Whitney U test). Surprisingly, however, the patients with bulbar course were additionally present with a significantly lower median age of onset (31 years, CI 24–36 vs. 40 years, CI 36–43,  $P = 0.025$ , Mann-Whitney U test, Fig. 4B and C).

Considering that the site of initial symptoms had a significant effect on both AoO and OTSE, one could deduce that the higher proportion of patients with bulbar disease might result in the decreased OTSE and earlier age at onset for the selected groups in Figure 3. However, when analyzing the OTSE for bulbar or spinal patients (Fig. 4D), no clear differences became obvious suggesting that additional modifiers might influence the disease phenotype, especially in the P525L group.

### Analysis of malignancy burden in FUS-ALS

Recent reports show that FUS mutations cause impairment of proper DNA damage response,<sup>13,15,25</sup> which was most strikingly seen in P525L, truncating mutations, and R521C. Therefore, we hypothesized that this might be reflected by increased abundance of malignancies in FUS mutation carriers. Data for neoplasms were available for 40 patients, most of whom belonging to cohort 1. Among all included individuals, we identified only one patient who suffered from a malignancy prior to ALS, namely an acute lymphoblastic leukemia (ALL), which was diagnosed during his childhood

(Table 1). This results in a prevalence for malignancies of 2.5% of the FUS-ALS patients, which is not significantly different from the prevalence data from control population (1.6%) provided by data from the German cancer statistics from 2004<sup>22</sup> (Fisher's exact test;  $P = 0.477$ ). Considering that the study by Haberland et al. only covered a 5-year prevalence, whereas our data can be understood as a lifetime prevalence, we recalculated with data from a register-based study.<sup>20</sup> Fang and colleagues did not detect a difference in malignancy burden between ALS cases and a healthy control population, but the rate for tumor prevalence in ALS cases was higher (10%) than in our study. Nevertheless, their ALS cohort and control patients did not differ significantly from our FUS-ALS cohort regarding cancer prevalence (Fisher's exact test;  $P = 0.18$ ).

Interestingly, the affected patient, who had a severe FUS frameshift mutation R495Qfs\*527 leading to truncation of the NLS, received prophylactic whole-brain radiation during his ALL therapy. Later on, he was diagnosed with a meningioma and eventually with ALS.

Conclusively, our data did not indicate an increased risk for malignancies in FUS-ALS patients.

### Discussion

In this study, we provide the largest so far reported cohort of 186 FUS-ALS patients and thereby enable a careful prediction of the clinical course in newly

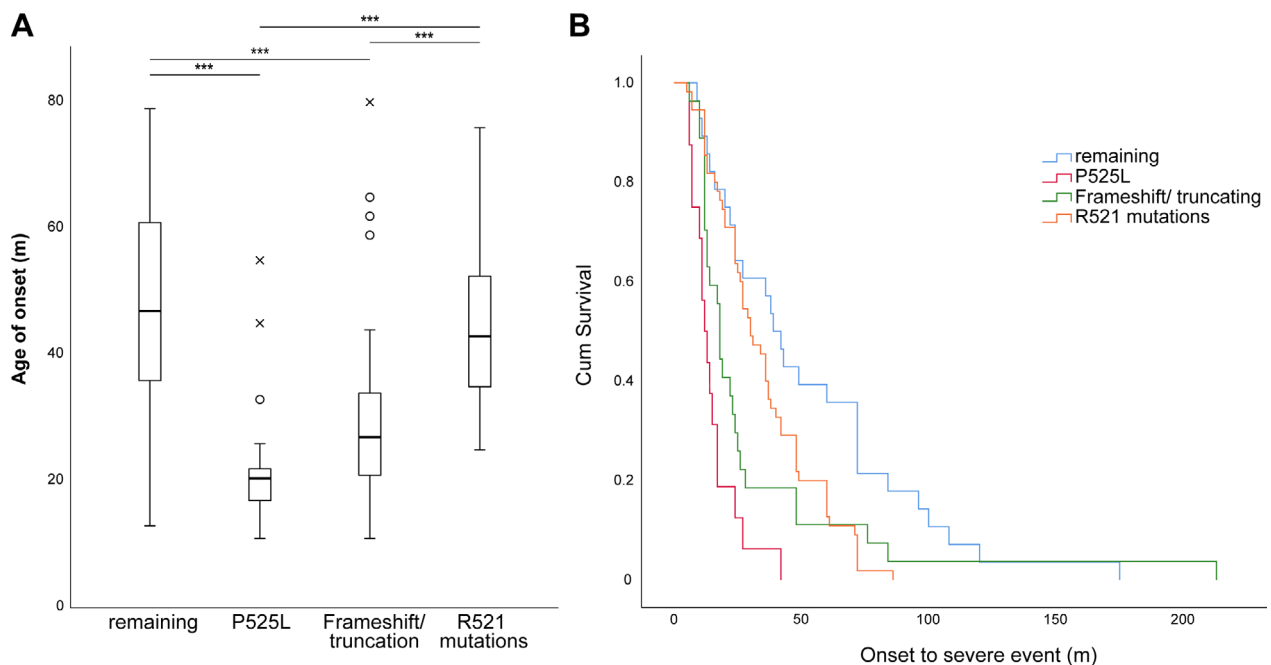


**Figure 3.** (A) Box plots showing the median age of onset for selected patient groups with the highest frequencies in the cohort. Statistical testing was performed using a Kruskal-Wallis test followed by Bonferroni correction,  $***P < 0.001$ . (B) Kaplan-Meier survival curve measuring the OTSE. The groups were found to have significantly different cum. survival rates as demonstrated by the Log-rank test,  $P < 0.001$ .

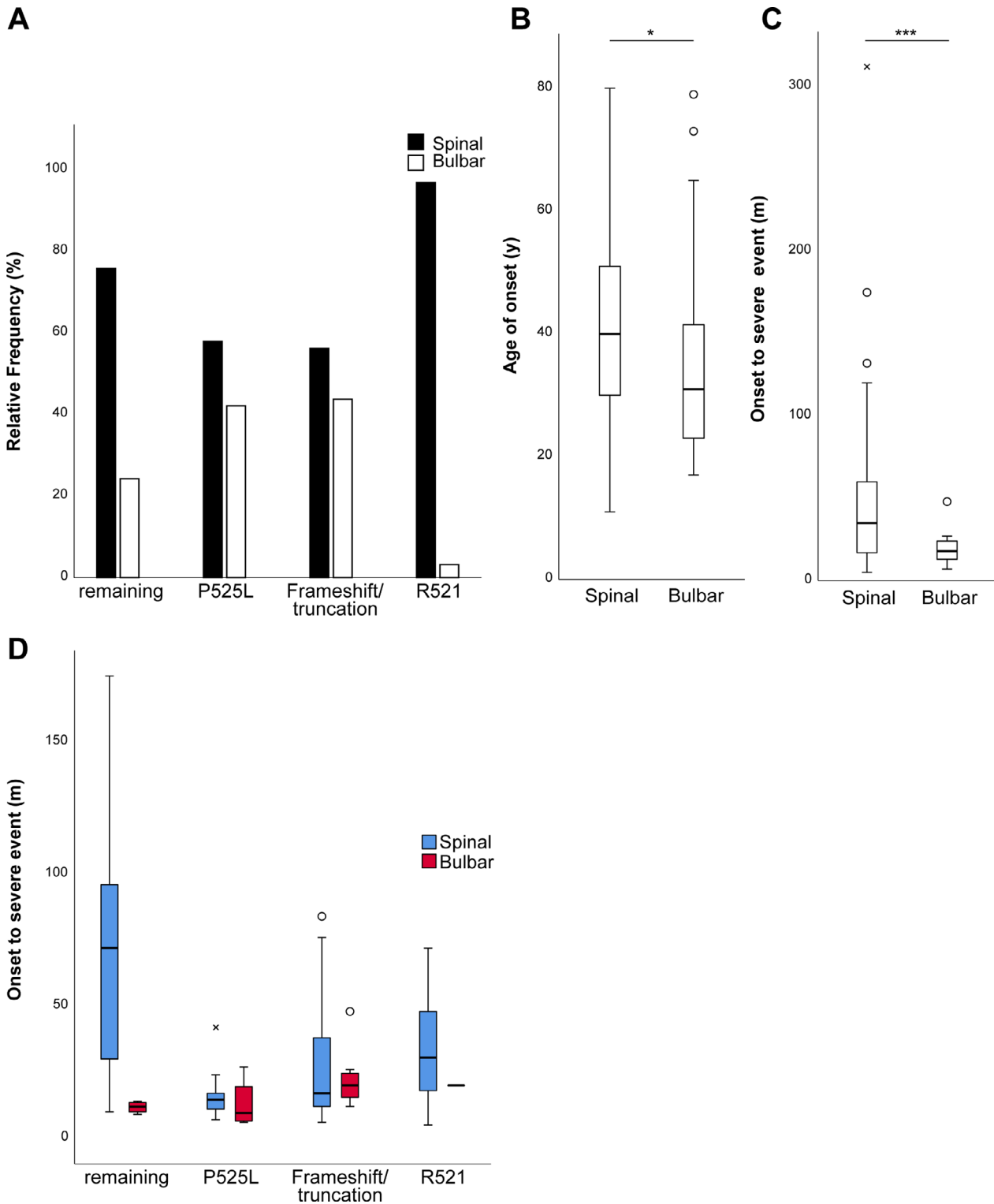


**Figure 4.** (A) Percentage of spinal vs. bulbar onset for the four most prevalent groups. Note the high rate of patients with a P525L or frameshift/truncating mutation presenting with bulbar disease, whereas R521 carriers mostly show spinal disease course. (B) Median age of onset and (C) OTSE grouped by spinal or bulbar disease onset. FUS-ALS patients with bulbar onset had a significantly lower age of onset and survival as revealed by Mann-Whitney U test. (D) Median survival time for selected mutation carriers grouped by side of onset. \* $P < 0.05$ , \*\*\* $P < 0.001$ .

diagnosed patients and their families carrying the more common amino acid changes. FUS-ALS patients showed a younger disease onset (median 39 years) than sporadic ALS patients.<sup>10,24</sup> This was, however, driven mainly by P525L and truncation/frameshift mutations leading to a higher frequency of bulbar onset and shorter survival. The less frequent Y526C mutation was also associated with particularly young onset, rapid disease progression, and atypical clinical signs as similarly demonstrated in a recent case report.<sup>26</sup> Therefore, FUS mutations should be considered in early onset and atypical forms of MN impairment including sporadic patients<sup>5</sup> with negative family history. We more often found *de novo* mutations in patients with a more drastic disease course and younger onset suggesting a possibly higher penetrance or lower chance to inherit the genetic change.

Our work extends previous work on genotype–phenotype correlations<sup>7,10</sup> by combining data from our patients with those FUS cases from the recent literature. This enabled us to identify patterns in the so far reported clinical heterogeneity by stratifying for certain mutations affecting the C-terminus, which once more became clear to be the major cause of FUS-ALS. Nevertheless, our study still lacks significant numbers of non-NLS mutations to describe their phenotypes properly. Furthermore, other modifying factors than the mutation itself must play a role considering the sometimes very different disease parameters within families carrying the same mutations (Table 1).

There is evidence for a lower risk of cancer in several neurodegenerative disorders like Alzheimer's, Parkinson's, and Huntington's disease.<sup>18,19,27</sup> On the other hand, patients with the ataxia-telangiectasia (AT) syndrome present with both neurodegeneration and higher risk for lymphoreticular malignancies and breast cancer. This is due to homozygous loss-of-function mutations in the *ATM* gene leading to insufficient DNA double-strand break repair,<sup>28,29</sup> which was also reported for *FUS* mutations.<sup>15</sup>

Thus, we addressed the clinical relevant question if FUS-ALS patients have a higher prevalence of malignant neoplasms. The retrospective assessment in our cohort revealed a lifetime prevalence of 2.5%. This was not significantly higher<sup>22</sup> or lower<sup>20</sup> than in the general population or in sporadic ALS. Even though the sample size is small and the study retrospective with the chance of underestimating neoplasm incidence, we consider the available data being sufficient to rule out an obvious co-occurrence of cancer as it is reported for AT syndromes.<sup>28</sup> It is important to stress that the calculation was done using prevalence data not considering the lifetime morbidity risk for a cancer disease, which is strongly age-dependent.<sup>22</sup> The retrospective database analysis of *Fang et al.* might be more suitable when comparing to FUS-ALS patients. FUS-ALS is otherwise

regarded to be the most frequent ALS subtype in juvenile patients (<35 years)<sup>5</sup> suggesting that a lower number of cancer cases could be due to young age of affected individuals with aggressive disease course leading to death before the classically increased risk for malignancies with higher age. Therefore, it would be important to follow-up the cases of unaffected family members of patients with evident *FUS* mutations and to compare with younger control cohorts.

Finally, there were only a few *FUS* mutations reported to influence DNA repair,<sup>13–15,25</sup> thus it is possible that the majority of patients not carrying those were not at risk for cancer which could not be addressed in our sample size. However, the most frequent FUS-ALS mutation R521C was described to impair proper DNA damage response resulting in increased DNA double-strand breaks evidently found in postmortem human tissue,<sup>15</sup> but none of our 12 R521C patients with partially late disease onset showed evidence for neoplasms.

To our knowledge, our survey has assessed the largest FUS-ALS patient collective so far. However, the rarity of the disease and the retrospective style has obvious limitations and warrants prospective validation. Still, we believe that our survey provides a sufficient cohort, which should be helpful when counseling patients and their families.

## Acknowledgments

We acknowledge all partners from the German ALS/MND NET and the Netherlands ALS foundation (“The Dutch ALS Tissue Bank”; EA). We thank the team who helped in the collection of ALS tissue samples (Prof. Dr. D. Troost and Prof. dr. M. de Visser).

## Author Contributions

M.N. and A.H. conceived and designed the study including statistics and data acquisition of previously published and newly reported patients and manuscript drafting. K.P. and R.G. contributed patient data and helped designing the manuscript. V.D., A.J.K., E.A., P.D., F.W., P.C., P.A., J.W., J.P., S.C., A.H., A.C.L., F.P., and A.G. contributed patient data, critically reviewed the manuscript, and helped designing it.

## Conflict of Interest

The authors report no conflict of interest.

## References

1. Brown RH, Al-Chalabi A. Amyotrophic lateral sclerosis. *N Engl J Med* 2017;377:162–172.



2. Renton AE, Chio A, Traynor BJ. State of play in amyotrophic lateral sclerosis genetics. *Nat Neurosci* 2014;17:17–23.
3. Müller K, Brenner D, Weydt P, et al. Comprehensive analysis of the mutation spectrum in 301 German ALS families. *J Neurol Neurosurg Psychiatry*. 2018;89:817–827.
4. Waibel S, Neumann M, Rosenbohm A, et al. Truncating mutations in FUS/TLS give rise to a more aggressive ALS-phenotype than missense mutations: a clinico-genetic study in Germany. *Eur J Neurol* 2013;20:540–546.
5. Hubers A, Just W, Rosenbohm A, et al. De novo FUS mutations are the most frequent genetic cause in early-onset German ALS patients. *Neurobiol Aging* 2015;36:1–3117.
6. Conte A, Lattante S, Zollino M, et al. P525L FUS mutation is consistently associated with a severe form of juvenile amyotrophic lateral sclerosis. *Neuromuscul Disord* 2012;22:73–75.
7. Akiyama T, Warita H, Kato M, et al. Genotype-phenotype relationships in familial amyotrophic lateral sclerosis with FUS/TLS mutations in Japan. *Muscle Nerve* 2016;54:398–404.
8. Chio A, Mora G, Leone M, et al. Early symptom progression rate is related to ALS outcome: a prospective population-based study. *Neurology* 2002;59:99–103.
9. Lattante S, Rouleau GA, Kabashi E. TARDBP and FUS mutations associated with amyotrophic lateral sclerosis: summary and update. *Hum Mutat* 2013;34:812–826.
10. Shang Y, Huang EJ. Mechanisms of FUS mutations in familial amyotrophic lateral sclerosis. *Brain Res* 2016;15:65–78.
11. Bosco DA, Lemay N, Ko HK, et al. Mutant FUS proteins that cause amyotrophic lateral sclerosis incorporate into stress granules. *Hum Mol Genet* 2010;19:4160–4175.
12. Lagier-Tourenne C, Polymenidou M, Cleveland DW. TDP-43 and FUS/TLS: emerging roles in RNA processing and neurodegeneration. *Hum Mol Genet* 2010;19(R1): R46–R64.
13. Naumann M, Pal A, Goswami A, et al. Impaired DNA damage response signaling by FUS-NLS mutations leads to neurodegeneration and FUS aggregate formation. *Nat Commun* 2018;9:335.
14. Qiu H, Lee S, Shang Y, et al. ALS-associated mutation FUS-R521C causes DNA damage and RNA splicing defects. *J Clin Invest* 2014;124:981–999.
15. Wang WY, Pan L, Su SC, et al. Interaction of FUS and HDAC1 regulates DNA damage response and repair in neurons. *Nat Neurosci* 2013;16:1383–1391.
16. Hicks GG, Singh N, Nashabi A, et al. Fus deficiency in mice results in defective B-lymphocyte development and activation, high levels of chromosomal instability and perinatal death. *Nat Genet* 2000;24:175–179.
17. Kuroda M, Sok J, Webb L, et al. Male sterility and enhanced radiation sensitivity in TLS(-/-) mice. *EMBO J* 2000;19:453–462.
18. Bajaj A, Driver JA, Schernhammer ES. Parkinson's disease and cancer risk: a systematic review and meta-analysis. *Cancer Causes Control* 2010;21:697–707.
19. Driver JA, Beiser A, Au R, et al. Inverse association between cancer and Alzheimer's disease: results from the Framingham Heart Study. *BMJ* 2012;344:e1442.
20. Fang F, Al-Chalabi A, Ronnevi LO, et al. Amyotrophic lateral sclerosis and cancer: a register-based study in Sweden. *Amyotroph Lateral Scler Frontotemporal Degener* 2013;14:362–368.
21. Brooks BR, Miller RG, Swash M, et al. El Escorial revisited: revised criteria for the diagnosis of amyotrophic lateral sclerosis. *Amyotroph Lateral Scler Other Motor Neuron Disord* 2000;1:293–299.
22. Haberland J, Bertz J, Wolf U, et al. German cancer statistics 2004. *BMC Cancer* 2010;22:52.
23. Chiò A, Logroscino G, Hardiman O, et al. Prognostic factors in ALS: A critical review. *Amyotroph Lateral Scler* 2009;10:310–323.
24. Rosenbohm A, Peter RS, Erhardt S, et al. Epidemiology of amyotrophic lateral sclerosis in Southern Germany. *J Neurol* 2017;264:749–757.
25. Higelin J, Demestre M, Putz S, et al. FUS mislocalization and vulnerability to DNA damage in ALS patients derived hiPSCs and aging motoneurons. *Front Cell Neurosci* 2016;10:290.
26. Corcia P, Danel V, Lacour A, et al. A novel mutation of the C-terminal amino acid of FUS (Y526C) strengthens FUS gene as the most frequent genetic factor in aggressive juvenile ALS. *Amyotroph Lateral Scler Frontotemporal Degener* 2017;18:298–301.
27. Ji J, Sundquist K, Sundquist J. Cancer incidence in patients with polyglutamine diseases: a population-based study in Sweden. *Lancet Oncol*. 2012;13: 642–648.
28. Reiman A, Srinivasan V, Barone G, et al. Lymphoid tumours and breast cancer in ataxia telangiectasia; substantial protective effect of residual ATM kinase activity against childhood tumours. *Br J Cancer* 2011;105:586–591.
29. Teive HA, Moro A, Moscovich M, et al. Ataxia-telangiectasia - A historical review and a proposal for a new designation: ATM syndrome. *J Neurol Sci* 2015;355:3–6.
30. Damme PV, Goris A, Race V, et al. The occurrence of mutations in FUS in a Belgian cohort of patients with familial ALS. *Eur J Neurol* 2010;17:754–756.



## Supporting Information

Additional supporting information may be found online in the Supporting Information section at the end of the article.

**Figure S1.** Depiction of the individual age of onset of all patients (cohort 1 and 2) relative to the median (39), which illustrates the clinical heterogeneity of the disease.

**Table S1.** FUS-ALS patients identified by pubmed review and novel patients

**Table S2.** Descriptive data of newly identified patients (cohort 1).

**Table S3.** Descriptive data of previously published cases (cohort 2).

**Table S4.** Descriptive data of the combined cohorts (cohort 1 + 2).

**Data S1.** Additional file providing raw data on published FUS-ALS cases including their source and descriptive data. Figure S1 similarly to Figure 1 depicts the individual AoO but for all patients of the study.

#### 4. Discussion

The presented publications demonstrate the successful use of human iPSC-derived sMNs for the modelling of FUS-ALS, which is extended by the effort to substantiate these results with the most comprehensive meta-analysis of FUS-ALS patients and their clinical symptoms to date. The *in-vitro* findings suggest that FUS-ALS is caused by an impaired DNA damage response, which subsequently leads to neurodegeneration and aggregate formation. Based on the live-cell imaging inhibitor experiments, a vicious cycle of FUS-nucleocytoplasmic traffic could be hypothesised. *FUS-NLS* mutations impaired the nuclear import of FUS and lowered its nuclear concentration. This resulted in a nuclear loss of function, which led to chronically increased signs of DNA damage. Subsequently, the constantly overactive DDR led to the exclusion of the remaining FUS from the nucleus by DNA-PK activity, which closed the vicious cycle by progressively reducing the nuclear FUS pool.

This theory of a primary nuclear dysfunction of FUS in the disease cascade challenges current therapeutic approaches that focus on mechanisms of protein aggregation and its clearance (Burke, Janke, Rhine, & Fawzi, 2015; Murakami et al., 2015; Patel et al., 2015). On the contrary, the work carried out implies that activation of DNA damage pathways in FUS-ALS is the key upstream event affecting both pathological protein aggregation and axonal trafficking. Therefore, intervening in DDR pathways could be more advantageous in terms of screening for therapeutic options. For example, inhibitors of PARP1 activity such as Olaparib have been approved by the FDA for the treatment of cancer with hereditary BRCA1 and BRCA2 mutations (Fong et al., 2009), and an inhibitor of PARG activity has recently been shown to make ovarian cells more susceptible to cell damage (Pillay et al., 2019). Thus, future ALS trials could benefit from this mutual interest in DNA damage response-interfering strategies. This could be clinically relevant in many ways. For example, PARP1 inhibition has recently been proposed as a therapeutic strategy for neurodegenerative diseases in general (Martire, Mosca, & d'Erme, 2015). However, the role of PARP1 in neurodegeneration is not yet fully understood. The experimental results of this work implied the inhibition of PARP1 as a functional phenotype copy of the mutated *FUS* condition. On the other hand, *PARP1* knockout mice were shown to be unremarkable except for higher rates of non-malignant skin diseases (Z. Q. Wang et al., 1995), suggesting that its function could be restored by other repair factors. However, others reported accelerated ageing, higher rates of malignant neoplasms, and increased aneuploidy in other *PARP1* knockout mouse strains (Piskunova et al., 2008; Simbulan-Rosenthal et al., 1999). Indeed, there is evidence that the functional outcome of sufficient DNA damage repair differs between PARP1 knockout and inhibition, the latter leading to an accumulation of PARP1 clusters at the DDS and a significant slowdown of SSB repair (Godon et al., 2008), while the former could lead to chromosomal aberrations. The abortive function in the SSB repair was recently shown for mutated *FUS* (H. Wang et al., 2018), suggesting that both *FUS* mutation

and PARP inhibition lead to a distal axonal phenotype via the SSB repair pathway and further downstream effectors in sMNs, which need to be investigated in future studies. One limitation of pharmacological PARP inhibition is the non-specific blockage of both PARP1 and PARP2 enzyme activity, which, however, mutually share functions in the DDR (Beck et al., 2014).

The strict regulation of PAR metabolism has become a new key element in the field of neurodegeneration in general in recent years. The pathological hyperactivity of PARP1 also seems to promote neuronal cell death. A growing list of rare neurodegenerative diseases has been shown to be characterised by PARP1 hyperactivation due to defective DNA damage repair mechanisms (E. F. Fang et al., 2014; Hoch et al., 2017). Furthermore, it has been shown to enhance the toxicity of alpha-synuclein, which adds a dysbalanced PAR metabolism to the pathogenesis of Parkinson's disease (Kam et al., 2018). If some of these diseases are mediated by the newly formed term "Parthanatos" (David, Andrabi, Dawson, & Dawson, 2009), a specific variant of cell death, which is caused by the mitochondrial release of AIF as a result of excessive PAR production (Yu et al., 2002), remains to be studied in the future. However, another mechanism that was discussed was the depletion of NAD<sup>+</sup> and acetyl-CoA following excessive PARP1 activity in a Xeroderma pigmentosum A cell model due to insufficient nucleotide excision repair (E. F. Fang et al., 2016). The authors found a reduced activity of the NAD<sup>+</sup>-dependant deacetylase sirtuin 1 (SIRT1), which led to lower deacetylation of the mitochondrial master transcription factor PGC1-alpha. PGC1-alpha has been described as a key regulator of mitochondrial homeostasis by indirectly modulating mitochondrial ROS and mitophagy, which are believed to be compromised by insufficient SIRT1-PGC1-alpha signalling. This mechanism would provide evidence for DNA-damage-induced nucleo-mitochondrial crosstalk in neurons, similar to that found in *Naumann & Pal et al. 2018*. In line with these considerations, a completely abolished PGC1-alpha signalling was observed in a neuronal model derived from iPSC with *FUS* C-terminal frameshift mutation (Bayer et al., 2017).

Furthermore, ATM has been shown to activate SIRT1 by phosphorylation, which in turn deacetylates HDAC1 in neurons after the induction of DSBs (Dobbin et al., 2013). One could hypothesize that nucleo-axonal impairment following DNA damage mediated by *FUS* insufficiency or direct induction of DNA damage, as demonstrated in Figure 5h (Naumann & Pal et al. 2018) could be related to the ATM-SIRT1-PGC1-alpha mechanism. It appears plausible that a primary physiological mechanism could exist in neurons that ensures mitochondrial spatial redistribution to the vicinity of the nucleus in case of constantly high nuclear DNA damage, which would require energy-consuming repair. However, constant neglect of axonal mitochondria and axonal energy demand could eventually lead to a potential Wallerian-like degeneration phenotype as previously suggested (Section 3.2.1). Nonetheless, experimental evidence for this theory is still missing. Importantly, another recent study also

described an axonal phenotype in iPSC-derived neurons with *FUS* mutation that was partially reversible after inhibition of cytoplasmic HDAC6 (Guo et al., 2017), confirming the findings presented here.

Taken together, both the chemical inhibition and the excessive activation of PARP1 lead to cell death via different pathways. Although inhibition of PARG improved the relevant phenotypes in the presented human sMNs with *FUS* mutation (Figure 6g, Naumann & Pal et al. 2018), the long-term effects on cellular survival must be evaluated because of the hazardous effect of PAR accumulation on neuronal survival and mitophagy (E. F. Fang et al., 2014; Hoch et al., 2017). Furthermore, more emphasis should be put on the respective PAR levels when intervening in its *in-vitro* generation or degradation. Mild PARP1 inhibition could have been beneficial in the sMN *FUS* mutant cell model as proposed for other neurodegenerative diseases.

Evidence of a role in the DDR has been reported for many ALS-related proteins, but currently, only the importance of *FUS* in this setting is corroborated by a growing number of publications. However, the influence of *FUS*-NLS mutations associated with ALS on the DDR was reported in different ways. While the presented publication and another one (Rulten et al., 2014) argue for a clear pathological involvement, others saw only minor changes in *FUS* mutants (Mastrocola et al., 2013a) or no differences at all (W. Y. Wang et al., 2013). The variety of these observations could be explained by the application of different cell models and *FUS* overexpression methods. In particular, the study by Wang et al. (2013) was very well-conceived, and strict control of the expression levels was given. However, their use of murine primary neuronal culture with ectopic expression of human *FUS* appears to be difficult to compare with endogenous *FUS* in human neuronal cells. This is underlined by a recent study based on a human neuronal model derived from hiPSC, which demonstrated the importance of *FUS* in the single-stranded DNA damage repair pathway (H. Wang et al., 2018). A role in homologous recombination or NHEJ pathways of DSB repair for *FUS* was not described in this study, which is in contrast to the murine-based study (W. Y. Wang et al., 2013), which demonstrated that *FUS* physically interacts with HDAC1 to ensure DSB repair. This would also be in line with the experimental results indicating sufficient DSB repair after etoposide treatment in both WT and *FUS* mutated neurons (Figure 5e, f; Naumann & Pal et al. 2018). Importantly, *FUS* is subject to N-terminal phosphorylation by ATM (Gardiner, Toth, Vandermoere, Morrice, & Rouse, 2008) and DNA-PK (Deng et al., 2014). More importantly, phosphorylation by DNA-PK after NHEJ activation leads to nuclear egress of the P-*FUS* into the cytoplasm. However, the biological relevance of this process is unclear to date. It is speculative if *FUS* could be important primarily for a sufficient DDR, but has to fulfil another task in the cytoplasm, secondary to the DNA damage induction. A major drawback of the study by Deng et al. (2014) was a relatively strong presence of cytoplasmic *FUS* in the control

conditions without induction of DNA damage. Although there are other reports that contradict a nucleo-cytoplasmic shift of phosphorylated FUS (Rhoads et al., 2018), the data presented in *Naumann & Pal et al. (2018)* argue in favour of a cytoplasmic translocation of FUS via DNA-PK-mediated phosphorylation. It could be shown that after treatment with etoposide, there was a delayed shift of FUS-WT-GFP into the cytoplasm. Of note is that upon pharmacological PARP inhibition, this process was visually even faster, presumably due to the disruption of its nuclear tether. Both conditions led to the observed axonal phenotype. On the contrary, pharmacological inhibition of the DNA-PK enzyme caused a shift of FUS-P525L-GFP into the nucleus, thus restoring sufficient recruitment to the DDS. Interestingly, under this condition, the signal peak was lower at the DDS but more extended than in the WT mock condition (Figure 6d; *Naumann & Pal et al. 2018*), suggesting an influence of posttranslational modifications on local protein organisation. In parallel, the initially detected axonal mitochondrial phenotype was similarly reversed in the mutant sMNs after DNA-PK inhibition.

Apart from its influence on the shuttling of FUS, it has also been reported that the N-terminal phosphorylation of FUS by DNA-PK attenuates liquid-liquid phase separation of multiple FUS proteins (Han et al., 2012; Monahan et al., 2017). This self-aggregation process, which is mediated by the interaction of the low-complexity domains of the respective FUS proteins, leads to the formation of viscous, membrane-less compartments at physiological concentrations (Patel et al., 2015). This formation could be related to the physiological processes in which FUS is involved, for instance, DNA repair and the formation of stress granules. However, it has been shown that FUS-ALS-associated mutations alter the equilibrium of the phase-separated droplets and thus induce a liquid-to-solid phase transition. It is assumed that the resulting irreversible aggregates have a significant influence on cellular survival (Patel et al., 2015). Blocking the activity of DNA-PK, which possibly dissolves the phase-separated FUS droplets, would therefore probably worsen the disease condition. On the other hand, there is growing evidence for the necessity of an active change in this phase-separated status to facilitate physiological processes such as DNA repair. Phase separation of proteins has been proposed as a key condition for the shaping of the DNA damage site for efficient repair (Nott et al., 2016). It has been shown that the nascent droplets act as filters for proteins associated with DNA damage repair and that they stabilize ssDNA and melt dsDNA. Moreover, the seeding of the negatively charged biopolymer PAR greatly increased the phase separation of the FET protein family involving FUS, TAF15, and EWS at the DDS (Altmeyer et al., 2015), which was shown to be mediated by electrostatic interaction with the positively charged RGG in their N-terminal domains. The higher complexity of this compartment could allow the spatial and temporal control of such elemental processes as the DDR, which is corroborated by the dynamic exchange of constituents through posttranslational modification such as phosphorylation or ubiquitination (Altmeyer et al., 2015) that regulate the sequence of

the DDR. Thus, there is growing evidence that FUS is a very early factor in the DDR cascade. However, the N-terminal phosphorylation at different S/T-Q motifs would hypothetically abolish the PAR interaction, which would lead to the exclusion of P-FUS from the DNA damage compartment. That way, it would be ensured that more downstream proteins can get access to the DDS and perform their function. As a consequence, this could secondarily lead to a passive egress of FUS into the cytoplasm (Deng et al., 2014). Whether there is another biological purpose for P-FUS in the cytoplasm after the DDR or whether this is only a stalling technique needs to be investigated in future studies. Nonetheless, this reasoning would explain the improvement of the cytoplasmic phenotype in mutated FUS sMNs by DNA-PK inhibition. It suggests a possibility to break the vicious cycle caused by a less efficient nuclear import of mutated FUS, resulting in a diminished DNA damage repair, higher rates of DNA damage, and even more FUS phosphorylation. If these considerations prove plausible, two questions arise. (1) Phosphorylated cytoplasmic FUS should be protected from liquid-liquid segregation and subsequent liquid-to-solid phase transition. Which phosphatases are responsible for the dephosphorylation of P-FUS and, by inhibiting them, would that prevent the formation of cytoplasmic FUS aggregates and even more so their spreading? (2) Would it be safe to inhibit DNA-PK in a long-term manner considering that DNA-PKc-deficient mice showed accelerated ageing (Espejel et al., 2004), or are there other post-translational modifiers that could cope with the loss? However, as the main component of the NHEJ, DNA-PK is likely to be irreplaceable for this instance, but not for its presumed function in spatially and temporally regulating the membrane-less DDR compartment by phosphorylation of FUS, which could be hypothesised considering that DNA-PK inhibition might prolong the presence of FUS-GFP at the DDS (Figure 6d; Naumann & Pal et al. 2018). In summary, both DNA-PK and PARG inhibition lead to complex and partially not well-understood biomolecular consequences, but they offer potential therapeutic options for (FUS)-ALS patients. At present, however, much more evidence of the efficacy and safety of these inhibitors must be gathered, including in animal models, before possible human trials can be discussed.

To dynamically measure the extent of FUS mislocalisation, recruitment to the DDS and protein aggregation, isogenic iPSC-derived neuronal lines with GFP tagged FUS generated by CRISPR/Cas9n were applied. Thus, isogenic control conditions were given, which implied that the obtained results can only be explained by the underlying heterozygous *FUS* mutation. The influence of random Cas9n integration events on the results seemed less likely due to the strategy of designing the probes (Material & Methods, Naumann & Pal et al. 2018). At present, there is no evidence of a clear bias of the GFP tag as all relevant phenotypes could be reproduced in a similar way by using iPSC-derived neurons with endogenous *FUS* mutation from affected patients, who evidently suffered from the disease.



It is assumed that the classical NHEJ is the main resource for DSB repair in neurons, due to their post-mitotic state in contrast to the highly efficient homologous recombination through which cycling cells predominantly repair occurring DSBs. The latter requires the presence of the identical sister chromatid, which is present during late S- and G2-phases of the cell cycle, but allows for error-free repair. Therefore, DSBs represent a serious condition for neurons that are only able to perform the error-prone NHEJ or the even less accurate microhomology-mediated end joining. Therefore, critical control and rapid repair of more benign damage entities like DNA single-strand nicks are essential to prevent transformation to hazardous DSBs as part of the genome protection for neurons. Consequently, it is widely accepted that mutations in DNA damage repair factors lead disproportionately often to neurological phenotypes. Previous reports and the presented publication (Naumann et al. 2019) thus add FUS-ALS to the class of neurodegenerative diseases with impaired DDR signalling, such as Ataxia telangiectasia (A-T), AOA1 (Ataxia oculomotor apraxia), AOA2, SCA3 (Spinocerebellar ataxia), SCAN1, and SCAN2 (Spinocerebellar ataxia with axonal neuropathy) (Madabhushi, Pan, & Tsai, 2014; Reynolds & Stewart, 2013). Of note is that the A-T syndrome is characterized by more than purely neurological symptoms, as it is evident in the other syndromes listed. Biallelic mutations of *ATM* in A-T are associated with a higher prevalence for lymphoma, leukaemia, or breast cancer (Stankovic et al., 1998). Importantly, *FUS*  $-/-$  mice were reported to exhibit high genomic instability (Hicks et al., 2000) and increased radiation sensitivity (Kuroda et al., 2000), which has also been reported for A-T. Moreover, it has been demonstrated that neurodegenerative diseases in general correlate with altered risk of cancer. There is evidence for lower risk in Alzheimer's and Parkinson's disease (Bajaj, Driver, & Schernhammer, 2010; Driver et al., 2012), whereas, in a register-based study, no difference could be found in ALS patients compared to the general population (F. Fang et al., 2013). The question of whether FUS-ALS patients are therefore more susceptible to the development of malignant disease or hypersensitive to radiation was of immense clinical importance as radiation of salivary glands could currently be used to treat pseudohypersalivation in ALS patients. However, the multicentre retrospective analysis identified only one in 40 FUS-ALS patients who had leukaemia in his childhood. From the genetic point of view, he harboured a frameshift mutation that functionally affected the C-terminal NLS of FUS. Importantly, his derived iPSC, neural progenitor cells, and sMNs all exhibited a clear cytoplasmatic FUS signal (data not shown) and dramatically increased DNA damage as indicated by staining for gamma-H2A.X (Figure 5g; Naumann & Pal et al. 2018). On the other hand, many other studied FUS-ALS patients showed in some cases even worse neurological symptoms and striking signs of DNA damage, without any documented malignant disease suggesting the influence of additional protective factors. However, due to the small patient cohort, it is difficult to obtain a statistically convincing result, but considering the prevalence of around 3-5 per 10,000,000,

implies the difficulty of the need for bigger cohorts. Furthermore, it appeared possible that a higher susceptibility to malignant cell transformations could be masked by the very limited survival time of patients as well as the young onset of the disease. However, from a clinical point of view, FUS-ALS is similar to the other neurological conditions mentioned above in that they are all characterized exclusively by neurological symptoms, while A-T patients additionally suffer from telangiectasias, pulmonary and endocrine dysfunction, immunodeficiency, and an increased risk of some malignant neoplasms (Verhagen et al., 2012). A possible explanation for the absence of malignancies in neurological disorders associated with impaired SSB nick repair like FUS-ALS (H. Wang et al., 2018), AOA1, AOA2, and SCAN1 (Reynolds & Stewart, 2013) could be that in non-neuronal cells, regular ATM activity provides sufficient control of the cell cycle and p53-mediated apoptosis mechanisms, thereby diminishing the influence of accumulated DNA damage, but this is not the case in A-T due to loss of ATM function. Taken together, no increased risk of cancer in FUS-ALS patients could be identified in the cohort surveyed. Nonetheless, prospective studies are recommended, especially involving unaffected family members who carry the heterozygous mutation without exhibiting neurological symptoms. The reasons for the incomplete penetrance are not known, but it appeared that the clinically more benign mutations at the R521 locus were more likely associated with a familial pattern, while the most severe mutations such as P525L were found only sporadically, probably due to the young age at onset or a possible negative effect on the egg/sperm cells. The presented, so far most comprehensive phenotype-genotype correlation for FUS-ALS patients could in the future enable better counselling of newly diagnosed patients when evaluating the individual course of the disease.

## 5. Summary

**Background:** The submitted cumulative dissertation is based on two intertwined main studies with biomolecular foundation and clinical perspective on FUS-ALS complemented by two follow-up projects. This subtype of Amyotrophic lateral sclerosis is caused by heterozygous mutations mainly in the NLS of the *FUS* gene, which interferes with the proper nuclear import of the gene product. To date, there is no sufficient therapy available for this devastating neurodegenerative disease due to an incomplete pathophysiological understanding. Furthermore, not much is known about the specific clinical phenotype of FUS-ALS patients, including the influence of distinct *FUS* mutations due to the rarity of the disease. FUS is a DNA/RNA-binding protein that is mainly located in the nucleus and has essential functions in splicing, mRNA transport, transcription, and DNA damage repair.

### Hypothesis:

1. It was hypothesized that the human-induced pluripotent stem-cell technique enables to create a sufficient motor neuron *in-vitro* cell model, which should provide new insights into unknown pathophysiological processes compared to previous cell models of FUS-ALS due to its patient-specific and human character. Thus, screening for potential therapeutic substances should be feasible using this model system.
2. Judging from the previously demonstrated, essential function of FUS in the DNA damage repair, *FUS* mutations are expected to increase the risk of malignant diseases in affected patients. Moreover, specific correlations between the nature of the mutation and the clinical, neurological phenotype appear plausible.

**Material & methods:** First, an *in-vitro* cell culture model of FUS-ALS was established. For this purpose, a patient-specific, induced pluripotent stem cell-derived SMN culture was generated, which contained spinal motor neurons with mutations in the gene *FUS* or WT control cells. The Microfluidic Chamber system was used for the selective analysis of axons, which enabled the live-cell imaging of lysosomes and mitochondria using TIRF microscopy. For the analysis of DNA damage and its repair, gamma-H2A.X immunofluorescence staining was used on the one hand and live-cell laser ablation microscopy on the other, which allowed the precise induction of DNA damage and the monitoring of the repair response. For this purpose, isogenic FUS-GFP cell lines generated via CRISPR-Cas9n were used. A multicentre, retrospective cross-sectional study was conducted to determine genotype-phenotype correlations and the prevalence of malignant neoplasms in FUS-ALS. Previously published FUS-ALS cases have been added to perform a meta-analysis of clinical features.

**Results:** Primarily, correct neuronal differentiation was observed prior to neurodegenerative phenotypes, perfectly mimicking a neurodegenerative disease in the dish. The typical cellular

pathology of cytoplasmatic FUS deposition could be reproduced, making it a suitable model for more in-depth pathophysiological studies. Furthermore, the use of Microfluidic Chambers enabled the guided cultivation of neurons with somato-axonal direction of neurite outgrowth along tiny microchannels *in silico*, resulting in a pure motoneuronal, axonal model. Within the distal axonal compartment of these channels, a loss of motility of both lysosomes and mitochondria was observed in parallel with a loss of the mitochondrial membrane potential, followed by the secondary degeneration of the distal axons of the sMNs with *FUS* mutation. A pathological increase in nuclear DNA damage has been identified as the cause of the distal-axonal phenotypes. This was due to a reduced nuclear FUS abundance as a result of the *FUS*-NLS mutation, which impaired proper nuclear import. There was evidence of a vicious cycle in this setting because the loss of the nuclear function of FUS disrupted the proper PAR-dependent DNA damage response, resulting in sustained DNA damage. Moreover, the remaining nuclear FUS was transferred into the cytoplasm upon phosphorylation by DNA-PK in a DNA damage response dependent manner, which is to date a process of unclear biological relevance. However, pharmacological inhibition of either the degradation of the PAR biopolymer or DNA-PK improved the nuclear presence of mutant FUS, restored its function in the DNA damage response, and finally prevented the distal axonal phenotype.

Furthermore, the multicentric cohort study included 36 newly diagnosed patients. Only one in 40 patients was diagnosed with a malignant disease. By combining the newly diagnosed patients with previously published cases (186 cases in total), the so far most comprehensive database of *FUS*-ALS patients has been created. This allowed a thorough genotype-phenotype analysis, which showed a clear correlation between individual *FUS* mutations and the clinical phenotype.

**Conclusion:** The experimental results indicated a primary nuclear insufficiency of mutated *FUS*, which is due to an impaired nuclear import and leads to a secondary axonal degeneration and finally to neuronal demise (“Dying-Back”). Potential therapeutic options have been identified, but their applicability and safety must be determined in prospective studies. The hypothesis of a generally increased risk of malignant diseases in the analysed *FUS*-ALS patient group was rejected. However, the clinical data of the meta-analysis are helpful in the counselling of newly diagnosed *FUS*-ALS patients, including the decision making of the therapeutic management and clearly add *FUS*-ALS to the family of diseases characterised by deficient DNA damage repair with purely neurological phenotypes such as AOA1, AOA2, and SCAN1.

## 6. Zusammenfassung

**Hintergrund:** Die vorgelegte Arbeit beinhaltet die Vereinigung zweier ineinandergreifender Hauptprojekte mit grundlagenwissenschaftlicher Ausgangslage und klinischer Perspektive zur Pathophysiologie der FUS-ALS, die ergänzt werden von zwei aufbauenden Nachfolgeprojekten. Als Unterform der Amyotrophen Lateralsklerose wird die FUS-ALS durch heterozygote Mutationen in der NLS des *FUS* Gens verursacht, wodurch der physiologische, nukleäre Import des Genprodukts beeinträchtigt wird. Für diese schwere neurodegenerative Krankheit existiert bis heute keine zufriedenstellende Therapie aufgrund unvollständiger Kenntnis der pathologischen Mechanismen. Durch die Seltenheit der Krankheit ist der klinische Phänotyp der FUS-ALS wenig charakterisiert auch im Hinblick des Einflusses verschiedener *FUS* Mutationen. FUS ist als DNS/RNS-bindendes, primär nukleäres Protein essentiell beteiligt an zellbiologischen Prozessen wie Splicing, mRNA Transport oder DNS Schaden Reparatur.

### **Hypothese:**

1. Es wurde hypothetisiert, dass die humane, induzierte pluripotente Stammzelltechnik die Generierung eines suffizienten *in vitro* Motoneuronmodells ermöglicht, welches neue Erkenntnisse zu bisher unbekanntem pathophysiologischen Prozessen ermöglichen sollte im Vergleich zu bisherigen Zellmodellen der FUS-ALS aufgrund des Patienten-spezifischen und humanen Charakters. Unter Verwendung dieses Modells sollten nachfolgend Screeningverfahren zur Testung potentieller Therapeutika möglich sein.
2. Basierend auf der bekannten, essentiellen Funktion von FUS im Rahmen der DNS Schadenreparatur ist ein generell erhöhtes Risiko an malignen Neoplasien zu erkranken im Falle von *FUS* Mutationen für betroffene Patienten zu erwarten. Weiterhin erscheint es plausibel, dass verschiedene *FUS* Mutationen assoziiert sind mit spezifischen, klinisch-neurologischen Phänotypen

**Material & Methoden:** Im ersten Schritt wurde ein *in vitro* Zellkulturmodell der FUS-ALS etabliert. Dazu wurden Patienten-spezifische, von induzierten pluripotenten Stammzellen abgeleitet, spinale Motoneurone mit heterozygoten Mutationen im *FUS* Gen generiert. Zur selektiven Analyse von Axonen gelang die Kultivierung in Microfluidic Chambers. Darin wurden mittels live-cell-imaging TIRF Mikroskopie Lysosomen und Mitochondrien visualisiert. Zur Analyse von DNS Schäden wurde zum einen die gamma-H2A.X Immunfluoreszenzfärbung verwendet, zum anderen Laserablationsmikroskopie um in lebenden Zellen zeitlich und räumlich präzise DNS Schaden zu induzieren und dynamisch die Reparaturantwort darzustellen. Dazu wurden isogene FUS-GFP Zelllinien verwendet, die zuvor mittels CRISPR-Cas9n kreiert und zur Verfügung gestellt worden sind. Zur Erfassung des klinischen Phänotyps

erfolgte eine multizentrische, retrospektive Studie neuer FUS-ALS Patienten und Metaanalyse mit bereits publizierten Fällen.

**Ergebnisse:** Es wurde primär regelrechte neuronale Differenzierung der FUS-ALS MN beobachtet, bevor sich ein neurodegenerativer Phänotyp *in-vitro* entwickelte passend zum Charakter neurodegenerativer Erkrankungen. Die typische zelluläre Pathologie in Form von zytoplasmatischen FUS Ablagerungen konnte im Anschluss in spinalen humanen Motoneuronen dargestellt werden, sodass von einem suffizienten Modell auszugehen war. Unter Verwendung sogenannter Microfluidic Chambers gelang die gerichtete Kultivierung der Neurone mit somato-axonaler Orientierung des Neuritenauswuchses entlang von Mikrokanälen *in-silico*. Dabei wurde ein distal axonaler Phänotyp im Sinne eines Motilitätsverlusts von Mitochondrien und Lysosomen und Zusammenbruch des mitochondrialen Membranpotentials gesehen, gefolgt vom progredienten Verlust der Axone spinaler Motoneurone mit *FUS* Mutation. Diese pathologische Veränderung konnte kausal auf erhöhten nukleären DNS Schaden zurückgeführt werden. Experimentell wurde ursächlich eine verminderte nukleäre FUS Konzentration identifiziert, was zu einem pathologischen Teufelskreis führte, da der nukleäre Funktionsverlust von FUS PAR-abhängige DNS Reparaturprozesse negativ beeinflusste, woraus chronische DNS Schädigung und Reparaturantwort folgte. Der verbleibende nukleäre FUS Pool wurde darauf weiterhin vermindert durch DNS Reparatur assoziierte DNA-PK Aktivität, was zur Phosphorylierung und nachfolgend zytoplasmatischen Translokation von FUS führte. Die biologische Funktion dieses Prozesses bleibt bis jetzt unklar. Durch Inhibition des Abbaus des PAR Biopolymers oder der DNA-PK konnte die nukleäre Konzentration von mutiertem FUS erhöht werden, was sowohl die Funktion im Rahmen der DNS Reparatur wiederherstellte, als auch den axonalen Phänotyp verhinderte.

Weiterhin wurden im Rahmen der multizentrischen, retrospektiven Studie 36 neu diagnostizierte FUS-ALS Patienten beschrieben. Nur in einem von 40 Fällen wurde eine maligne Tumorerkrankung festgestellt. Unter Einbeziehung bisher publizierter Patienten umfasste die Metaanalyse anamnestischer und klinischer Parameter insgesamt 186 Patienten. Die Genotyp-Phänotyp Analyse zeigte klare Zusammenhänge zwischen der Art und Lokalisation individueller Mutationen im *FUS* Gen und dem klinischen Phänotyp.

**Schlussfolgerung:** Die Zellkulturdaten weisen auf eine primär nukleäre Insuffizienz des FUS Proteins hin, was zu sekundärer axonaler Schädigung und letztlich axoneuronalem Zelltod führte („Dying-Back“). Potentiell kausale Therapeutika wurden identifiziert, die zukünftig weiter untersucht werden müssen hinsichtlich Wirksamkeit und Sicherheit. Die Hypothese eines erhöhten Risikos für maligne Erkrankungen in der FUS-ALS Studienpopulation wurde abgelehnt. Allerdings können die Daten der Metaanalyse genutzt werden bei der Beratung und



therapeutischem Management neuer FUS-ALS Patienten in der klinischen Praxis und erlauben eine Einordnung der FUS-ALS in die Familie von Krankheiten mit ausschließlich neurologischem Phänotyp und gestörter DNA Schaden Reparatur wie AOA1, AOA2 and SCAN1.

## 7. Acknowledgements

This work would not have been possible without the constant support and help of the team within the groups of Prof. Dr. Dr. A. Hermann and Prof. Dr. A. Storch. This project was carried out in close partnership with Dr. rer. nat. Arun Pal. His commitment had a particular impact on this project, which would not have had the same high quality without him. He introduced many practical experiments, methods (including TIRF and laser ablation microscopy), and scientific ideas, making a great and significant contribution to our joint paper *Naumann & Pal et al.* (2018). Similarly, I would like to thank Prof. Dr. Dr. A. Hermann, who provided me with this interesting project, which opened up the world of science to me, which influences and will always have an impact on my thinking and my work. He never tired of discussing new aspects and scientific ideas, and not rarely, he contributed to the planning and scheduling of new experiments at all hours of the day. Furthermore, I would like to express my special thanks to Dr. Hannes Glass, whose support and friendship cannot be described in mere words. If a problem arose in the lab, he knew what to do. For their help in the preparation of the hiPSC culture and the provision of various cell lines, I would like to thank Dr. Xenia Lojewski, Dr. Peter Reinhard, and Dr. Jared Sternecker, including Dr. Julia Japtok, for creating the processed CRISPR-Cas9n cell lines. Furthermore, I would like to express my gratitude to Dr. Anand Goswami, Prof. Dr. Joachim Weis, and Prof. Dr. Eleonora Aronica for their significant contribution to the post-mortem FUS-ALS studies. My special thanks go to the Light Microscopy Facility (LMF) of CMCB (Center for Molecular and Cellular Bioengineering, *Technische Universität Dresden*) for their help in questions of imaging issues and the creation of efficient readout software (Dr. Ronny Czech). Moreover, my thanks are due to Prof. Dr. Stephan Grill for the excellent help he provided by enabling Dr. Pal and me to perform the laser ablation assay in his laboratory, and to Prof. Dr. Nils Cordes and Dr. Anne Vehlow for their advice on DNA damage-related assays and contribution on the Western blot data. I also would like to deeply acknowledge the support of the *Else-Kröner-Promotionskolleg*, which was founded by Prof. Dr. A. Deußen at the Medical Faculty of the Technical University Dresden with the help of the Else-Kröner-Fresenius Stiftung, because it paved my first steps in science. In addition, this work was supported by the *Deutsche Gesellschaft für Muskelerkrankungen* (He2/2), the Roland Ernst Stiftung Saxony, the MeDDrive program of the Medical Faculty at the Technical University Dresden, the BIOCREA GMBH, the NOMIS Foundation and the Helmholtz Virtual Institute 'RNA dysmetabolism in ALS and FTD (VH-VI-510)'. It is important that my thanks and condolences go to the patients and their families. Finally, I would like to thank my family, my parents, my brother Philipp, and my girlfriend Anna for their interest and perseverance that this work required. Especially my grandmother was always very interested to hear what I was doing with the 'worms' in the laboratory.

## 8. References

- Akiyama, T., Warita, H., Kato, M., Nishiyama, A., Izumi, R., Ikeda, C., Kamada, M., Suzuki, N., & Aoki, M. (2016). Genotype-phenotype relationships in familial amyotrophic lateral sclerosis with FUS/TLS mutations in Japan. *Muscle Nerve*, *54*(3), 398-404. doi:10.1002/mus.25061
- Al-Chalabi, A., & Hardiman, O. (2013). The epidemiology of ALS: a conspiracy of genes, environment and time. *Nat Rev Neurol*, *9*(11), 617-628. doi:10.1038/nrneurol.2013.203
- Altmeyer, M., Neelsen, K. J., Teloni, F., Pozdnyakova, I., Pellegrino, S., Grøfte, M., Rask, M. D., Streicher, W., Jungmichel, S., Nielsen, M. L., & Lukas, J. (2015). Liquid demixing of intrinsically disordered proteins is seeded by poly(ADP-ribose). *Nat Commun*, *6*, 8088. doi:10.1038/ncomms9088
- Baechtold, H., Kuroda, M., Sok, J., Ron, D., Lopez, B. S., & Akhmedov, A. T. (1999). Human 75-kDa DNA-pairing protein is identical to the pro-oncoprotein TLS/FUS and is able to promote D-loop formation. *J Biol Chem*, *274*(48), 34337-34342. doi:10.1074/jbc.274.48.34337
- Bajaj, A., Driver, J. A., & Schernhammer, E. S. (2010). Parkinson's disease and cancer risk: a systematic review and meta-analysis. *Cancer Causes Control*, *21*(5), 697-707. doi:10.1007/s10552-009-9497-6
- Bayer, H., Lang, K., Buck, E., Higelin, J., Barteczko, L., Pasquarelli, N., Sprissler, J., Lucas, T., Holzmann, K., Demestre, M., Lindenberg, K. S., Danzer, K. M., Boeckers, T., Ludolph, A. C., Dupuis, L., Weydt, P., & Witting, A. (2017). ALS-causing mutations differentially affect PGC-1 $\alpha$  expression and function in the brain vs. peripheral tissues. *Neurobiol Dis*, *97*(Pt A), 36-45. doi:10.1016/j.nbd.2016.11.001
- Beck, C., Robert, I., Reina-San-Martin, B., Schreiber, V., & Dantzer, F. (2014). Poly(ADP-ribose) polymerases in double-strand break repair: focus on PARP1, PARP2 and PARP3. *Exp. Cell Res.*, *329*(1), 18-25.
- Bertrand, P., Akhmedov, A. T., Delacote, F., Durrbach, A., & Lopez, B. S. (1999). Human POMp75 is identified as the pro-oncoprotein TLS/FUS: both POMp75 and POMp100 DNA homologous pairing activities are associated to cell proliferation. *Oncogene*, *18*(31), 4515-4521. doi:10.1038/sj.onc.1203048

- Bosco, D. A., Lemay, N., Ko, H. K., Zhou, H., Burke, C., Kwiatkowski, T. J., Sapp, P., McKenna-Yasek, D., Brown, R. H., & Hayward, L. J. (2010). Mutant FUS proteins that cause amyotrophic lateral sclerosis incorporate into stress granules. *Hum Mol Genet*, *19*(21), 4160-4175. doi:10.1093/hmg/ddq335
- Brenner, D., & Weishaupt, J. H. (2019). Update on amyotrophic lateral sclerosis genetics. *Curr Opin Neurol*, *32*(5), 735-739. doi:10.1097/WCO.0000000000000737
- Burke, K. A., Janke, A. M., Rhine, C. L., & Fawzi, N. L. (2015). Residue-by-Residue View of In Vitro FUS Granules that Bind the C-Terminal Domain of RNA Polymerase II. *Mol Cell*, *60*(2), 231-241. doi:10.1016/j.molcel.2015.09.006
- Conte, A., Lattante, S., Zollino, M., Marangi, G., Luigetti, M., Del Grande, A., Servidei, S., Trombetta, F., & Sabatelli, M. (2012). P525L FUS mutation is consistently associated with a severe form of juvenile amyotrophic lateral sclerosis. *Neuromuscul Disord*, *22*(1), 73-75. doi:10.1016/j.nmd.2011.08.003
- Crozat, A., Aman, P., Mandahl, N., & Ron, D. (1993). Fusion of CHOP to a novel RNA-binding protein in human myxoid liposarcoma. *Nature*, *363*(6430), 640-644.
- Cudkovicz, M. E., Katz, J., Moore, D. H., O'Neill, G., Glass, J. D., Mitsumoto, H., Appel, S., Ravina, B., Kiebertz, K., Shoulson, I., Kaufmann, P., Khan, J., Simpson, E., Shefner, J., Levin, B., Cwik, V., Schoenfeld, D., Aggarwal, S., McDermott, M. P., & Miller, R. G. (2010). Toward more efficient clinical trials for amyotrophic lateral sclerosis. *Amyotroph Lateral Scler*, *11*(3), 259-265. doi:10.3109/17482960903358865
- David, K. K., Andrabi, S. A., Dawson, T. M., & Dawson, V. L. (2009). Parthanatos, a messenger of death. *Front Biosci (Landmark Ed)*, *14*, 1116-1128. doi:10.2741/3297
- De Vos, K. J., & Hafezparast, M. (2017). Neurobiology of axonal transport defects in motor neuron diseases: Opportunities for translational research? *Neurobiol Dis*, *105*, 283-299. doi:10.1016/j.nbd.2017.02.004
- Deng, Q., Holler, C. J., Taylor, G., Hudson, K. F., Watkins, W., Gearing, M., Ito, D., Murray, M. E., Dickson, D. W., Seyfried, N. T., & Kukar, T. (2014). FUS is phosphorylated by DNA-PK and accumulates in the cytoplasm after DNA damage. *J. Neurosci.*, *34*(23), 7802-7813.
- Devoy, A., Kalmar, B., Stewart, M., Park, H., Burke, B., Noy, S. J., Redhead, Y., Humphrey, J., Lo, K., Jaeger, J., Mejia Maza, A., Sivakumar, P., Bertolin, C., Soraru, G., Plagnol, V., Greensmith, L., Acevedo Arozena, A., Isaacs, A. M., Davies, B., Fratta, P., &

- Fisher, E. M. C. (2017). Humanized mutant FUS drives progressive motor neuron degeneration without aggregation in 'FUSDelta14' knockin mice. *Brain*, *140*(11), 2797-2805. doi:10.1093/brain/awx248
- Dobbin, M. M., Madabhushi, R., Pan, L., Chen, Y., Kim, D., Gao, J., Ahanonu, B., Pao, P. C., Qiu, Y., Zhao, Y., & Tsai, L. H. (2013). SIRT1 collaborates with ATM and HDAC1 to maintain genomic stability in neurons. *Nat. Neurosci.*, *16*(8), 1008-1015.
- Dormann, D., Madl, T., Valori, C. F., Bentmann, E., Tahirovic, S., Abou-Ajram, C., Kremmer, E., Ansorge, O., Mackenzie, I. R., Neumann, M., & Haass, C. (2012). Arginine methylation next to the PY-NLS modulates Transportin binding and nuclear import of FUS. *EMBO J.*, *31*(22), 4258-4275.
- Dormann, D., Rodde, R., Edbauer, D., Bentmann, E., Fischer, I., Hruscha, A., Than, M. E., Mackenzie, I. R., Capell, A., Schmid, B., Neumann, M., & Haass, C. (2010). ALS-associated fused in sarcoma (FUS) mutations disrupt Transportin-mediated nuclear import. *EMBO J.*, *29*(16), 2841-2857.
- Driver, J. A., Beiser, A., Au, R., Kreger, B. E., Splansky, G. L., Kurth, T., Kiel, D. P., Lu, K. P., Seshadri, S., & Wolf, P. A. (2012). Inverse association between cancer and Alzheimer's disease: results from the Framingham Heart Study. *BMJ*, *344*, e1442. doi:10.1136/bmj.e1442
- Espejel, S., Martín, M., Klatt, P., Martín-Caballero, J., Flores, J. M., & Blasco, M. A. (2004). Shorter telomeres, accelerated ageing and increased lymphoma in DNA-PKcs-deficient mice. *EMBO Rep*, *5*(5), 503-509. doi:10.1038/sj.embor.7400127
- Fang, E. F., Scheibye-Knudsen, M., Brace, L. E., Kassahun, H., SenGupta, T., Nilsen, H., Mitchell, J. R., Croteau, D. L., & Bohr, V. A. (2014). Defective mitophagy in XPA via PARP-1 hyperactivation and NAD(+)/SIRT1 reduction. *Cell*, *157*(4), 882-896. doi:10.1016/j.cell.2014.03.026
- Fang, E. F., Scheibye-Knudsen, M., Chua, K. F., Mattson, M. P., Croteau, D. L., & Bohr, V. A. (2016). Nuclear DNA damage signalling to mitochondria in ageing. *Nat Rev Mol Cell Biol*, *17*(5), 308-321. doi:10.1038/nrm.2016.14
- Fang, F., Al-Chalabi, A., Ronnevi, L. O., Turner, M. R., Wirdefeldt, K., Kamel, F., & Ye, W. (2013). Amyotrophic lateral sclerosis and cancer: a register-based study in Sweden. *Amyotroph Lateral Scler Frontotemporal Degener*, *14*(5-6), 362-368. doi:10.3109/21678421.2013.775309

- Fong, P. C., Boss, D. S., Yap, T. A., Tutt, A., Wu, P., Mergui-Roelvink, M., Mortimer, P., Swaisland, H., Lau, A., O'Connor, M. J., Ashworth, A., Carmichael, J., Kaye, S. B., Schellens, J. H., & de Bono, J. S. (2009). Inhibition of poly(ADP-ribose) polymerase in tumors from BRCA mutation carriers. *N Engl J Med*, *361*(2), 123-134. doi:10.1056/NEJMoa0900212
- Gardiner, M., Toth, R., Vandermoere, F., Morrice, N. A., & Rouse, J. (2008). Identification and characterization of FUS/TLS as a new target of ATM. *Biochem. J.*, *415*(2), 297-307.
- Ghasemi, M., & Brown, R. H. (2018). Genetics of Amyotrophic Lateral Sclerosis. *Cold Spring Harb Perspect Med*, *8*(5). doi:10.1101/cshperspect.a024125
- Godon, C., Cordelières, F. P., Biard, D., Giocanti, N., Mégnin-Chanet, F., Hall, J., & Favaudon, V. (2008). PARP inhibition versus PARP-1 silencing: different outcomes in terms of single-strand break repair and radiation susceptibility. *Nucleic Acids Res*, *36*(13), 4454-4464. doi:10.1093/nar/gkn403
- Guo, W., Naujock, M., Fumagalli, L., Vandoorne, T., Baatsen, P., Boon, R., Ordovás, L., Patel, A., Welters, M., Vanwelden, T., Geens, N., Tricot, T., Benoy, V., Steyaert, J., Lefebvre-Omar, C., Boesmans, W., Jarpe, M., Sterneckert, J., Wegner, F., Petri, S., Bohl, D., Vanden Berghe, P., Robberecht, W., Van Damme, P., Verfaillie, C., & Van Den Bosch, L. (2017). HDAC6 inhibition reverses axonal transport defects in motor neurons derived from FUS-ALS patients. *Nat Commun*, *8*(1), 861. doi:10.1038/s41467-017-00911-y
- Haberland, J., Bertz, J., Wolf, U., Ziese, T., & Kurth, B. M. (2010). German cancer statistics 2004. *BMC Cancer*, *10*, 52. doi:10.1186/1471-2407-10-52
- Han, T. W., Kato, M., Xie, S., Wu, L. C., Mirzaei, H., Pei, J., Chen, M., Xie, Y., Allen, J., Xiao, G., & McKnight, S. L. (2012). Cell-free formation of RNA granules: bound RNAs identify features and components of cellular assemblies. *Cell*, *149*(4), 768-779. doi:10.1016/j.cell.2012.04.016
- Hardiman, O., Al-Chalabi, A., Brayne, C., Beghi, E., van den Berg, L. H., Chio, A., Martin, S., Logroscino, G., & Rooney, J. (2017). The changing picture of amyotrophic lateral sclerosis: lessons from European registers. *J Neurol Neurosurg Psychiatry*, *88*(7), 557-563. doi:10.1136/jnnp-2016-314495



- Hardy, J. A., & Higgins, G. A. (1992). Alzheimer's disease: the amyloid cascade hypothesis. *Science*, 256(5054), 184-185. doi:10.1126/science.1566067
- Hicks, G. G., Singh, N., Nashabi, A., Mai, S., Bozek, G., Klewes, L., Arapovic, D., White, E. K., Koury, M. J., Oltz, E. M., Van Kaer, L., & Ruley, H. E. (2000). Fus deficiency in mice results in defective B-lymphocyte development and activation, high levels of chromosomal instability and perinatal death. *Nat. Genet.*, 24(2), 175-179.
- Hill, S. J., Mordes, D. A., Cameron, L. A., Neuberg, D. S., Landini, S., Eggan, K., & Livingston, D. M. (2016). Two familial ALS proteins function in prevention/repair of transcription-associated DNA damage. *Proc Natl Acad Sci U S A*, 113(48), E7701-E7709. doi:10.1073/pnas.1611673113
- Hoch, N. C., Hanzlikova, H., Rulten, S. L., Tétreault, M., Komulainen, E., Ju, L., Hornyak, P., Zeng, Z., Gittens, W., Rey, S. A., Staras, K., Mancini, G. M., McKinnon, P. J., Wang, Z. Q., Wagner, J. D., Yoon, G., Caldecott, K. W., & Consortium, C. R. C. (2017). XRCC1 mutation is associated with PARP1 hyperactivation and cerebellar ataxia. *Nature*, 541(7635), 87-91. doi:10.1038/nature20790
- Hübers, A., Just, W., Rosenbohm, A., Müller, K., Marroquin, N., Goebel, I., Högel, J., Thiele, H., Altmüller, J., Nürnberg, P., Weishaupt, J. H., Kubisch, C., Ludolph, A. C., & Volk, A. E. (2015). De novo FUS mutations are the most frequent genetic cause in early-onset German ALS patients. *Neurobiol Aging*, 36(11), 3117.e3111-3117.e3116. doi:10.1016/j.neurobiolaging.2015.08.005
- Japtok, J., Lojewski, X., Naumann, M., Klingenstein, M., Reinhardt, P., Sternecker, J., Putz, S., Demestre, M., Boeckers, T. M., Ludolph, A. C., Liebau, S., Storch, A., & Hermann, A. (2015). Stepwise acquirement of hallmark neuropathology in FUS-ALS iPSC models depends on mutation type and neuronal aging. *Neurobiol Dis*, 82, 420-429. doi:10.1016/j.nbd.2015.07.017
- Kabashi, E., Valdmanis, P. N., Dion, P., Spiegelman, D., McConkey, B. J., Vande Velde, C., Bouchard, J. P., Lacomblez, L., Pochigaeva, K., Salachas, F., Pradat, P. F., Camu, W., Meininger, V., Dupre, N., & Rouleau, G. A. (2008). TARDBP mutations in individuals with sporadic and familial amyotrophic lateral sclerosis. *Nat Genet*, 40(5), 572-574. doi:10.1038/ng.132
- Kam, T. I., Mao, X., Park, H., Chou, S. C., Karuppagounder, S. S., Umanah, G. E., Yun, S. P., Brahmachari, S., Panicker, N., Chen, R., Andrabi, S. A., Qi, C., Poirier, G. G., Pletnikova, O., Troncoso, J. C., Bekris, L. M., Leverenz, J. B., Pantelyat, A., Ko, H. S.,

- Rosenthal, L. S., Dawson, T. M., & Dawson, V. L. (2018). Poly(ADP-ribose) drives pathologic  $\alpha$ -synuclein neurodegeneration in Parkinson's disease. *Science*, 362(6414). doi:10.1126/science.aat8407
- Kiernan, M. C., Vucic, S., Cheah, B. C., Turner, M. R., Eisen, A., Hardiman, O., Burrell, J. R., & Zoing, M. C. (2011). Amyotrophic lateral sclerosis. *Lancet*, 377(9769), 942-955. doi:10.1016/S0140-6736(10)61156-7
- King, O. D., Gitler, A. D., & Shorter, J. (2012). The tip of the iceberg: RNA-binding proteins with prion-like domains in neurodegenerative disease. *Brain Res*, 1462, 61-80. doi:10.1016/j.brainres.2012.01.016
- Kuroda, M., Sok, J., Webb, L., Baechtold, H., Urano, F., Yin, Y., Chung, P., de Rooij, D. G., Akhmedov, A., Ashley, T., & Ron, D. (2000). Male sterility and enhanced radiation sensitivity in TLS(-/-) mice. *EMBO J*, 19(3), 453-462. doi:10.1093/emboj/19.3.453
- Kwiatkowski, T. J., Bosco, D. A., Leclerc, A. L., Tamrazian, E., Vanderburg, C. R., Russ, C., Davis, A., Gilchrist, J., Kasarskis, E. J., Munsat, T., Valdmanis, P., Rouleau, G. A., Hosler, B. A., Cortelli, P., de Jong, P. J., Yoshinaga, Y., Haines, J. L., Pericak-Vance, M. A., Yan, J., Ticozzi, N., Siddique, T., McKenna-Yasek, D., Sapp, P. C., Horvitz, H. R., Landers, J. E., & Brown, R. H. (2009). Mutations in the FUS/TLS gene on chromosome 16 cause familial amyotrophic lateral sclerosis. *Science*, 323(5918), 1205-1208. doi:10.1126/science.1166066
- Lattante, S., Rouleau, G. A., & Kabashi, E. (2013). TARDBP and FUS mutations associated with amyotrophic lateral sclerosis: summary and update. *Hum Mutat*, 34(6), 812-826. doi:10.1002/humu.22319
- Madabhushi, R., Pan, L., & Tsai, L. H. (2014). DNA damage and its links to neurodegeneration. *Neuron*, 83(2), 266-282. doi:10.1016/j.neuron.2014.06.034
- Martinez-Macias, M. I., Moore, D. A., Green, R. L., Gomez-Herreros, F., Naumann, M., Hermann, A., Van Damme, P., Hafezparast, M., & Caldecott, K. W. (2019). FUS (fused in sarcoma) is a component of the cellular response to topoisomerase I-induced DNA breakage and transcriptional stress. *Life Sci Alliance*, 2(2). doi:10.26508/lsa.201800222
- Martire, S., Mosca, L., & d'Erme, M. (2015). PARP-1 involvement in neurodegeneration: A focus on Alzheimer's and Parkinson's diseases. *Mech Ageing Dev*, 146-148, 53-64. doi:10.1016/j.mad.2015.04.001

- Mastrocola, A. S., Kim, S. H., Trinh, A. T., Rodenkirch, L. A., & Tibbetts, R. S. (2013a). The RNA-binding protein fused in sarcoma (FUS) functions downstream of poly(ADP-ribose) polymerase (PARP) in response to DNA damage. *J Biol Chem*, *288*(34), 24731-24741. doi:10.1074/jbc.M113.497974
- Mastrocola, A. S., Kim, S. H., Trinh, A. T., Rodenkirch, L. A., & Tibbetts, R. S. (2013b). The RNA-binding protein fused in sarcoma (FUS) functions downstream of poly(ADP-ribose) polymerase (PARP) in response to DNA damage. *J. Biol. Chem.*, *288*(34), 24731-24741.
- McKinnon, P. J. (2017). Genome integrity and disease prevention in the nervous system. *Genes Dev*, *31*(12), 1180-1194. doi:10.1101/gad.301325.117
- Mehta, P., Kaye, W., Raymond, J., Wu, R., Larson, T., Punjani, R., Heller, D., Cohen, J., Peters, T., Muravov, O., & Horton, K. (2018). Prevalence of Amyotrophic Lateral Sclerosis - United States, 2014. *MMWR Morb Mortal Wkly Rep*, *67*(7), 216-218. doi:10.15585/mmwr.mm6707a3
- Miller, R. G., Mitchell, J. D., Lyon, M., & Moore, D. H. (2003). Riluzole for amyotrophic lateral sclerosis (ALS)/motor neuron disease (MND). *Amyotroph. Lateral Scler. Other Motor Neuron Disord.*, *4*(3), 191-206.
- Monahan, Z., Ryan, V. H., Janke, A. M., Burke, K. A., Rhoads, S. N., Zerze, G. H., O'Meally, R., Dignon, G. L., Conicella, A. E., Zheng, W., Best, R. B., Cole, R. N., Mittal, J., Shewmaker, F., & Fawzi, N. L. (2017). Phosphorylation of the FUS low-complexity domain disrupts phase separation, aggregation, and toxicity. *EMBO J*, *36*(20), 2951-2967. doi:10.15252/embj.201696394
- Müller, K., Brenner, D., Weydt, P., Meyer, T., Grehl, T., Petri, S., Grosskreutz, J., Schuster, J., Volk, A. E., Borck, G., Kubisch, C., Klopstock, T., Zeller, D., Jablonka, S., Sendtner, M., Klebe, S., Knehr, A., Günther, K., Weis, J., Claeys, K. G., Schrank, B., Sperfeld, A. D., Hübers, A., Otto, M., Dorst, J., Meitinger, T., Strom, T. M., Andersen, P. M., Ludolph, A. C., Weishaupt, J. H., & MND-NET, G. A. n. (2018). Comprehensive analysis of the mutation spectrum in 301 German ALS families. *J Neurol Neurosurg Psychiatry*, *89*(8), 817-827. doi:10.1136/jnnp-2017-317611
- Murakami, T., Qamar, S., Lin, J. Q., Schierle, G. S., Rees, E., Miyashita, A., Costa, A. R., Dodd, R. B., Chan, F. T., Michel, C. H., Kronenberg-Versteeg, D., Li, Y., Yang, S. P., Wakutani, Y., Meadows, W., Ferry, R. R., Dong, L., Tartaglia, G. G., Favrin, G., Lin, W. L., Dickson, D. W., Zhen, M., Ron, D., Schmitt-Ulms, G., Fraser, P. E., Shneider,

- N. A., Holt, C., Vendruscolo, M., Kaminski, C. F., & St George-Hyslop, P. (2015). ALS/FTD Mutation-Induced Phase Transition of FUS Liquid Droplets and Reversible Hydrogels into Irreversible Hydrogels Impairs RNP Granule Function. *Neuron*, *88*(4), 678-690. doi:10.1016/j.neuron.2015.10.030
- Murthy, A. C., Dignon, G. L., Kan, Y., Zerze, G. H., Parekh, S. H., Mittal, J., & Fawzi, N. L. (2019). Molecular interactions underlying liquid-liquid phase separation of the FUS low-complexity domain. *Nat Struct Mol Biol*, *26*(7), 637-648. doi:10.1038/s41594-019-0250-x
- Neumann, M., Rademakers, R., Roeber, S., Baker, M., Kretzschmar, H. A., & Mackenzie, I. R. (2009). A new subtype of frontotemporal lobar degeneration with FUS pathology. *Brain*, *132*(Pt 11), 2922-2931.
- Neumann, M., Sampathu, D. M., Kwong, L. K., Truax, A. C., Micsenyi, M. C., Chou, T. T., Bruce, J., Schuck, T., Grossman, M., Clark, C. M., McCluskey, L. F., Miller, B. L., Masliah, E., Mackenzie, I. R., Feldman, H., Feiden, W., Kretzschmar, H. A., Trojanowski, J. Q., & Lee, V. M. (2006). Ubiquitinated TDP-43 in frontotemporal lobar degeneration and amyotrophic lateral sclerosis. *Science*, *314*(5796), 130-133.
- Nott, T. J., Craggs, T. D., & Baldwin, A. J. (2016). Membraneless organelles can melt nucleic acid duplexes and act as biomolecular filters. *Nat Chem*, *8*(6), 569-575. doi:10.1038/nchem.2519
- Pal, A., Glaß, H., Naumann, M., Kreiter, N., JapTok, J., Sczech, R., & Hermann, A. (2018). High content organelle trafficking enables disease state profiling as powerful tool for disease modelling. *Sci Data*, *5*, 180241. doi:10.1038/sdata.2018.241
- Pascal, J. M. (2018). The comings and goings of PARP-1 in response to DNA damage. *DNA Repair (Amst)*, *71*, 177-182. doi:10.1016/j.dnarep.2018.08.022
- Patel, A., Lee, H. O., Jawerth, L., Maharana, S., Jahnel, M., Hein, M. Y., Stoyanov, S., Mahamid, J., Saha, S., Franzmann, T. M., Pozniakovski, A., Poser, I., Maghelli, N., Royer, L. A., Weigert, M., Myers, E. W., Grill, S., Drechsel, D., Hyman, A. A., & Alberti, S. (2015). A Liquid-to-Solid Phase Transition of the ALS Protein FUS Accelerated by Disease Mutation. *Cell*, *162*(5), 1066-1077. doi:10.1016/j.cell.2015.07.047
- Pillay, N., Tighe, A., Nelson, L., Littler, S., Coulson-Gilmer, C., Bah, N., Golder, A., Bakker, B., Spierings, D. C. J., James, D. I., Smith, K. M., Jordan, A. M., Morgan, R. D.,

- Ogilvie, D. J., Foijer, F., Jackson, D. A., & Taylor, S. S. (2019). DNA Replication Vulnerabilities Render Ovarian Cancer Cells Sensitive to Poly(ADP-Ribose) Glycohydrolase Inhibitors. *Cancer Cell*, 35(3), 519-533.e518. doi:10.1016/j.ccell.2019.02.004
- Piskunova, T. S., Yurova, M. N., Ovsiyannikov, A. I., Semenchenko, A. V., Zabezhinski, M. A., Popovich, I. G., Wang, Z. Q., & Anisimov, V. N. (2008). Deficiency in Poly(ADP-ribose) Polymerase-1 (PARP-1) Accelerates Aging and Spontaneous Carcinogenesis in Mice. *Curr Gerontol Geriatr Res*, 754190. doi:10.1155/2008/754190
- Rabbitts, T. H., Forster, A., Larson, R., & Nathan, P. (1993). Fusion of the dominant negative transcription regulator CHOP with a novel gene FUS by translocation t(12;16) in malignant liposarcoma. *Nat. Genet.*, 4(2), 175-180.
- Reinhardt, P., Glatza, M., Hemmer, K., Tsytsyura, Y., Thiel, C. S., Hoing, S., Moritz, S., Parga, J. A., Wagner, L., Bruder, J. M., Wu, G., Schmid, B., Ropke, A., Klingauf, J., Schwamborn, J. C., Gasser, T., Scholer, H. R., & Sternecker, J. (2013). Derivation and expansion using only small molecules of human neural progenitors for neurodegenerative disease modeling. *PLoS ONE*, 8(3), e59252-e59252.
- Renton, A. E., Chiò, A., & Traynor, B. J. (2014). State of play in amyotrophic lateral sclerosis genetics. *Nat Neurosci*, 17(1), 17-23. doi:10.1038/nn.3584
- Reynolds, J. J., & Stewart, G. S. (2013). A single strand that links multiple neuropathologies in human disease. *Brain*, 136(Pt 1), 14-27. doi:10.1093/brain/aws310
- Rhoads, S. N., Monahan, Z. T., Yee, D. S., Leung, A. Y., Newcombe, C. G., O'Meally, R. N., Cole, R. N., & Shewmaker, F. P. (2018). The prionlike domain of FUS is multiphosphorylated following DNA damage without altering nuclear localization. *Mol Biol Cell*, 29(15), 1786-1797. doi:10.1091/mbc.E17-12-0735
- Rosen, D. R., Siddique, T., Patterson, D., Figlewicz, D. A., Sapp, P., Hentati, A., Donaldson, D., Goto, J., O'Regan, J. P., & Deng, H. X. (1993). Mutations in Cu/Zn superoxide dismutase gene are associated with familial amyotrophic lateral sclerosis. *Nature*, 362(6415), 59-62.
- Rowland, L. P., & Shneider, N. A. (2001). Amyotrophic lateral sclerosis. *N Engl J Med*, 344(22), 1688-1700. doi:10.1056/NEJM200105313442207
- Rulten, S. L., Rotheray, A., Green, R. L., Grundy, G. J., Moore, D. A., Gómez-Herreros, F., Hafezparast, M., & Caldecott, K. W. (2014). PARP-1 dependent recruitment of the

- amyotrophic lateral sclerosis-associated protein FUS/TLS to sites of oxidative DNA damage. *Nucleic Acids Res*, 42(1), 307-314. doi:10.1093/nar/gkt835
- Scekic-Zahirovic, J., Oussini, H. E., Mersmann, S., Drenner, K., Wagner, M., Sun, Y., Allmeroth, K., Dieterlé, S., Sinniger, J., Dirrig-Grosch, S., René, F., Dormann, D., Haass, C., Ludolph, A. C., Lagier-Tourenne, C., Storkebaum, E., & Dupuis, L. (2017). Motor neuron intrinsic and extrinsic mechanisms contribute to the pathogenesis of FUS-associated amyotrophic lateral sclerosis. *Acta Neuropathol*, 133(6), 887-906. doi:10.1007/s00401-017-1687-9
- Shang, Y., & Huang, E. J. (2016). Mechanisms of FUS mutations in familial amyotrophic lateral sclerosis. *Brain Res*, 1647, 65-78. doi:10.1016/j.brainres.2016.03.036
- Simbulan-Rosenthal, C. M., Haddad, B. R., Rosenthal, D. S., Weaver, Z., Coleman, A., Luo, R., Young, H. M., Wang, Z. Q., Ried, T., & Smulson, M. E. (1999). Chromosomal aberrations in PARP(-/-) mice: genome stabilization in immortalized cells by reintroduction of poly(ADP-ribose) polymerase cDNA. *Proc Natl Acad Sci U S A*, 96(23), 13191-13196. doi:10.1073/pnas.96.23.13191
- Spillantini, M. G., Schmidt, M. L., Lee, V. M., Trojanowski, J. Q., Jakes, R., & Goedert, M. (1997). Alpha-synuclein in Lewy bodies. *Nature*, 388(6645), 839-840. doi:10.1038/42166
- Sreedharan, J., Blair, I. P., Tripathi, V. B., Hu, X., Vance, C., Rogelj, B., Ackerley, S., Durnall, J. C., Williams, K. L., Buratti, E., Baralle, F., de Belleruche, J., Mitchell, J. D., Leigh, P. N., Al-Chalabi, A., Miller, C. C., Nicholson, G., & Shaw, C. E. (2008). TDP-43 mutations in familial and sporadic amyotrophic lateral sclerosis. *Science*, 319(5870), 1668-1672. doi:10.1126/science.1154584
- Stankovic, T., Kidd, A. M., Sutcliffe, A., McGuire, G. M., Robinson, P., Weber, P., Bedenham, T., Bradwell, A. R., Easton, D. F., Lennox, G. G., Haites, N., Byrd, P. J., & Taylor, A. M. (1998). ATM mutations and phenotypes in ataxia-telangiectasia families in the British Isles: expression of mutant ATM and the risk of leukemia, lymphoma, and breast cancer. *Am J Hum Genet*, 62(2), 334-345. doi:10.1086/301706
- Takahashi, K., Tanabe, K., Ohnuki, M., Narita, M., Ichisaka, T., Tomoda, K., & Yamanaka, S. (2007). Induction of pluripotent stem cells from adult human fibroblasts by defined factors. *Cell*, 131(5), 861-872.



- Takahashi, K., & Yamanaka, S. (2006). Induction of pluripotent stem cells from mouse embryonic and adult fibroblast cultures by defined factors. *Cell*, 126(4), 663-676.
- Taylor, J. P., Brown, R. H., & Cleveland, D. W. (2016). Decoding ALS: from genes to mechanism. *Nature*, 539(7628), 197-206. doi:10.1038/nature20413
- Vance, C., Rogelj, B., Hortobágyi, T., De Vos, K. J., Nishimura, A. L., Sreedharan, J., Hu, X., Smith, B., Ruddy, D., Wright, P., Ganesalingam, J., Williams, K. L., Tripathi, V., Al-Saraj, S., Al-Chalabi, A., Leigh, P. N., Blair, I. P., Nicholson, G., de Belleruche, J., Gallo, J. M., Miller, C. C., & Shaw, C. E. (2009). Mutations in FUS, an RNA processing protein, cause familial amyotrophic lateral sclerosis type 6. *Science*, 323(5918), 1208-1211.
- Vance, C., Rogelj, B., Hortobágyi, T., De Vos, K. J., Nishimura, A. L., Sreedharan, J., Hu, X., Smith, B., Ruddy, D., Wright, P., Ganesalingam, J., Williams, K. L., Tripathi, V., Al-Saraj, S., Al-Chalabi, A., Leigh, P. N., Blair, I. P., Nicholson, G., de Belleruche, J., Gallo, J. M., Miller, C. C., & Shaw, C. E. (2009). Mutations in FUS, an RNA processing protein, cause familial amyotrophic lateral sclerosis type 6. *Science*, 323(5918), 1208-1211. doi:10.1126/science.1165942
- Verhagen, M. M., Last, J. I., Hogervorst, F. B., Smeets, D. F., Roeleveld, N., Verheijen, F., Catsman-Berrevoets, C. E., Wulffraat, N. M., Cobben, J. M., Hiel, J., Brunt, E. R., Peeters, E. A., Gómez Garcia, E. B., van der Knaap, M. S., Lincke, C. R., Laan, L. A., Tijssen, M. A., van Rijn, M. A., Majoor-Krakauer, D., Visser, M., van 't Veer, L. J., Kleijer, W. J., van de Warrenburg, B. P., Warris, A., de Groot, I. J., de Groot, R., Broeks, A., Preijers, F., Kremer, B. H., Weemaes, C. M., Taylor, M. A., van Deuren, M., & Willemsen, M. A. (2012). Presence of ATM protein and residual kinase activity correlates with the phenotype in ataxia-telangiectasia: a genotype-phenotype study. *Hum Mutat*, 33(3), 561-571. doi:10.1002/humu.22016
- Waibel, S., Neumann, M., Rosenbohm, A., Birve, A., Volk, A. E., Weishaupt, J. H., Meyer, T., Müller, U., Andersen, P. M., & Ludolph, A. C. (2013). Truncating mutations in FUS/TLS give rise to a more aggressive ALS-phenotype than missense mutations: a clinico-genetic study in Germany. *Eur. J. Neurol.*, 20(3), 540-546.
- Wang, H., Guo, W., Mitra, J., Hegde, P. M., Vandoorne, T., Eckelmann, B. J., Mitra, S., Tomkinson, A. E., Van Den Bosch, L., & Hegde, M. L. (2018). Mutant FUS causes DNA ligation defects to inhibit oxidative damage repair in Amyotrophic Lateral Sclerosis. *Nat Commun*, 9(1), 3683. doi:10.1038/s41467-018-06111-6

- Wang, W. Y., Pan, L., Su, S. C., Quinn, E. J., Sasaki, M., Jimenez, J. C., Mackenzie, I. R., Huang, E. J., & Tsai, L. H. (2013). Interaction of FUS and HDAC1 regulates DNA damage response and repair in neurons. *Nat. Neurosci.*, *16*(10), 1383-1391.
- Wang, Z. Q., Auer, B., Stingl, L., Berghammer, H., Haidacher, D., Schweiger, M., & Wagner, E. F. (1995). Mice lacking ADPRT and poly(ADP-ribosyl)ation develop normally but are susceptible to skin disease. *Genes Dev*, *9*(5), 509-520. doi:10.1101/gad.9.5.509
- Yu, S. W., Wang, H., Poitras, M. F., Coombs, C., Bowers, W. J., Federoff, H. J., Poirier, G. G., Dawson, T. M., & Dawson, V. L. (2002). Mediation of poly(ADP-ribose) polymerase-1-dependent cell death by apoptosis-inducing factor. *Science*, *297*(5579), 259-263. doi:10.1126/science.1072221
- Zarei, S., Carr, K., Reiley, L., Diaz, K., Guerra, O., Altamirano, P. F., Pagani, W., Lodin, D., Orozco, G., & Chinea, A. (2015). A comprehensive review of amyotrophic lateral sclerosis. *Surg Neurol Int*, *6*, 171. doi:10.4103/2152-7806.169561

## 9. Appendix

### 9.1 Anlage 1

#### Erklärungen zur Eröffnung des Promotionsverfahrens

1. Hiermit versichere ich, dass ich die vorliegende Arbeit ohne unzulässige Hilfe Dritter und ohne Benutzung anderer als der angegebenen Hilfsmittel angefertigt habe; die aus fremden Quellen direkt oder indirekt übernommenen Gedanken sind als solche kenntlich gemacht.

2. Bei der Auswahl und Auswertung des Materials sowie bei der Herstellung des Manuskripts habe ich Unterstützungsleistungen von folgenden Personen erhalten:

*Unterstützung bei Planung und Design: Prof. Dr. Dr. Andreas Hermann*

3. Weitere Personen waren an der geistigen Herstellung der vorliegenden Arbeit nicht beteiligt. Insbesondere habe ich nicht die Hilfe eines kommerziellen Promotionsberaters in Anspruch genommen. Dritte haben von mir weder unmittelbar noch mittelbar geldwerte Leistungen für Arbeiten erhalten, die im Zusammenhang mit dem Inhalt der vorgelegten Dissertation stehen.

4. Die Arbeit wurde bisher weder im Inland noch im Ausland in gleicher oder ähnlicher Form einer anderen Prüfungsbehörde vorgelegt.

5. Die Inhalte dieser Dissertation wurden in folgender Form veröffentlicht:

**Naumann M, Pal A, Goswami A, Lojewski X, Japtok J, Vehlow A, Naujock M, Günther R, Jin M, Stanslawski N, Reinhardt P, Sternecker J, Frickenhaus M, Pan-Montojo F, Storkebaum E, Poser I, Freischmidt A, Weishaupt JH, Holzmann K, Troost D, Ludolph AC, Boeckers TM, Liebau S, Petri S, Cordes N, Hyman A, Wegner F, Grill S, Weis J, Storch A, Hermann A.** *Impaired DNA damage response signaling by FUS-NLS mutations leads to neurodegeneration and aggregation formation. Nature Communications (2018), 9:335. DOI: 10.1038/s41467-017-02299-1*

*Journal impact factor 2018: 11.880*

**Naumann M, Peikert K, Günther R, van der Kooij AJ, Aronica E, Hübers A, Danel V, Corcia P, Pan-Montojo F, Cirak S, Haliloglu G, Ludolph AC, Goswami A, Andersen PM, Prudlo J, Wegner F, Van Damme P, Weishaupt JH, Hermann A.** *Phenotypes and malignancy risk of different FUS mutations in genetic amyotrophic lateral sclerosis. Ann Clin Transl Neurol. 2019 Nov 4. doi: 10.1002/acn3.50930*

*Journal impact factor 2019: 3.66*

6. Ich bestätige, dass es keine zurückliegenden erfolglosen Promotionsverfahren gab.

-----*entfällt*-----

7. Ich bestätige, dass ich die Promotionsordnung der Medizinischen Fakultät der Technischen Universität Dresden anerkenne.

8. Ich habe die Zitierrichtlinien für Dissertationen an der Medizinischen Fakultät der Technischen Universität Dresden zur Kenntnis genommen und befolgt.

9. Ich bin mit den "Richtlinien zur Sicherung guter wissenschaftlicher Praxis, zur Vermeidung wissenschaftlichen Fehlverhaltens und für den Umgang mit Verstößen" der Technischen Universität Dresden einverstanden.

Rostock, 09.07.2020

Unterschrift des Doktoranden

## 9.2 Anlage 2

### Erklärung über die Einhaltung gesetzlicher Bestimmungen

Hiermit bestätige ich die Einhaltung der folgenden aktuellen gesetzlichen Vorgaben im Rahmen meiner Dissertation

× das zustimmende Votum der Ethikkommission bei Klinischen Studien, epidemiologischen Untersuchungen mit Personenbezug oder Sachverhalten, die das Medizinproduktegesetz betreffen

Aktenzeichen der zuständigen Ethikkommission: *EK45022009, EK393122012, EK49022016*

die Einhaltung der Bestimmungen des Tierschutzgesetzes

Aktenzeichen der Genehmigungsbehörde zum Vorhaben/zur Mitwirkung: *entfällt*

× die Einhaltung des Gentechnikgesetzes/Projektnummer: *Projektnummer: 56.8811.71/170-7*

× die Einhaltung von Datenschutzbestimmungen der Medizinischen Fakultät und des Universitätsklinikums Carl Gustav Carus.

Rostock, 09.07.2020

Unterschrift des Doktoranden

### 9.3 Erklärung zum Eigenanteil der gemeinschaftlichen Publikationen

1. **Naumann M**, Pal A, Goswami A, Lojewski X, Japtok J, Vehlow A, Naujock M, Günther R, Jin M, Stanslawski N, Reinhardt P, Sternecker J, Frickenhaus M, Pan-Montojo F, Storkebaum E, Poser I, Freischmidt A, Weishaupt JH, Holzmann K, Troost D, Ludolph AC, Boeckers TM, Liebau S, Petri S, Cordes N, Hyman A, Wegner F, Grill S, Weis J, Storch A, Hermann A. Impaired DNA damage response signaling by FUS-NLS mutations leads to neurodegeneration and aggregation formation. Nature Communications (2018), 9:335. DOI: 10.1038/s41467-017-02299-1

- Mitarbeit an der konzeptionellen Projektplanung und eigenverantwortliche Detailplanung der Experimente
- Methodenetablierung (Differenzierungsprotokoll sMN, MFC Kultur, DNA damage assays)
- praktische Durchführung der Kultivierung von spinalen Motoneuronen und davon abgeleitete Experimente
- anteilsweise Durchführung live-cell imaging (TIRF-Mikroskopie und Laserablationsmikroskopie)
- Datenanalyse, Auswertung
- Anteilsweise Miterstellung der Publikation

2. **Naumann M**, Peikert K, Günther R, van der Kooij AJ, Aronica E, Hübers A, Danel V, Corcia P, Pan-Montojo F, Cirak S, Haliloglu G, Ludolph AC, Goswami A, Andersen PM, Prudlo J, Wegner F, Van Damme P, Weishaupt JH, Hermann A. Phenotypes and malignancy risk of different FUS mutations in genetic amyotrophic lateral sclerosis. Ann Clin Transl Neurol. 2019 Nov 4. doi: 10.1002/acn3.50930

- Mitarbeit an der konzeptionellen Projektplanung eigenverantwortliche Detailanalysen inklusive Literaturrecherche
- Datenbankrecherchen und Rohdatengewinnung mit Unterstützung von Kollaborationspartnern
- Datenanalyse, statistische Aufarbeitung und Auswertung
- Erstellung der Publikation

Rostock, 09.07.2020

Unterschrift des Doktoranden